

Fig. 1: FT-IR spectra of a) benzoxazine monomer. b) polybenzoxazine. c) BA-a/PU 60/40 before curing. d) BA-a/PU 60/40 after fully cured.

Table 1: Properties of BA-a/PU Polymers

BA-a/PU	Tg (°C)	E' at rubbery plateau (MPa)	Crosslink density (mol/m³)	Flexural strength (MPa)	Flexural modulus (GPa)
100:0	166	56	4661	130	5.49
90:10	177	78	5202	142	4.10
80:20	192	102	5613	120	3.47
70:30	220	118	5833	89	2.57
60:40	245	148	7955	60	2.11

Viscoelastic properties of BA-a/PU systems were shown in Table 1. Synergistic behavior of Tg of the polymer network is evidently observed i.e. the Tg's of all copolymers are greater than the values of 166°C of BA-a and -70°C of PU. The Tg of the BA-a/PU copolymers increased with the PU contents.

Crosslink density of polymer network can be estimated by an equation from the statistical theory of rubber elasticity by Nielson [4].

$$\log\left(\frac{E'}{3}\right) = 7.0 + 293(\rho_x) \tag{1}$$

Where E' is a storage modulus in rubbery plateau, ρ_x is crosslink density that means the mole number of network chains per volume of the polymers. Table 1 suggested that the crosslink density of the BA-a/PU copolymers increased with the mass fraction of the PU. A higher crosslink density of the alloys led to a higher T_g of the matrix as described by Fox and Loshaek equation.

$$Tg = Tg(\infty) - \frac{k}{M_n} + k_x \rho_x \tag{2}$$

Where $Tg(\infty)$ is the Tg of infinite molecular weight linear polymer. k and kx are the numerical constant. M_n is the number averaged molecular weight and ρ_x is the crosslink density respectively.

Table 1 also exhibits flexural properties of BA-a/PU alloys at various compositions. The flexural strength of the BA-a/PU ratio at a 90/10 was observed to show a maximum value. In principle, the addition of the softer PU fraction in the alloys should result in the decrease of their strength. However, we also knew that the addition of PU helped improve the crosslink density. This implies that the effect of crosslink density on the alloy's strength dominates the effect of the lower stiffness of the PU if the PU mass fraction is below 10wt%. Finally, the lower flexural modulus with the PU addition was due to the presence of the softer urethane elastomer in the more rigid polybenzoxazine [3].

4. Conclusions

Hybrid network structures were formed in curing of PU prepolymer with BA-a resin with disappearance of IR bands at 941, 1230 cm⁻¹ (C-O-C) and 2242 cm⁻¹ (NCO). BA-a/PU alloys showed synergistic behavior in Tg. A maximum in flexural strength was also observed at the BA-a/PU mass ratio of 90/10. Finally, the flexural modulus of the alloys was found to systematically decrease with an addition of the PU. These high thermal and mechanical properties suggested that BA-a/PU can be potentially used as high performance polymers or composite matrices for part of the electronic and ballistic armor in Thailand.

Acknowledgments

This work is supported by the research grant for TRF Research Scholar (S. Rimdusit) and by TRF-MAG scholarship (W. Bangsen) of the Thailand Research Fund.

- [1] H. Ishida, D.J. Allen, Polymer 37 (1996) 4487-4495.
- [2] T. Takeichi, T.J. Guo, Agag, Polym. Sci., 38 (2000) 4165.
- [3] S. Rimdusit, et al., Polym. Eng. Sci. 45 (2005) 228.
- [4] L.E. Nielsen, R.F. Landel, Mechanical Properties of Polymers and Composites, Marcel Dekker, New York, 1994, pp. 131– 232.

101 NS-E03

High Thermomechanical Performance Hybrids of Dianhydride Containing Polybenzoxazine

Chanchira Jubsilp¹, Tsutomu Takeichi², and Sarawut Rimdusit^{3,*}

¹Department of Chemical Engineering, Faculty of Engineering, Srinakharinwirot University, Nakhonnayok, Thailand

²School of Materials Science, Toyohashi University of Technology, Tempaku-cho, Toyohashi 441-8580, Japan.

³Polymer Engineering Laboratory, Department of Chemical Engineering, Faculty of Engineering, Chulalongkorn University, Bangkok, 10330, Thailand

Tel.: +66-2-218-6862, Fax: +66-2-218-6877, *E-mail address: sarawut.r@chula.ac.th

Thermomechanical properties of benzophenone-3,3',4,4'-tetracarboxylic dianhydride (BTDA) containing polybenzoxazine (BA-a) was investigated. The experimental results reveal that the enhancement in the glass transition temperature (Tg) which depicted with the viscoelastic analysis of the BA-a/BTDA blends is clearly observed, i.e., Tg of the BA-a/BTDA blends are significantly higher (Tg beyond 200°C) than that of polybenzoxazine, i.e. 165°C. The enhanced Tg of the BA-a/BTDA blend at 1.5/1 mole ratio is found to be 250°C. Furthermore, the degradation temperature and the char yield values with the thermogravimetric analyzer (TGA) of the BA-a/BTDA blends are found to significantly improve with the presence of the BTDA which is molecular structure consisted of aromatic rings. Increasingly, the flexibility of the crosslinked BA-a/BTDA was greatly enhanced compared with the neat poly(BA-a).

1. Introduction

The polybenzoxazine is a novel class of thermosetting polymer that combined the thermal properties and flame retardant of phenolic resin with mechanical performance and molecular design flexibility of epoxy resin [1-2]. The chemistry of benzoxazine synthesis offers a wide range of molecular design flexibility by using derivatives of phenol, aldehyde, and primary Improvements of polybenzoxazine properties to be excellent candidates for highperformance materials such as high thermal stability, high char yield, and high glass transition temperature (Tg), are becoming more and more attractive in many methods, which can be mainly classified into two procedures. By taking advantage of its design flexibility of benzoxazine chemistry, thermal and thermo oxidative stabilities of polybenzoxazine have been improved by altering the functional group on the phenol and/or amine. However, the functional groups of the aromatic amines are difficult to prepare and significantly raise the product's cost. The other procedure to obtain high-performance materials is modification utilizing polymer alloy/or blend technology. Therefore, the purpose of this work is to study effect of BTDA incorporated polybenzoxazine on thermal properties and mechanical characteristics as a high performance polymer, which makes them suitable for more extensive applications, i.e., in protecting coating, thermal insulating materials through the investigation of thermal stability, and dynamic moduli.

2. Methodology

The BA-a/BTDA mixtures to be investigated are BA-a/BTDA 1:1 to BA-a/BTDA 5:1. The number after letters is the mol ratio of the benzoxazine resin and BTDA in the respective order. The mixture was dissolved and

stirred in NMP at 80°C for few minutes until the homogeneous mixture was obtained and then the solution was cast. The NMP solvent was removed by drying in vacuum oven at 80°C for 24 h before undergoing a step cure in an air-circulating oven. The sample were then cured sequentially at 170°C-240°C for 1 h to ensure fully cure of the mixture.

Dynamic viscoelastic measurements were conducted on Perkin Elmer model Pyris Diamond in the tension geometry at 1 Hz from 30 to 350°C at 2°C/min. TGA was determined with Perkin Elmer model Diamond TG/DTA. Sample mass of 10 mg was heated from 40 to 820°C at a heating rate of 20°C/min under nitrogen.

3. Results and Discussion

Dynamic mechanical analysis can provide important viscoelastic properties of BA-a/BTDA blend systems as illustrated in Fig. 1. From the figure, we can clearly see that the storage modulus of the BA-a/BTDA blends is higher than that of the neat poly(BA-a). The storage moduli at the room temperature of the BAa/BTDA blend systems exhibit the values in the ranges of 6.6-9.4 GPa at desirable compositions whereas that of the neat poly(BA-a) is of 4.5 GPa. The increase of the storage modulus value may be due to a result of the more rigid molecular characterization of dianhydride used. Since the BTDA molecule contains a number of the rigid molecule structure of benzene ring which significantly induced the materials more rigid. Thus, we can see that the modulus in the rubbery plateau of the BA-a/BTDA blend systems was clearly increased with the content of the BTDA. This evidence suggests that the increase of the BTDA composition results in a greater cross-linked density of the BA-a/BTDA blend systems.



of BA-a/BTDA All blends were homogeneous and transparent, implying that no phase separation occurred at the scale exceeding the wavelength of visible light. However, the BA-a/BTDA blends were subjected to thermal analysis to confirm the miscible characteristic with considering glass transition temperature (Tg) behavior. From the inset in Fig.1, the Tg value determined from the maximum of the loss modulus curve of the neat poly(BA-a) was reported to be about 165°C and the Tg value of the neat poly(BA-a) was found to enhance by blending with the BTDA. For the cured BA-

a/BTDA blends, the compositions of these blends show single Tg's, i.e. 200°C to 250°C. Interesting feature was observed that the BA-a/BTDA 1.5:1 blend shows synergistic behavior compared to other BA-a/BTDA blend compositions, which expects that the reaction of the functional groups by stoichiometric ratio between the BA-a resin and the BTDA may be strongly affected.

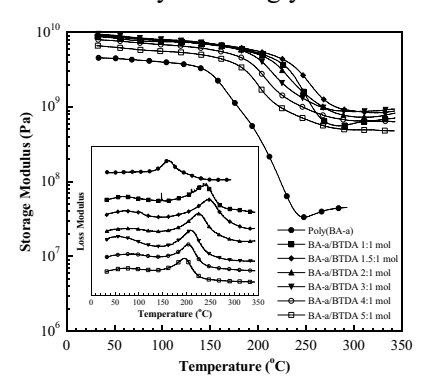


Fig. 1 Viscoelastic analysis of Ba-A/BTDA blends

The thermal stability of BA-a/BTDA blends was investigated by TGA. The values of 5 and 10% weight loss temperatures and the char yield are summarized in Table 1. As evidently seen in the table, the degradation temperature (Td) reported at 5 and 10% weight loss of the BTDA containing poly(BA-a) showed higher than these of the neat poly(BA-a). Again, the synergistic behavior is observed, with the Td of 364°C belonging to BA-a/BTDA 1.5:1 composition while the Td of the neat poly(BA-a) used in this study has been reported to be about 339°C at 5% weight loss due to the presence of the BTDA into poly(BA-a) is plausible to propose that weight loss from segmental decomposition via gaseous fragments could be suppressed by an aromatic structure of the BTDA. Thus, incorporating the BTDA into poly(BA-a) can open an effective way to an improvement on the thermal stability of the neat poly(BA-a).

Another interesting feature in the Table 1 is a char yield value of the BA-a/BTDA blend systems reported at the temperature 800°C. Positive deviation (synergism) of char yield values was observed in the BA-a/BTDA blend systems as also observed in the Tg behavior, i.e., the char yields of all compositions show the values greater than that of the neat poly(BA-a). In particular, the cured BA-a/BTDA 1.5:1 synergistic composition shows behavior compared to the other compositions, which suggests that this is due to the presence of the BTDA structure consisted of aromatic rings into the polybenzoxazine. The highest char residue of the BA-a/BTDA 1.5:1 is remarkably high considering the good processibility of the poly(BA-a) containing BTDA as well as the relative flammability also can be judged from their char residue.

Composition (mole ratio)	Td (°C) at 5% wt loss	Td (°C) at 10% wt loss	Char yield at 800°C (%)
Poly (BA-a)	339	369	39.9
BA-a/BTDA1:1	353	432	59.8
BA-a/BTDA1.5:	1 364	414	61.5
BA-a/BTDA2:1	363	405	59.3
BA-a/BTDA3:1	345	395	59.5
BA-a/BTDA4:1	336	381	57.5
BA-a/BTDA5:1	331	378	54.7

Table 1 Heat resistance of BA-a/BTDA blends

The appearances of the cured BA-a/BTDA blend samples are shown in Fig. 2. The poly(BA-a) sample of 100 µm thickness is very brittle, and the sample can be not bent more than as is shown in Fig. 2(a) whereas all the BA-a/BTDA blend samples as seen in Fig. 2(b-d) showed remarkably improved flexibility.

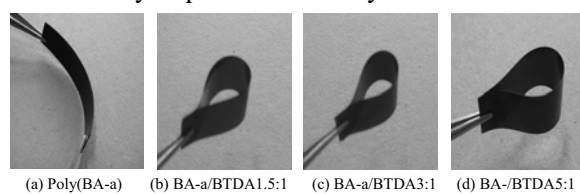


Fig. 2 Appearance of the fully cured BA-a/BTDA

4. Conclusions and Recommendations for **Thailand**

Poly(BA-a) blends with improved thermal, some mechanical properties and flexibility characteristic have been achieved. The Tg values of the BA-a/BTDA blend were 200-250°C, much higher than the Tg of the typical poly(BA-a) [165°C]. The incorporation of the BTDA into the poly(BA-a) can improve the stiffness. Thermal stability of the BA-a/BTDA blend systems depended on the BTDA content. Therefore, high performance polymers with high thermal stability as indicated by those experimental results are increasing demanded in an advanced composite system as a matrix resin and in the electronic industry for packaging application in Thailand.

Acknowledgements

This work is supported by the research grant for TRF Research Scholar (S. Rimdusit) and by TRF-MAG scholarship (W. Bangsen and P. Kunopast) of the Thailand Research Fund.

- [1] H. Ishida, US Patent 5,543,516 (1996).
- [2] N.N. Ghosh, B. Kiskan, Y. Yagci, Prog. Polym. Sci. 32 (2007) 1344-1391.

NS-E04

Mechanical and Physical Properties of HDPE/Corn Starch Composite

Supaphorn Thumsorn^{1,*}, Jessada Wong-on², Yew Wei Leong¹, Hiroyuki Hamada¹

¹Department of Advanced Fibro-Science, Kyoto Institute of Technology, Kyoto, Japan ²Department of Industrial Engineering, Pathumwan Institute of Technology, Thailand Tel.:+81-7-5724-7844, Fax: +81-7-5724 -7800, *E-mail address: nooh17@yahoo.com

This research has concerned feasibility study on using corn starch, as filler in high density polyethylene (HDPE). The filler content used range between 0-40 percent by weight. The HDPE/corn starch compounding was prepared by using a single screw extruder. From the results, it was found that the incorporation of corn starch into HDPE increased tensile modulus of the composite material at the expensed of its tensile strength. The decreases in the mechanical properties of HDPE with corn starch were explained in the light of the presence of interface defects between corn starch and polymer. Degradation studies demonstrated that the higher filler contents of HDPE/corn starch composites increased degradability at the given degradable environment. The information implies that this composite could be utilized as a degradable plastic.

1. Introduction

Starch is an abundant, inexpensive and natural raw material which is available from corn or other crops. Starch is totally biodegradable in wide variety of environments and could permit the development of degradable products for market demands. Degradation or incineration of starch products would recycle atmospheric CO₂ trapped by starch-producing plants and would not increase potential global warming [1]. Starch can be used as natural filler in traditional plastics and particularly in polyolefins. Since polyethylene is one of the most extensively produced nondegradable polymer and various types of polyethylenes are used in many field including food-packaging film and agricultural [2]. With the development of the plastic industry, starch/polyethylene with good degradability and compatibility are increasingly desired [3]. Starch-filled polyethylene plastics have been reported by many researchers [2-3]. The dry native starch was directly mixed in the polyethylene matrix with blends used for many products. An example of the contribution of starch is promoting of photodegradable low density polyethylene (LDPE). This research study of physical and mechanical properties of high density polyethylene (HDPE) filled with corn starch. The effect of starch content will be study on degradable property of the composites.

2. Methodology

Commercial-grade HDPE and corn starch were compounded in high speed mixer before compounding in single screw extruder (HAAKE/Polydrive Rheomex R25) at 0-40 percent by weight of starch. Mixing temperatures at zone 1, zone 2, zone 3 and die

zone were 140/150/160/170 °C, respectively at speed of 60 rpm. Compounds were molded in compression molding. Molded dogbone-type specimen dimension was in accordance with ASTM D638. The molded specimens were used in determination of tensile properties on universal tensile testing machine (Instron 5569) at speed of 100 mm/min. Thermal analysis of about 10 mg. of the compound in Al pan was done using Differential Scanning Calorimeter (Perkin Elmer/DSC7) within 50 °C - 200 °C range. The heating rate was 20 °C. Finally measure weight loss of the specimen before and after bury in soil. The weight loss percent was determined as the following method: Prior to the experiment, the specimen was accurately weighed. After the specimens were buried in soil for 3 months, they were also accurately weighed. The ratio of the weight reduction of the film after degradation to the original weight of the specimen prior to degradation was defined as weight loss percent. The formula of weight loss percent was as follows:

weightloss (%) =
$$\frac{(w_0 - w_1) \times 100}{w_0}$$
 (1)

where w_1 refers to the weight of the specimen after degradation; w_0 refers to the weight of the specimen before degradation.

⊗TJIA

3. Results and Discussion

3.1 Mechanical Properties of HDPE/Corn Starch Composite

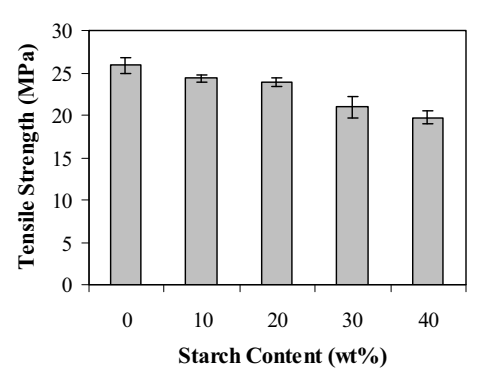


Fig. 1 Tensile Strength of HDPE filled corn starch 0-40 wt%

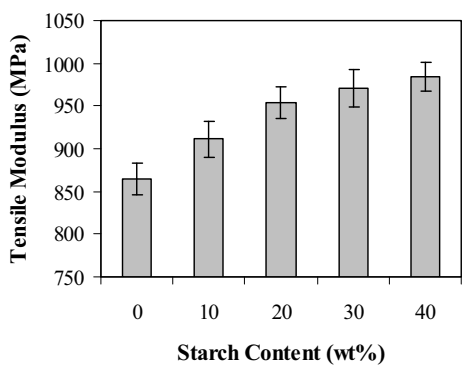


Fig. 2 Tensile Modulus of HDPE filled corn starch 0-40 wt%

The tensile strength of all HDPE/corn starch composites (Fig. 1) decreased with increasing starch content. This indicated that starch behaved as non-reinforcing filler and less interaction between the compounds resulted in decreasing the tensile strength. Tensile Modulus values in Fig. 2 increased when increasing starch content. In general, the modulus is closely related to the rigid domains of the material [4]. Starch added up the rigidity which increased stiffness of the composites.

3.2 Weight Loss Percent of HDPE/Corn Starch Composite

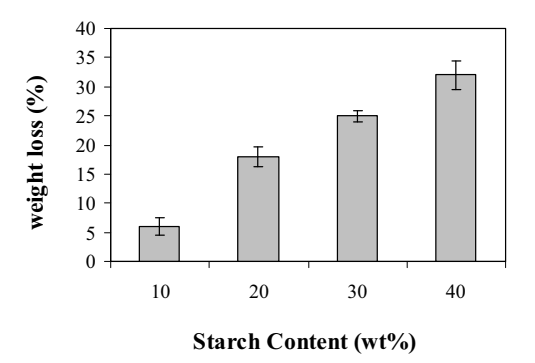


Fig. 3 Weight Loss of HDPE filled corn starch 10-40 wt%

The higher starch content showed higher in weight loss in Fig. 3. The weight loss of the composite was due to the biodegradability or light-oxidation degradability under the given degradable environments. The reduction in weight of the composite revealed that higher in starch content had better degradability [3].

4. Conclusions and Recommendations for Thailand

Corn starch, as filler, increased tensile modulus of HDPE where as decreased in tensile strength of the composites. The starch also promoted properties in stiffness and increased degradability of the composites. The research showed not only the potential of using corn starch, natural biomaterials, as filler in HDPE but also the potential of the material for sustainable development in both the aspects of degradable which contributes for waste management and energy conservation in Thailand.

- [1] G. Scott and D. Gilead, Degradable Polymers, Chapman&Hall, London, 1995.
- [2] S. I. Yoo, T. Y. Lee, J. S. Yoon, I. M. Lee, M. N. Kim, H. S. Lee, J. Appl. Polm. Sci. 83 (2001) 767-776.
- [3] W. Shujun, Y. Jiugao, Y. Jinglin, J. Polym. Environ. 14 (2006) 65-70.
- [4] J. L. Jane, A. W. N. Schwabacher, S. N. Ramrattan, J. A. Moore J. Appl. Polm. Sci. 52 (1992) 617–628.

NS-E05

Development of Single Chamber Solid Oxide Fuel Cell using BaLaIn₂O_{5.5} (BLI) Solid Electrolyte: Introduction of Sublimation Materials as Pore Former in Electrode Preparation

Yuwa Chompoobutrgool, Hiroaki Suzuki, Mitsuhiro Hibino, Takeshi Yao

Graduate School of Energy Science, Kyoto University, Japan Tel.: +81-7-5753-4735, E-mail address: yuwa@donut.mbox.media.kyoto-u.ac.jp

BaLaIn₂O_{5.5} (BLI) exhibits higher oxide ion conductivity than yttria-stabilized zirconia; however, it is difficult to use as a solid electrolyte in conventional dual chamber solid oxide fuel cells (SOFCs) because In ion suffers reduction under reducing atmosphere in the vicinity of a fuel electrode. Since Single Chamber Solid Oxide Fuel Cells (SC-SOFCs) operate in a mixture of fuel and oxygen which has more benign reducing atmosphere than the dual chamber, BLI is applicable to the SC-SOCFs application. Pore-former materials have been employed to the electrode preparation. Its function is to create diffusion path for gas in electrodes, hence easing the gas flow and increasing the gas velocity. Here, a novel study proposed by our research group is the introduction of sublimation materials as pore formers. Two types of sublimation materials have been studied; phthalic acid and fumaric acid. The results have been compared to the common pore former; carbon. According to the results, it was found that the performance of cells with sublimation materials as pore formers were better than the cells with carbon materials. This suggests that the cell performance of SC-SOFCs can be improved by enhancing the gas diffusion in electrodes by means of sublimation materials.

1. Introduction

Due to its higher oxide ionic conductivity than yttria-stabilized zirconia (YSZ) [1], BaLaIn₂O_{5.5} (BLI) [2-4], which has a defective perovskite-related structure, is chosen to serve as solid electrolyte in solid oxide fuel cell. In a conventional dual chamber system, BLI cannot be utilized because indium ion is reduced at oxygen partial pressure as low as that of fuel electrode. Therefore, we have developed a single chamber system with mild reducing atmosphere such as a mixture of methane and air, which allowed the utilization of BLI.

It has been observed that one of the major causes to low performance of solid oxide fuel cell in the single chamber system is its impedance, especially, from electrochemical reaction occurring at the electrode. The aim of this study is, thus, to improve cell performance by enhancing the electrochemical reactions by means of utilization of sublimation materials as pore formers in electrode material preparation.

2. Experimental

BaLaIn₂O_{5.5} (BLI) powder was prepared by a solid-state reaction of barium carbonate, indium oxide, and lanthanum oxide. The obtained powder was shaped into a disk, pressed under 392 MPa and sintered at 1400°C for 10 h. An 11-to-15-mm in diameter pellet electrolyte with a thickness of 0.5 mm was then obtained. (La_{0.75}Sr_{0.25})_{0.9}Cr_{0.5}Mn_{0.5}O_{0.3} (LSCM) mixed with 5wt% NiO and Sm_{0.5}Sr_{0.5}CoO₃ (SSC) were used as anode and

cathode, respectively. In this study, phthalic acid, fumaric acid, and benzoic acid were selected as pore-former materials due to their sublimation property. Each material was added both LSCM and SSC at various compositions. The compositions of the poreformer materials were tested at 5, 10, 15, 20 and 30 wt%. The mixture was then painted on each face of BLI electrolyte pellet. The painted pellets were thermally treated for sublimation of the pore former and then pores or voids the created within electrodes. were Subsequently, the pellets were heated at 1000-1200°C. The power generation tests at 800°C were carried out to examine the cell performance. A mixture of methane and air was supplied with 1:1 volume ratio.

3. Results and Discussion

The cell performance was investigated by generation test through measurement of cell's open-circuited voltage (OCV) and maximum power density (MPD). The power generation results obtained at optimum composition of each sublimation pore-former material, 10 wt% for phthalic acid, 30 wt% for fumaric acid, and 10 wt% for benzoic acid, are shown in Fig. 1. For comparison, the results of carbon materials, acetylene black (AB), ketjen black (KB), and artificial graphite, as pore formers are shown in Fig. 2. Such carbon materials were often employed as pore formers. The composition ratios of these carbons were optimized. In



addition, the results from sublimation poreformer materials and carbon pore-former materials are compared and summarized in Table 1. The sublimation pore-former materials achieved higher performance than the carbons in terms of MPD.

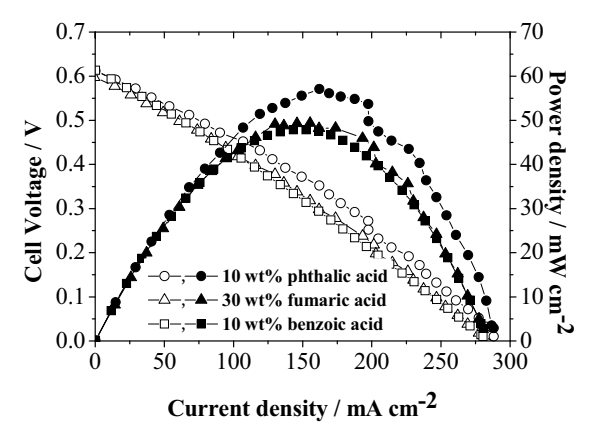


Fig.1 Power generation results of single chamber cell using BLI fabricated with sublimation poreformer materials.

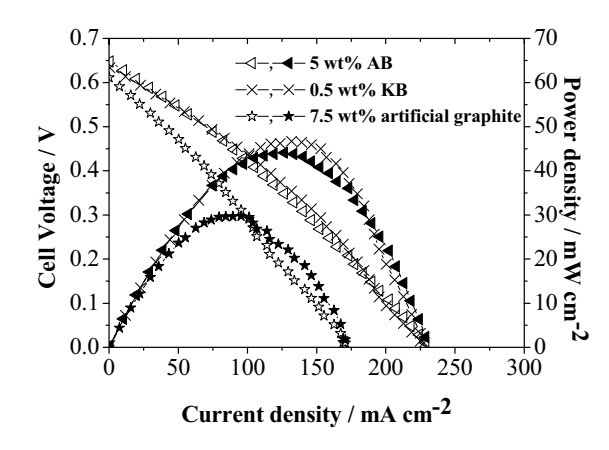


Fig.2 Power generation results of single chamber cell using BLI fabricated with carbon pore-former materials.

Table 1 Performance of the single chamber cell using BLI

pore-former materials	OCV/mV	MPD/ mWcm ⁻²
10 wt% phthalic	612	57.1
30 wt% fumaric	598	49.4
10 wt% benzoic	614	47.8
5 wt% AB	648	44.1
0.5 wt% KB	633	46.6
7.5 wt% artificial graphite	611	29.7

In conclusion, BLI cell fabricated with 10 wt% phthalic acid yielded the highest performance in all pore-former materials in this study. It is proved that sublimation pore formers are promising materials that can be applied to electrode for BLI electrolyte utilization to enhance the BLI cell performance.

4. Recommendations for Thailand

At present, the number of researches about fuel concerning cells has increasing. This research can be contributed as a reference source to the research and development of solid oxide fuel cell as an energy alternative source in Thailand. However, the technology level of this research has not yet reached the practical application. Further research and development are required in order to apply this project into industrial process.

- [1] S.Asahara, D.Michiba, M.Hibino, T.Yao, Electrochem. Solid-State Lett. 8 (2005) A449-A451.
- [2] T.Yao, Y.Uchimoto et al., Solid State Ionics 132 (2000) 189-198.
- [3] Y. Uchimoto, T. Yao, H. Takagi et al., Electochemistry 68 (2000) 531
- [4] K. Kakinuma, H.Yamamura et al., Solid State Ionics 140 (2001) 301-306.

107 NS-E06

Development of an Electric Wheelchair Using PEM Fuel Cell

Chan Anyapo, Kazuo Saito, Toshihiko Noguchi

Department of Electrical Engineering, Nagaoka University of Technology, Japan Tel./Fax: +81-2-5847-9541, E-mail address: chan@stn.nagaokaut.ac.jp

This paper introduces a prototype of electric wheelchair using fuel cell, and refers to energy management of the wheelchair system. It consists of a PEM fuel cell stack as a power supply, an EDLC bank as an energy buffer, and two electric DC motors which are driven by a newly designed four-quadrant DC chopper, etc. The study aims to save energy by managing energy flow of the wheelchair system, and to accomplish efficient drive of the DC motors. In order to achieve high efficiency of the system, the EDLC bank works properly depending on drive conditions of the system. Essential characteristics of the fuel cell and performance of the wheelchair have been investigated by many kinds of experiments. According to the experimental results, fundamental driving ability of the wheelchair has already been proved. Also, it is cleared that the fuel cell has enough capability and is appropriate to the electric wheelchair system. Consequently, some ideas and technologies which are applied to the system will be able to contribute to design for other kinds of electric vehicles and transportation in the near future.

1. Introduction

Recently, many discussions on fuel cells have come up. For problems of the global environment and exhaustion of the fossil fuels, the studies on application of fuel cells are notable issues. On the other hand, several types of electric vehicles have been developed by a lot of car manufacturers and institutes. Then, investigation into combination of fuel cells and electric vehicles, which include wheelchair, is important subject [1]-[2].

In particular, there is a big problem of air pollution in many metropolises, even in Thailand. From the viewpoint of it, this study is supposed to be worthwhile.

This paper shows a prototype of electric wheelchair using a PEM (Proton Exchange Membrane) fuel cell stack. The wheelchair system also has an EDLC (Electric Double Layer Capacitor) bank as an energy buffer, and a four-quadrant DC chopper which drives two electric DC motors. The motors are mounted on both of the wheels.

2. Structure of Wheelchair System

Figure 1 shows a picture of the electric wheelchair. It originally has the following specifications; diameter of both the wheels is 22 inches, maximum speed is 6km/h, output power of both DC motors is 90W, power supply is a Li-ion battery (25.9V/6Ah).

The electric wheelchair has been improved on several points. Especially, the power supply has been replaced by the PEM fuel cell stack with a set of hydrogen storage alloys, which are shown in Fig. 2. The two DC motors are driven by the newly designed DC chopper, and the EDLC bank is employed to manage energy flow of the system.



Fig. 1 Electric wheelchair

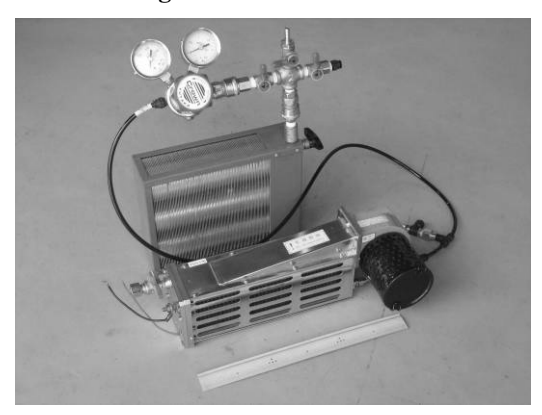


Fig. 2 PEM Fuel cell & Hydrogen storage alloys



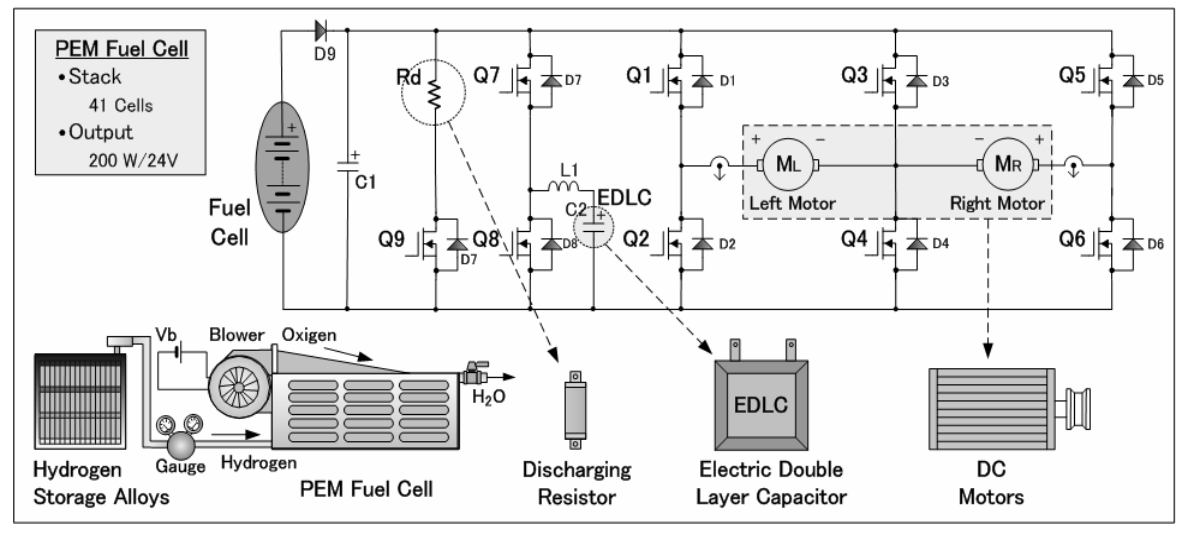


Fig. 3 Energy management and motor drive

Major specifications of the main devices of the wheelchair system are as follows.

(1) PEM fuel cell (output): 200W-24V, (2) Hydrogen storage alloys (capacity of H₂): 500 liters, (3) DC motor (output power): 90W, (4) EDLC: 1350F-2.7V.

Figure 3 shows the architecture of energy management of the system and the drive circuit for the two DC motors. Regarding to the PEM fuel cell stack, hydrogen is supplied from the hydrogen storage alloys, and oxygen contained in the air is inhaled using a blower.

The EDLC bank is charged or discharged depending on drive conditions of the system. For example, it supplies energy to the motors when the output power of the fuel cell lacks for motor drive. When regeneration occurs, energy flows from the motors to the EDLC bank.

3. Experiments and Discussion

As described above, the prototype of electric wheelchair system using the PEM fuel cell stack have already been completed. To examine the performances of the fuel cell and the motor drive circuit, many kinds of experiments were carried out.

According to the experimental results, some important knowledge has been obtained. Firstly, the fuel cell has sufficient output power (about 200W) because the maximum power of the two motors is 180W. Secondly, the motor drive circuit operates adequately for essential drive modes, i. e., forward or backward drive, right or left turn, pivot movement, and combination of these modes [3]-[4].

The next stage of the study is to inspect energy management and to achieve high efficiency of the electric wheelchair system. Therefore, it is important to analyze the energy flow for any conditions of the system by computer simulations and experiments.

4. Conclusions and Recommendations for Thailand

The problem of air pollution has been discussed amazingly these days in Thailand, especially in Bangkok. This study will surely contribute to the problem because fuel cells do not exhaust any harmful gases. Naturally, some ideas and technologies applied on the electric wheelchair system will be able to utilize for design of the future vehicles. In addition, the means of energy management and save energy would contribute to the future transportation and lifestyle, not only in Japan but also in Thailand.

- [1] J. Larminie, A. Dicks, Fuel Cell Systems Explained (2nd Ed.), John Wiley & Sons Ltd., UK, 2003.
- [2] S. Iizuka, Possibility of Fuel Cell Cars and Electric Vehicles, Grand Prix Publisher Co., Ltd., Japan, 2006.
- [3] K.Saito, C. Anyapo, T. Noguchi, The Inter-national Workshop on Mechatronics, 2006, pp. 44-46.
- [4] K.Saito, P. Kamjitjam, T. Noguchi, The 2nd Technology and Innovation for Sustainable Development Conf., 2008, pp.347-351.

High Efficient Dye-Sensitized Solar Cells Using TiO₂ Nanoparticles/ Nanofibers as Photoelectrode

Surawut Chuangchote, Takashi Sagawa, Susumu Yoshikawa

Institute of Advanced Energy, Kyoto University, Kyoto, Japan Tel: 81-80-3814-9493, Fax: 81-7-7438-3508, E-mail address: surawut@iae.kyoto-u.ac.jp

Specific applications of 1-D materials are being developed in order to improve the electron transport and enhance the light confinement leading to higher conversion efficiencies of dye-sensitized solar cells (DSCs). Electrospun TiO₂ nanofibers are one of the promising 1-D materials. Recently, we have successfully prepared electrospun TiO₂ nanofibers which were very long over several cm. Calcination of the composite fibers at 450°C resulted in predominant content of anatase titania nanofibers. The effects of temperature and time of calcination on the crystalline phase and size of the as-spun TiO₂ fibers were also investigated. When the TiO₂ nanofibers were fabricated on top of the particle-electrode, we observed remarkable enhancement of photovoltaic performance attained power conversion efficiency of 8.14% (0.25 cm²) compared with conventional TiO₂ nanoparticles (7.47%). The maximal power conversion efficiency was attained to be 10.3% (N719 dye system) by using 0.0515 cm² mask.

1. Introduction

Dye-sensitized solar cells (DSCs) by using TiO₂ nanoparticles have been studied for over a decade expected as low cost alternatives to conventional silicon devices. One limiting factor in the performance of DSCs with nanoparticles is electron transport. Grain boundaries and small cross-sectional area at the interfaces of the nanoparticles lead to the enhancement of the scattering of free electrons, and such scattered electrons reduce the electron mobility and promote the electron recombination.

Specific applications of 1-D materials are being developed in our laboratory in order to improve the electron transport and enhance the light confinement leading to higher power conversion efficiencies. Electrospun TiO₂ nanofibers are one of the promising 1-D materials [1,2]. In this context, a specific application of electrospun TiO₂ nanofibers was reported for electrodes of DSCs as a light harvesting layer.

2. Experimental

The TiO₂ nanoparticles-paste was first coated on fluorine-doped SnO₂ conducting glass (FTO) by doctor-blade technique. TiO₂ nanofibers were electrospun directly onto the nanoparticles from a solution in methanol of poly(vinyl pyrrolidone) (PVP), titanium(IV) butoxide (TiBu), and acetylacetone (ACA), which is different from other previously reported procedures [3]. ACA was used to slowdown the hydrolysis and the condensation reactions for preventing of breakage of fibers during those reactions. The spinning solution was loaded into a syringe and connected to a

high voltage power supply. An electrical potential of 15 kV was applied between a nozzle and the ground over the collection distance of 15 cm. The obtained fibers were left exposed to moisture for approximately 5 h to allow complete hydrolysis.

In order to prepare the DSC, obtained nanoparticles/nanofibers electrode consequently subjected to calcination at 450°C for 3 h. The microstructure and crystalline structure of the prepared nanofibers and electrode obtained were observed measured by using a scanning electron microscopy (SEM) and X-ray diffraction (XRD), respectively. Calcined TiO₂ electrodes were sensitized by immersing in a 0.3 mM of ruthenium (II) dye (known as N719) in a mixture of t-butanol and acetonitrile. The electrolyte which we utilized in this work was composed of dimethylpropyl imidazolium iodide, lithium iodide (LiI), iodide (I2), and 4tert-butylpyridine in acetonitrile. Photocurrentvoltage (I-V) curve was measured under simulated solar light (AM 1.5, 100 mW/cm²).

3. Results and Discussion

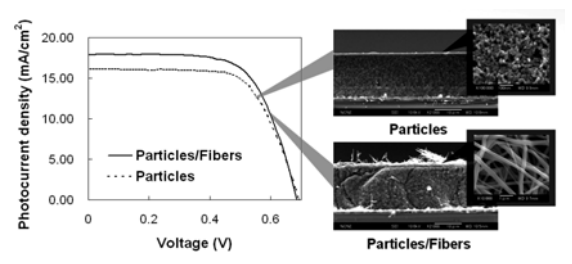
The obtained TiO₂ nanofibers showed 1-D structure with diameters ca. 250 nm, which were very long over several cm. Calcination of the composite fibers at 450°C for 3 hr resulted in predominant content of anatase titania nanofibers with high crystallinity.

Figure 1 (right) shows SEM images of both types of obtained photoelectrodes (nanoparticle electrodes with and without nanofibers). Size of nanoparticles was ca. 15 nm which is beneficial for high surface area and high dye adsorption. The nanofibers-layer

109

NS-E07

with thickness up to ca. 1 µm could be fabricated. From UV-vis absorption spectra of both of electrodes, nanoparticles/nanofibers electrode showed higher light absorption in visible region. It can be described that the optical path length of incident light with longer wavelength could be prolonged by light scattering at the layer of TiO₂ nanofibers. In other words, light harvesting efficiency was improved by a combination of nanofibers.



Photocurrent density versus characteristics (left) and SEM images (right) of DSCs with and without TiO₂ nanofibers-introduced on nanoparticles-electrode [3].

Figure 1 (left) shows some examples of photocurrent-voltage characteristics of the devices with nanoparticles/nanofibers compared with conventional TiO₂ nanoparticle DSCs. When the TiO₂ nanofiber electrode was used, enhanced photovoltaic performance was attained with power conversion efficiency of 8.14% compared with conventional TiO₂ nanoparticles (7.47%). The maximal power conversion efficiency was attained to be 10.34% (N719 dye system with 0.0515 cm² mask) by some optimizations. The successful about 8% increase in efficiency combination of thin nanofibers-layer indicates the increasing in light harvest efficiency as described above. Addition of large sized nanoparticles on top of photoelectrode acting as light-scattering layers to increase the light harvest efficiency was also reported previously. The nanofibers showed more advantageous than that topology as: (1) The well aligned nanofibrils in 1-D nanofibers may contribute to better charge transportation (2) efficient penetration of the electrolyte into the TiO₂ particles-electrode can occur easily through many pores in the web, and (3) nanofibers can be directly fabricated on top of particles-electrode in one step with uniform large-area and good adhesion with particles. In addition, the details of microstructures, physical properties, and photovoltaic properties of the other devices with TiO2 nanofibers were also investigated and will be reported.

4. Conclusions and Recommendations for **Thailand**

Anatase TiO₂ nanofibers were directly fabricated on thick nanoparticles electrode through electrospinning and sol-gel techniques, and applied for dye sensitized solar cells. IPCE of 85% at the wavelength of 540 nm and conversion efficiencies of 8.14 and 10.3% with area of 0.25 and 0.0515 cm², respectively, were obtained. These results suggest light harvesting 1-D nanofibers-combined nanoparticles might be very promising materials for the electrode of DSC. This research is beneficial for Thailand because Thailand is a tropical country which has sunshine in several months a year. Thailand's climate makes it an ideal location for the development of renewable energy technologies, especially solar cells. fabrication of DSC photoelectrodes combination of TiO₂ particles and nanofibers by above simple method is seems to be able to carryout in Thailand. However, it still needs to undergo further research and development to enhance its efficiency versus cost and the potential to use DSCs in a commercial level.

- [1] S. Chuangchote, T. Sagawa, S. Yoshikawa, Jpn. J. Appl. Phys. 47 (2008) 787.
- [2] S. Chuangchote, T. Sagawa, S. Yoshikawa, Macromol. Symp. 264 (2008) 80.
- [3] S. Chuangchote, T. Sagawa, S. Yoshikawa, Appl. Phys. Lett. 93 (2008) 033310.

111 NS-F01

Microstructure and Fatigue Crack Growth Behavior of Friction Stir Welded 6063 T-5 Aluminium Alloys

Kiraphat Paenduang^{1,2}, Masakazu Okazaki², Supachai Surapunt¹, Tran Hung Tra²

Department of Industrial Engineering, Thammasat University, Thailand

Department of Material Science & Engineering, Nagaoka University of Technology, Japan Tel.: +66-8-6593-2552, E-mail address: kiraphat engr@msn.com

The influence of friction stir welding on the microstructure and fatigue crack growth behaviour of 6063 T-5 aluminum alloys were investigated. For this propose, fatigue crack growth (FCG) curves were determined for crack growing in different locations of notch, including base materials (BM), middle of welded zone and heat affect zone (HAZ). The crack initiation and crack propagation of the FSW specimens were presented slower than base material specimens. Results are completed with microhardness measurements and scanning electron microscopy (SEM) observations. The material affected by the welding process presents a fine stirred grain structure and the material near the heat affected zone (HAZ) presents regular grains.

1. Introduction

Friction stir welding (FSW), is a solid-state joining process developed and patented by Wayne Thomas at TWI in 1991 [1-4], This joining technique has enabled us to butt-weld aluminum alloys, which are often difficult to fusion weld, without voids, cracking, or distortion. Furthermore it is energy efficient, environment friendly and versatile [1].

The process was developed initially for aluminum alloys,[1-4] but since then FSW was found suitable for joining a large number of materials. In aeronautics, riveting is the preferred manufacturing process for aircraft fuselage structures [2]

In this study is contribution about the influence of the FSW technique on the fatigue crack growth and microstructure of FS welded and base materials specimens of AA 6063 T-5.

2. Experimental procedures

The base material used in this present study was the Al alloy 6063 T-5. The Chemical composition shown in Table 1 The 5 mm-thick plates were friction stir welded.

Table 1 Chemical composition of the Al 6065 T-5

Al	Cu	Fe	Mg	Mn	Si	Ti	Zn
Bal	0.01	0.18	0.48	0.04	0.44	0.01	0.01

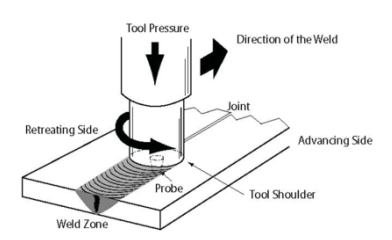


Fig. 1 Shows metal plates butted together with probe and tool shoulder of FSW process

The middle tension, M(T), specimens were used in FCG test. The geometry are in accordance with ASTM specification E 647-95a [5].

Stress intensity factor range, ΔK of M(T) specimen were calculated as follow:

$$\Delta K = \frac{\Delta P}{B} \sqrt{\frac{\pi \cos}{2W} \sec \frac{\pi \cos}{2}}$$
 (1)

Where $\infty = 2a/W$; 2a/W < 0.95

B: Thickness, W: Width

Scanning electron microscopy (SEM) were used for observation of grain structure and hardness were measured on transverse cross-section of weld.

3. Results and Discussion

3.1 Microstructure analysis

The friction stir weld is characterized by three different zones as shown in Fig.2 as follow: stir zone (SZ) included; thermo mechanically affect zone (TMAZ) and welded nugget, heat affect zone (HAZ) which surrounding the SZ, and unaffected base metal (BM). In Fig. 2 (1),(z2),(3) the effected zone by FSW presented a fine grain size .On the other hand HAZ (3) and base material (5),(6) presented regular grains size.



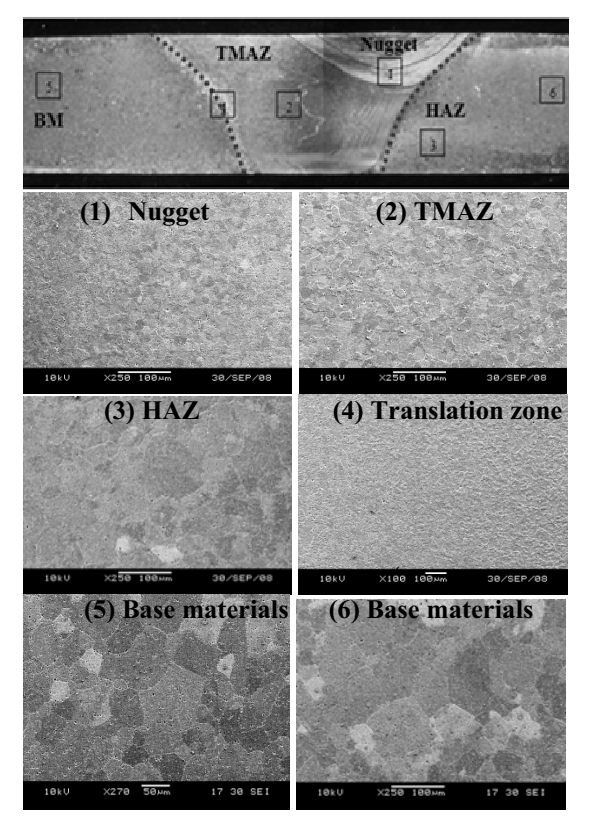


Fig. 2 Macro and microstructure

To determine the grain size diameter ,the grain size on base material have an average diameter of 60-70 μm and weld zone (TMAZ and nugget) present diameter of 25-30 μm .

3.2 Microhardness measurements

The Vickers micro hardness test obtained along 3 lines (Top, mid and bottom) on cross-section are presented in Fig.3. Hardness minimum appeared in heat affected zone and hardness decrease in weld zone was found to be significantly slightly lower than the base material. This hardness variation was due to the different micro- structures of base material (BM) and welded zone.

3.3 Fatigue crack growth curves

Fig.4 summarizes the results obtained for different location of notch under R=0.1

The crack initiation and crack propagation rate of the middle welded are lower than crack initiation and crack propagation rate of HAZ and base material. This behavior relate to different grain size at different location of notch.

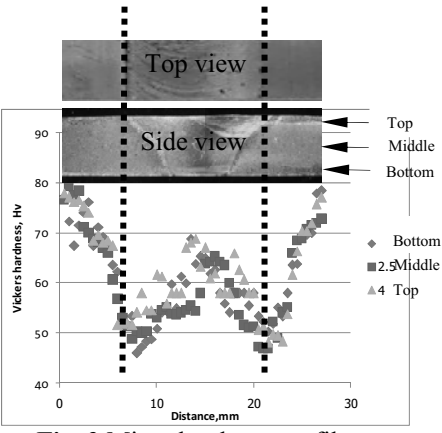


Fig. 3 Micro hardness profile

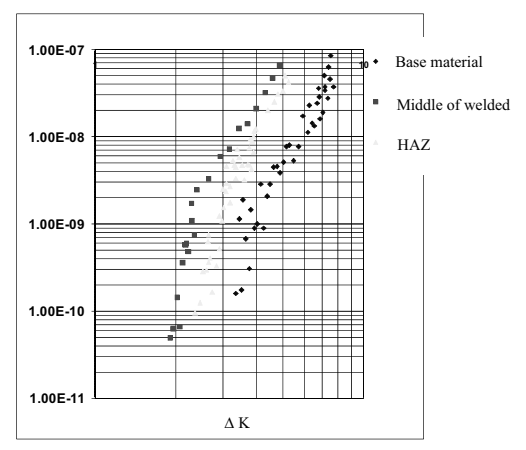


Fig. 4 Fatigue crack growth curves

4. Conclusions and Recommendations for Thailand

The fatigue crack growth of the FS welded of 6063 T-5 Al alloy present the crack initiation and crack propagation of the FSW specimens are slower than base material specimens and microstructure presents a fine stirred grain structure of welded zone and the base material near the heat affected zone (HAZ) presents regular grains due to the hardness test was found to be significantly slightly lower than the base material. The papers can contribution to Thailand.

- [1] R.S. Mishra, Z.Y. Ma, Mater. Sci Eng. R 50 (2005) 1-78
- [2] P.M.G.P. Moreira, F.M.F. de Oliveira, Mater. Processing Tech. (2008).
- [3] S. A. Khodir, T. Shibayanagi, Mater. Sci. Eng.B. 148 (2008) 82-87.
- [4] S. Di, X. Yang, G. Luan, B. Jian, Mater. Sci. Eng.A. 1435-436 (2006) 389-395.
- [5] ASTM standard E-647-95a, Annual Book of ASTM standard, Vol.3 (1) (1998) 562-575

113 NS-F02

Robust Pattern Detection Using Quantum-Inspired Evolutionary Algorithms

Vorapong Suppakitpaisarn

The University of Tokyo, Tokyo, Japan
Tel.:+81-90-6483-7724, E-mail address: mr t dtone@is.s.u-tokyo.ac.jp

In this research, we apply Quantum-Inspired Evolutionary Algorithms to the Pattern Detection problem. Quantum-Inspired Evolutionary Algorithms are the learning algorithms based on the basis of Quantum Computation, the new paradigm of computing. Even though Quantum-Inspired Evolutionary Algorithms are processed on classical computer model, it uses many elegant concepts from Quantum Computation such as the analog representation on the probability of each data and chromosome. That makes it suitable for Artificial Intelligence system and has been applied widely. In this research, we will apply Quantum-Inspired Evolutionary Algorithms to Pattern Detection problem focused on Robot Vision System. The result shows that we can produce fast and correct Pattern Detection System using this method.

1. Introduction

Quantum Computation [1] is the new paradigm of computing that is expected to replace personal computer in the next few decades [2]. Using Quantum Mechanics as a base to build a new type of computer, Quantum Computer is not only compact and fast, but also changing the way to solve computational problems make computer able to solve many problems, which are mostly hard to solve in classical computer. Factoring, Discrete Logarithm, and Abelian Hidden Subgroup Problems [3] are examples of this type of problems. Moreover, because of the fact that Quantum Computer processes the data parallel, Quantum Grover's Search Algorithm [4] is significantly faster than any classical search algorithm. Since most of Artificial Intelligence system is based on searching, this makes Quantum Computation suitable for AI system. Quantum Neural Network and Quantum Genetic Algorithms is said to be faster, and more natural.

Although, D-Wave have announced that they have public the first Quantum Computer and use their Quantum Computer to solve many problems such as Image Matching [5], Factoring, and Quantum Cryptography, many believe that we are still far from the commercial Quantum Computer. Despite that fact, we can use many interesting concepts from Quantum Computation to make the algorithms in classical computer better. Quantum-Inspired Evolutionary Algorithms (QEAs) [6] are the algorithms interested in this research. Using the concept about the linear superposition of the qubits and the rotation of qubits in Grover's Search Algorithm, QEAs have been shown faster, and consume much less memory. Because of this fact, it has been

applied widely to Combinatorial Optimization Problem [7], Image Segmentation [8], Face Detection [9], or User Detection in Wireless Sensor Network [10]. In this paper, we will focus on another Image Processing Problem that is Pattern Detection in Robot Vision. This problem has already been explored in the paper about Quantum Robotics by Benioff [11] and Dong et al. [12], but they research on the algorithm on Quantum Computer, contrast to Quantum-Inspired Algorithm in classical computer in our research.

2. Methodology

The QEA consists of 2 parts, training and evaluation. Training is the process that we use a large number of examples to train the computer to recognize our patterns, and evaluation is the process which we make the computer decides whether the input image can match our patterns. Our Algorithm is based on Principal Component Analysis (PCA) method.

For Training process, we use 100 examples. In each example, we do some image preprocessing [13] such as remove noise, resize into 50x50 pixels image, and convert into Monotone Picture. Then, we find the eigenvalues and eigenvectors. The eigenvectors that correspond to a large eigenvalues seem to present the important information in the image. We call these eigenvectors as "Principal". Assuming that the pattern can be rotated into any angle, we rotate every image to make the first Principal of them point to the same way.

Next, we find the pattern of the training examples by finding the covariance matrix of each point in 50x50 pixels image. We will use this covariance matrix together with QEA to recognize the patterns.

To detect the pattern from the image, we first find candidate of the pattern by using Hough Transformation or other simple object recognition techniques. As a result of those techniques, we select 100 candidates that have the most possibility to match our patterns. Then, we apply the preprocessing algorithms that have been applied on the training examples and extract the covariance matrix. comparison between the covariance matrix and training example's covariance matrix is used to evaluate whether the input can be matched to the pattern using QEA.

QEA is almost the same as Genetic Algorithm. The algorithm consists of the generation of the initial population, the mutation, the crossing over similar to Genetic Algorithm. But each bit in chromosome is replaced by qubits that is the bits that we are unable to decide what it is -0 or 1, until we measure it, but the possibility of 0 or 1 will be computable. Since we use qubits instead of the classical bits, in the end of the genetic loop, we perform the measurement and use the result of the measurement to evaluate the chromosome.

3. Conclusions and Recommendations for Thailand

Theoretical Computer Science is very broad, but the number of researchers in Thailand on this field is so few. Thus, Thai researchers can hardly pursuee the advance on this field. Besides, Quantum Computation is relatively new and interesting topic that we have not been explored. In the near future, as Quantum Computer gain more importance, using this technology as a pioneer might be very beneficial for Thailand.

- [1] M.A. Nielsen, I.L. Chuang, Quantum Computation and Information, 1st ed., Cambridge, 2000.
- [2] A. Raghuvanshi, Y. Fan, M. Woyke, M. Perkowski, Proc. International Symp. on Multiple-Valued Logic, 37(2007).
- [3] P.W. Shor, Proc. FOCS, 35(1994) 124-134.
- [4] L.K. Grover, Proc. STOC, 28(1996) 212-219.
- [5] H. Neven, G. Rose, W.G. Macready, arXiv:0804.4457v1.
- [6] A. Narayanan, M. Moore, Proc. IEEE International Conf. on Evolutionary Computation, 1996, 61-66.

- [7] K.H. Han, J.H. Kim, IEEE Trans. on Evolutionary Computation, 6(2002) 580-593.
- [8] H. Talbi, M. Batouche, and A. Draa, Proc. WASET, 25(2007) 205-210.
- [9] J.S. Jang, K.H. Han, J.H. Kim, Proc. Congress on Evolutionary Computation, 2 (2004) 2100-2106.
- [10] S. Yang, M. Wang, L. Jiao, Congress on Evolutionary Computation, 1(2004) 820-826
- [11] P. Benioff, Physical Review A 58(1998) 893-904.
- [12] D. Dong et al., Robotica 24(2006) 513-521
- [13] R.C. Gonzalez, K.E. Woods, Digital Image Processing, 2nd ed., Prentice Hall, 2002

Computer Vision for Thailand's Future

Chutisant Kerdvibulvech

Department of Information and Computer Science, Keio University, Yokohama, Kanagawa, Japan E-mail address: chutisant@ozawa.ics.keio.ac.jp

Computer vision is the technology of machines that see and analyze scientifically. Simply speaking, it is the use of computer techniques to theoretically extract and methodically interpret information in visual images. It is needed for automated systems to keep pace with real-world activities. Recently, computer vision is a rapidly developing and extremely interdisciplinary field of computer science. An increasing number of leading researchers around the world are turning their attention to the development of vision applications. In this paper, we survey the existing vision based-applications in recent years. Topics covered in the paper include: introduction to computer vision, computer vision in science fiction movies and computer vision for musical applications (i.e. piano and guitar). Also, we briefly address specific needs for computer vision research in the context of Thailand in the future. We believe that computer vision could be a useful key to emerge the innovative technologies in Thailand in coming future.

1. Introduction to Computer Vision

Vision is an important sense that humans have. Computer vision is the technology to endow machines with similar capabilities to interpret visual input, and to act upon it. Generally speaking, it is the method to allow computer to visually understand something from the images. Figure 1 shows a sample of recognizing emotions expressed by body pose using computer vision technology [1].

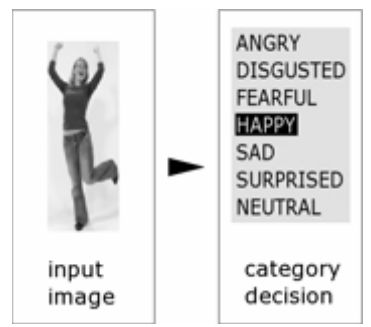


Fig. 1 Sample application of computer vision for recognizing emotions expressed by body pose [1]

Many ideas of computer vision have been appeared in various movies. For example, in the science fiction movie "Minority Report", in which Tom Cruise plays a futuristic police officer shuffling computerized information around simply by moving his hands and fingers (Figure 2), the idea of computer vision technology for hand detection has been appeared. Another example can be found in the science fiction movie "The Matrix Reloaded" (for new viewpoint analysis technology in computer vision). Moreover, in movie "Resident Evil", the concept of human detection in computer vision has been appeared. Imagine how interesting is if all of these ideas in the science fiction movies can

become true in real life with an emerging technology called computer vision.



Fig. 2 Tom Cruise in the science fiction movie "Minority Report" which inspires computer vision technologies in the future [www.imdb.com/title/tt0181689/]

2. Computer Vision for Musicians

Computer Vision can be applied to many fields. One of them is about vision-based research for musicians. For instance, Gorodnichy and Yogeswaran [2] present a system for monitoring and analyzing the movements executed by piano players, as shown in Figure 3.



Fig. 3 Vision-Based Monitoring of a Pianist's Movements [2]

Other vision-based research for musical applications is about guitars. It is also a popular topic in the field of computer vision for musical applications. For example, Maki-Patola et al. [3] propose an interesting system



called "Virtual Air Guitar" using computer vision (Figure 4). They create a virtual air guitar which does not require a real guitar (e.g. by using only a pair of colored gloves), but produces music similar to a player using a real guitar.

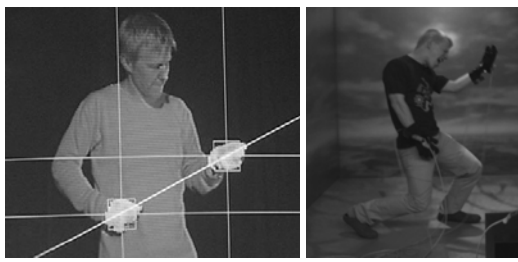


Fig. 4 "Virtual Air Guitar" [3]

Another vision-based application for guitar player is "Interactive Guitar Game" (Figure 5), in our research. By using computer vision technology, it assists guitar learners by automatically identifying whether the fingertip positions are correct and in accord with the fingertip positions required for the piece of music that is being played.



Fig. 5 "Interactive Guitar Game"

The aforementioned guitar application recognizes the guitar chord being played by a guitar learner based on the 3D position of fingering in the virtual guitar coordinate spaces. Then, the system gives real-time feedback to guitar learners telling them if they are using the correct chords required by the musical piece. This application would be invaluable as a teaching aid for guitar learners.

3. Conclusions and Recommendations for Thailand

Recent economic growth in developing regions, together with the widespread use of technology, suggests that there is a potential for technologies to have an impact on development. For this reason, researches about computer vision in developing regions are experiencing fast growth in recent years. Therefore, we believe that the idea of developing and emerging a new computer vision technology is essential for Thailand to keep our place in this world.

In the context of Thailand, computer vision could be beneficial to further apply to solve various existing problems in Thailand. For example, computer vision could be a useful tool to solve the problem of traffic jam in Bangkok by calculating the car used during every particular time. The only limitation of conducting this kind of researches in Thailand is lacking of supporting budgets. If there are enough budget supporters from either private companies or the government, we believe that computer vision technologies could be an emerging key to develop Thailand.

References

- [1] K. Schindler, L. van Gool, B. De Gelder. Recognizing Emotions Expressed by Body Pose: a Biologically Inspired Neural Model. Neural Networks, 2008.
- [2] D.O. Gorodnichy, A. Yogeswaran, Detection and Tracking of Pianist Hands and Fingers. CRV 2006.
- [3] T. Maki-Patola, J. Laitinen, A. Kanerva, T. Takala Experiments with Virtual Reality Instruments. NIME 2005.

Chutisant Kerdvibulvech received the B.E. degree (Hons) in computer engineering from Chulalongkorn University, Thailand, and M.E. degree in information and computer science from Keio University, Japan. Currently, he is a Ph.D. candidate in the Department of Information and Computer Science, Keio University. His work has mainly focused on the research area of computer vision, image processing, and pattern recognition.

117 NS-F04

Research on Weed Detection Methods for Precision Spraying in Lawns

Ukrit Watchareeruetai and Noboru Ohnishi

Department of Media Science, Graduate School of Information Science, Nagoya University, Nagoya, Japan

Tel.:+81-5-2789-5150, E-mail address: ukrit@ieee.org

This paper summarizes image processing based methods of lawn weed detections for automatic weed control systems. Three gray-scale based methods are briefly explained and compared. The performances of the methods together with a chemical-based system, which performs precision spraying, are shown. The methods can destroy more than 70% of weeds existing in the captured images, and can successfully reduce herbicide usages of more than 90%. Other topics which improve performance of the system, such as a post-processing technique, color-based method and hybrid system, and non-chemical based weed control systems, are also briefly described.

1. Introduction

There are many methods for controlling weeds but chemical-based method, i.e., to destroy weeds by using herbicide, is often used because it is convenient and less time required. However, the use of herbicide can cause adverse effects on the environment, and also increases the cost of weed control. Nowadays. automatic weed control systems become an alternative approach. Instead of spraying herbicide onto the entire area, the systems capture the field images, detect the area of weeds, and control a nozzle system to spray herbicide onto only the areas of detected weeds. Consequently, herbicide usages can be significantly reduced. This research focuses on weed detection in lawn fields by using image processing techniques.

2. Methodology

Figure 1 shows the flowcharts of three gray-scale based lawn weed detection methods. The first one (Fig. 1(a)) is called Bayes classifier based method (denoted by BC) [1]. It extracts two texture features from the edge image, and distinguishes weed pixels from lawn background by using Bayes classifier. The second method (Fig. 1(b)), called morphological operation (MO) based method, employs image morphological operations such as opening and closing to detect weed areas [1]. These two methods were proposed by the authors. The third one (Fig. 1(c)), proposed by Ahmad et al. [2], is called gray-scale uniformity analysis method (denoted by UA). It was implemented and compared with the BC and MO methods. The three methods were tested on a lawn weed database which consists of four different datasets taken from four different seasons in Japan. The database contains 20 training images and 100 test images. Examples of lawn weed images and

detected results are shown in Fig. 2 and Fig. 3, respectively.

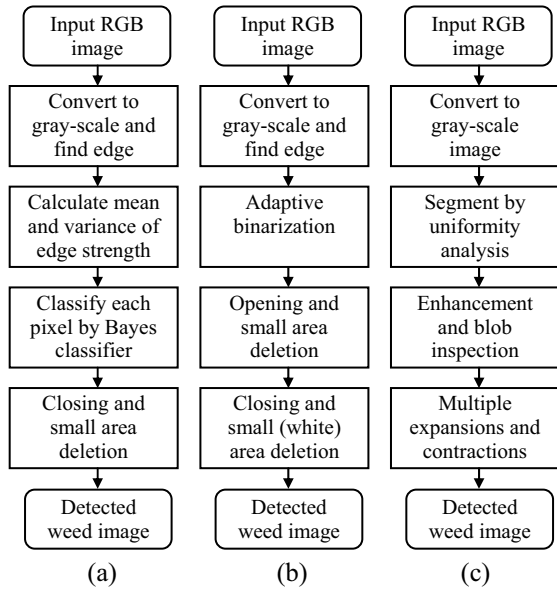


Fig. 1 Weed detection methods: BC methods (a), MO method (b), UA method (c).

3. Results and Discussion

Table 1 shows the performances of all three methods when they are simulated on a chemical-based weed control system. Three evaluation values are shown. Killed weed rate (KWR) is the ratio of destroyed weeds to all weeds existing in the test database. Correct spray rate (CSPR) describes accuracy of spraying. Herbicide reduction rate (HBR) describes how much herbicide can be reduced. compared with spraying herbicide onto the entire area. The result shows that all three methods succeed in herbicide reduction (HBRs of more than 90%) but the proposed methods (BC and MO) outperform the compared method (UA) in weed destruction performance (KWR) and spraying accuracy (CSPR). Because the proposed methods were designed







Fig. 2 Example of lawn weed images.

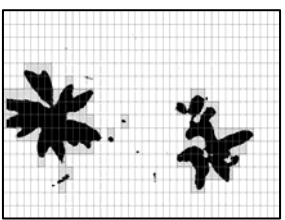




Fig. 3 Detected result of the weed images in Fig. 2 (black areas) and sprayed areas (grey blocks).

Table 1 Performance of chemical-based system

Method	KWR	CSPR	HBR
BC	72.87%	89.44%	93.94%
MO	73.94%	89.66%	92.92%
UA	70.74%	86.74%	93.49%

based on the difference of weed and lawn textures, they can still valid even in the case that weed density gets larger.

The other topics, which can be used to improve the performance of automatic weed control systems, are described as follows:

- In [3], a post-processing technique based on grass-edge model filterbank was proposed to remove misclassified blobs after weed detection was performed.
- In [4], a fast and simple color-based method for detecting weeds in winter (in which the lawn color has completely changed and is different from weed colors) was proposed. It outperforms the gray-scale based methods in detecting weeds of winter dataset. Also the idea of hybrid system that integrates both grayscale based and color-based methods was described.
- In [1], another type of automatic weed control system, i.e., electrical-based system, was considered and tested. The system would destroy weeds by using electrical spark discharges. Consequently, it does not use any chemical substance.

4. Conclusions and Recommendations for Thailand

Various techniques of lawn weed detection have been summarized, and a portion of results was shown. For Thailand, the target of the research (i.e., lawn fields) would be extended to agriculture fields because Thailand is an agriculture country. The use of automatic weed control systems would help farmers protect

their products effectively, increase quality and quantity of the products, and also reduce the amount of herbicide used in weed control, leading to cost reduction and environment preservation. For that case, we hope that it would highly benefit Thailand.

In the case of agriculture fields, color information can effectively be used to distinguish plants (weeds and crops) areas from soil backgrounds before performing weed/crop classification. The proposed lawn weed detections may be applied if the textures of weed and crop surfaces are different. However, when the shapes of weeds and crops are alike, it is difficult to classify them in visible-light domain. A hyperspectral imaging system should be exploited to capture the difference in the internal structures of weeds and crops in the other spectral bands.

- [1] U. Watchareeruetai, Y. Takeuchi, T. Matsumoto, H. Kudo, N. Ohnishi, Mach. Vis. and Appl. 17 (2006) 287-296.
- [2] U. Ahmad, N. Kondo, M. Monta, S. Arima, K. Mohri, Environ. Control. Biol. 36 (1998) 227-237.
- [3] U. Watchareeruetai, Y. Takeuchi, T. Matsumoto, H. Kudo, N. Ohnishi, in: M. Ishikawa et al. (Eds.), Neural Information Processing (Part II). LNCS 4985. Springer-Verlag, 2008, pp. 30-39.
- [4] U. Watchareeruetai, Y. Takeuchi, T. Matsumoto, H. Kudo, N. Ohnishi, Proc. IAPR Conf. on Machine Vision Applications (2007) 524-527.

119

NS-F05

Sustainable Management of Ground Anchor Maintenance using Markov Process

Thamrongsak Suwanishwong, Hiroyasu Ohtsu

Department of Urban Management, Graduate School of Engineering, Kyoto University Tel&Fax: +81-7-5383 3263, E-mail: suwanishwong@toshi.kuciv.kyoto-u.ac.jp

It has been highlighted that ground anchors deteriorate their performance with time as a result of physical and/or chemical effects. Nowadays, road administrators face serious problem associated with decisionmaking when and how to carry out inspection, maintenance and replace of a large number of pre-existing ground anchors under the limited budget allocated to road maintenance. This paper proposes a systematic method for maintenance management of ground anchor based on limited inspection data. The proposed method assumes that deterioration process can be modeled as a Markovian process using categorized inspection results.

1. Introduction

Ground anchors deteriorate performance with time as a result of physical and/or chemical degrading processes which are considered as a stochastic process. To clarify these tasks, Markov process is introduced in this research since Markov process is known as a special class of stochastic process that uniquely determines the future behavior by its present state.

Sharabah et al [1] has utilized the Markov deterioration modeling infrastructure assets owned by local councils in Australia. Mizutani [2] proposed maintenance planning method (MPM) for deteriorating structures using Markov chain associated with both maintenance and loss expenditures. However, very few of such a model was applied to strategic maintenance management of road slope considering ground anchor degradation. The problem is arisen when the state's prediction is situated under constraints of limited access to ground anchor condition data. In this paper, an approximation method is then proposed by utilizing iteration method in association with polynomial equation solving in order to determine the transition probability matrix based on the proposed assumptions using the categorized inspection results.

approximation method An is also combined with a discrete Markov chain model for future performance prediction to determine the optimum maintenance plan that complies with the budget constraints and satisfies the required objectives.

2. Methodology

A Markov chain is a special type of the Markov process whose development can be treated as a series of transition between certain

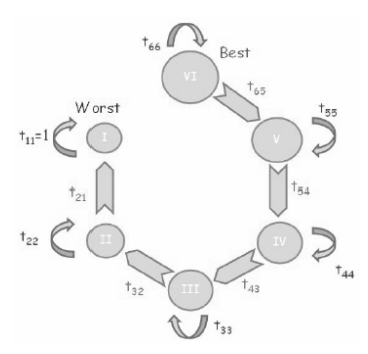


Fig. 1 Six-state Markov chain

states. When time is measured in discrete intervals the model is called the Discrete Time Markov Chain (DTMC). The performance of ground anchors were inspected and categorized into 6 ranks, best rank (VI) to the worst rank (I). Due to the short transition time, a decaying probability by more than one state in one year is assumed to be negligible as shown in Fig. 1. The Markov properties are characterized though the transition probability matrix. In this study, the Markov differential equation is developed by describing the probability of being in each of the state at time $t+\Delta t$ as a function of state of the system at time t resulting in the following equations:

$$\begin{bmatrix} dS_6(t)/dt \\ dS_5(t)/dt \\ dS_4(t)/dt \\ dS_3(t)/dt \\ dS_2(t)/dt \\ dS_1(t)/dt \end{bmatrix} = \begin{bmatrix} S_6(t) \\ S_5(t) \\ S_4(t) \\ S_3(t) \\ S_2(t) \\ S_1(t) \end{bmatrix}^T \begin{bmatrix} T_{66} & T_{65} & 0 & 0 & 0 & 0 \\ 0 & T_{55} & T_{54} & 0 & 0 & 0 \\ 0 & 0 & T_{44} & T_{43} & 0 & 0 \\ 0 & 0 & 0 & T_{33} & T_{32} & 0 \\ 0 & 0 & 0 & 0 & T_{22} & T_{21} \\ 0 & 0 & 0 & 0 & 0 & T_{11} \end{bmatrix}$$
or $\dot{S} = S \cdot T$

where Serepresents the state of system at time $t+\Delta t$, S represents the initial state of the system and T represents transition probability matrix.

The difficulties are arisen when the predictions of state are situated under



constraints of limited access to ground anchor condition data. Therefore the systematically method is proposed in the combination of iteration method and polynomial equation solving.

3. Results and Discussions

The total number of inspected ground anchor at 12th year, 16th year and 19th year after operation is 52, 208 and 391, respectively therefore the initial state matrix corresponding to each inspected year are expressed by

$$S_{12}(0) = \begin{bmatrix} 52 & 0 & 0 & 0 & 0 & 0 \\ S_{16}(0) = \begin{bmatrix} 208 & 0 & 0 & 0 & 0 & 0 \end{bmatrix}$$

 $S_{10}(0) = \begin{bmatrix} 391 & 0 & 0 & 0 & 0 & 0 \end{bmatrix}$

The state matrices at time t are presented by a number of inspected ground anchor corresponding to each condition rating as shown below:

$$S_{12}(12) = \begin{bmatrix} 0 & 11 & 36 & 4 & 1 & 0 \end{bmatrix}$$

 $S_{16}(16) = \begin{bmatrix} 0 & 0 & 206 & 0 & 2 & 0 \end{bmatrix}$
 $S_{19}(19) = \begin{bmatrix} 0 & 0 & 315 & 76 & 0 & 0 \end{bmatrix}$

Using iteration method, the trial transition matrix is obtained corresponding to each inspected year. Consequently, each inspected year is extended up to the final inspected year, which is 19th year in this case, using its trial transition matrix as shown below:

$$S_{12}(19) = \begin{bmatrix} 0 & 4 & 37.1 & 6.8 & 4 & 0.2 \end{bmatrix}$$

 $S_{16}(19) = \begin{bmatrix} 0 & 0 & 205.3 & 0.3 & 2.3 & 0.1 \end{bmatrix}$
 $S_{19}(19) = \begin{bmatrix} 0 & 0 & 316.3 & 74.1 & 0.4 & 0.2 \end{bmatrix}$

The optimized state matrix is defined as the state matrix obtained by summation of each equation above as shown below:

$$S(19) = \begin{bmatrix} 0 & 4 & 558.7 & 81.2 & 6.7 & 0.4 \end{bmatrix}$$

In consideration of the total number of inspected ground anchor, the initial state matrix can be obtained by summation of each equation in the initial state as expressed by

$$S(0) = [651 \ 0 \ 0 \ 0 \ 0]$$

optimized transition matrix is The obtained as shown below by polynomial equations in which the S(0) is used as input state and S(19) is used as output state.

$$T = \begin{bmatrix} 0.5580 & 0.4420 & 0 & 0 & 0 & 0 \\ 0 & 0.7273 & 0.2727 & 0 & 0 & 0 \\ 0 & 0 & 0.9889 & 0.0111 & 0 & 0 \\ 0 & 0 & 0 & 0.9876 & 0.0124 & 0 \\ 0 & 0 & 0 & 0 & 0.9929 & 0.0071 \\ 0 & 0 & 0 & 0 & 0 & 0 & 1 \end{bmatrix}$$

The predicted state using optimized transition probability matrix is compared with observed data as shown in Fig. 2. It was found that the predicted state using calculated transition matrix give a small different comparing with observed data in which such an error is caused by uncertainty involved in deteriorating process such as the random of inspected ground anchor as well as their numbers in each inspected year. Therefore, one can conclude that the deterioration process including future state of ground anchor can be clarified and predict efficiently using proposed method.

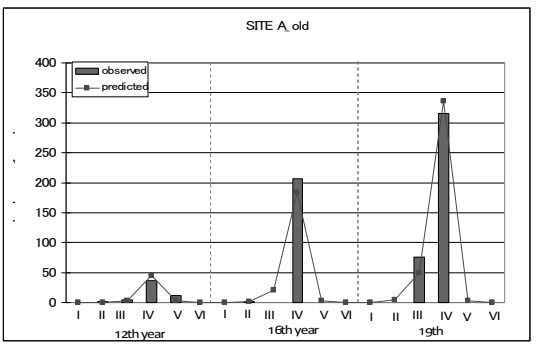


Fig. 2 Comparison between observed-input data

4. Recommendations for Thailand

In Thailand, awareness of infrastructure maintenance management is still deficient therefore the proposed method can be applied into not only ground anchor maintenance but also other infrastructures in which their deteriorating nature can be modeled as the Markovian properties.

- [1] A. Sharabah, S. Setunge, P. Zeephongsekul, Use of Markov chain for deterioration modeling and management of infrastructure assets, IEEE ICIA, 2006, pp. 384-389.
- [2] M. Mizutani, A maintenance planning method (MPM) for deteriorating structures, Structural Safety and Reliability, Shiraishi, Shinozuka & Wen (eds), Balkema, Rotterdam, 1998, pp. 443-450.

An Optimal Renewal Timing Markov Model for Water Supply Pipelines System

Le Thanh Nam, Kiyoyuki Kaito, Kiyoshi Kobayashi

Graduate School of Engineering, Department of Urban Management, Kyoto University, Kyoto, Japan E-mail address: info.tna@gmail.com

In megacities, the water work bereaus are facing major challenges with regard to the deterioration of their pipelines system. Pipelines are underground facilities that inspection and repair could not be easily implemented. As a matter of course, it exerts to have high uncertainty in deterioration speed. Under the occurence of leakage or breakdown, a huge loss in term of social cost and repairing cost would be accumulated. This paper takes into consideration of this risk and thus to develop a model in defining an optimal timing for pipeline replacement so as to minimize the total expected life cycle cost (LCC). The model employs the application of markov process to illustrate the deterioration process of pipelines system. An empirical study was carried out with pipelines system in Osaka city to further verify its applicability

1. Introduction

It has been widely known in the asset management of water supply pipelines system that the deterioration is due to various corrosion mechanisms, such as soil corrosion, bimetallic corrosion, and stray currents. As a sequel of deterioration, the leakage and breakdown will occur and lead to presume head losses, high repairing cost as well as social cost [1].

In the literature of asset management, especially for pipelines system, several methods have been studied in determining the optimal replacement strategies [2,3]. These studies focused both on repair and renewal rules based on the break rate and least LCC estimation approach. In which, homogeneous process were employed to illustrate the behavior of deterioration process. The application of Markov hazard model in management of pipelines is somewhat at the outset of development. This study proposes a mathematical model, which is formulated based on markov chain process with use of discrete distinguish conditional states to describe the deterioration, and further apply LCC analysis to define the optimal renewal timing.

2. Mathematical Model

The water distribution network comprises of many different types of pipelines k(k=1,...,K). The total length of one type is S^k (km). For ease of management, each section with a pre-defined length is assumed (for instance 0.1 km/section). We further denotes the condition state of pipelines as i=1,...,M, where M is regarded as absorbing state. The renewal process can be described by equation of time $t_r^d = t_0 + rd$ (r = 0,1,L). In which, d is

interval duration, and r is number of time in discrete order.

With use of markov hazard model, the deterioration process of section s(s=1,...,S) can be represented by conditional transition probability matrix.

 $Prob[h_s(t^d_{r+1}) = j \mid h_s(t^d_r) = i] = p_{ij}$ (1) after repair/renewal, the condition state of pipeline at time t^d_r and t^d_{r+1} are denoted as $h^o_s(t^d_r)$ and $h^o_s(t^d_{r+1}) = j'$. The probability P^{ξ}_{ij} of chagning the condition state $h^o_s(t^d_r) = i$ into $h^o_s(t^d_{r+1}) = j' = j'$ can be formed as the following equation

$$P_{ij}^{\xi} = \sum_{j=1}^{M} p_{ij} q_{jj}^{\xi}$$
 (2)

where q_{jj}^{ξ} is action matrix the value equal to 1

when $\eta^{\xi}(j) = j'$ and equal to 0 otherwise. j' is the state after repair/renewal being made (j=1,L,M;j'=1,L,j). The deterioration level of pipelines system can be seen as the relative frequency of total number of section S

$$\pi^{\xi}(t_r^d) = \left\{ \pi_1^{\xi}(t_r^d), L, \pi_M^{\xi}(t_r^d) \right\} \text{ and } \sum_{i=1}^{M} \pi_i^{\xi}(t_r^d) = 1 \quad (3)$$

 $\pi_i^{\xi}(t_r^d) = a_i^{\xi}(t_r^d)/S$, $a_i^{\xi}(t_r^d) = m_i$ (i = 1, L, M). m_i is measured in km. From (2), we obtain the following equation for the change of relative frequency from t_r^d to t_{r+1}^d .

$$\pi_{j}^{\xi}(t_{r+1}^{d}) = \sum_{i=1}^{M} P_{ij}^{\xi} \pi_{i}^{\xi}(t_{r}^{d})$$
 (4)

When taking into account the cost and risk under LCC estimation, we formulate the one-step unit expected cost w_k^{ξ} .



$$w_k^{\xi} = \sum_{i=1}^{M-1} \sum_{j=1}^{M} \sum_{j'=1}^{j} p_{ij}^k q_{jj'}^{\xi} c_j^{j'} S^k \pi_i^{k^{\xi}}$$
 (5)

with c_i^j is repair/renewal cost. It is obvious that the w_k^{ξ} is also a function of d. Therefore, the unit cost with respect to policy ξ can be in the form as

$$W^{\xi}(d) = \frac{\sum_{k=1}^{K} w_k^{\xi}(d)}{d}$$
 (6)

Beside the direct cost, other fixed cost c_R occurs as social cost due to the level of deterioration. This loss has its own probability $v = (v_1, L, v_M)$.

$$R^{\xi}(d) = \sum_{k=1}^{K} \sum_{i=1}^{M-1} \sum_{j=1}^{M} p_{ij}^{k} \nu_{j} c_{R} S^{k} \pi_{i}^{k^{\xi}}$$
 (7)

The optimal timing d can be defined by solving the minimimum condition of the following equation.

$$\min_{d,\xi} \{ W^{\xi}(d) + R^{\xi}(d) \} \tag{8}$$

3. Empirical Application

In this study, we used the data of water distribution network in OSAKA city. We used two condition state i=1 for normal operation and i=2 for breakdown state. Following results were obtained from numerical analysis on 8567 recorded pipelines sections.

Fig. 1 shows the deterioration curve representing by survival probability throughout the management terms. After about 60 years of operation, the survival probability decreases to 0.5. Fig. 2 displays the plot of expected life cycle cost. In which, the repair cost and social cost are 2,485,000 (yen) and 4,670,000 (yen) respectively. It can be observed from the figure that the minimum LCC gets its value of 12,346,003 (yen), which is equivalent to 44 years. After 64 years, there is a gradually small increase with respect to expected LCC. The value of probability ν is assumed to be v = (0, 0.002).

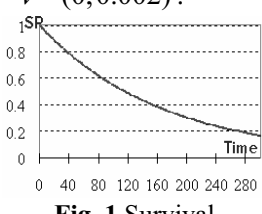


Fig. 1 Survival probability (SP)

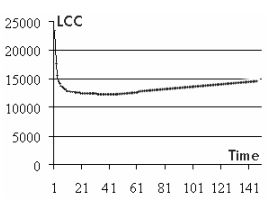


Fig. 2 Life cycle cost (1000 Yen)

4. Conclusions and Recommendations for **Thailand**

This paper introduces a method based on markov chain model to determine the optimal time for replacement of pipelines. The empirical study was conducted on the dataset of water pipelines system in Osaka city. The estimation shows a cumulative of about 44 years after the construction time for renewal policy to be implemented. The test of the model further proves that the ratio between social cost and repair cost has a great influence on the esimation result.

Regarding the recommendation Thailand, it can be obvious that the model can be used to apply for maintenance and repair work of pipelines or sewage system in megacity like Bangkok. Moreover, introduction of using markov process in asset management can bring significant positive development impact on the of asset management in Thailand, where asset management is still in early development stage.

- [1] A. Deb, J. Snyder, G. Logananthan, and Agbenowski, F. Grablutz, Pipeline Technologies, Security Safety (Proc. ASCE Int. Conf. on Pipeline Eng. and Construction), 2 (2003) 1002-1011.
- [2] H. Hong, E. Allouche, and M. Trivedi, J. Infrastruc. Syst. 12-3 (2006) 184-191.
- [3] Y. Kleiner, B. Adam, J. Comp. in Civ. Eng. 15-1 (2001) 15-26.

123

NS-F07

Sustainable Water Demand Management for Economic and Social Development in Thailand: Case of Lower Chao Phraya River Basin

Pongsak Suttinon

Research Center for Social Management, Kochi University of Technology, Kochi, Japan Tel.: +81-8-8757-2779, Fax: +81-8-8757-2811, E-mail address: pongsak.suttinon@kochi-tech.ac.jp

Water is the main natural resource that is used in many sectors including industry, agriculture, and domestic. Development of these economic and social activities with increasing population need more water; however, supported or supply water is limited. From this reason, the main question for policy makers is how to develop Thailand with the constraints of water capacity under satisfactions of each user. The aim of this study was therefore to develop water demand management model by integrating engineering (water resources), economic (input-output table and equilibrium analysis with water demand-supply curve), and financial (real option analysis) methods. In this paper, main economic and social activities (industrial, agricultural and domestic sector) in Lower Chao Phraya River Basin in Thailand including Bangkok, the capital of Thailand, were selected to analyses for next 20 years because this area is the center of development in urbanization, economic, and political part. The results show that this model can produce not only water demand in the future but effects from changing economic structure, pricing policy, and risk analysis also. This study suggests that water can be managed in line with demand, provided that combination of engineering, economic, and financial policies to control water demand are put in place.

1. Introduction

From the past, water use was more needed because of increasing population, urbanization, and industrialization. Most studies and designs in water resources engineering seem to agree that there are two schemes to manage water; water supply and demand schemes. Water supply approach is concentrated to increase new water source such as construction of dams or water supply systems but water demand idea reduces water use with constraints of new water sources, for example, recycle, pricing policy, and etc.

However, few studies have concentrated integration of water demand with combination among engineering, economic, and financial parts. Policy maker should design the possible national economic and social development plan at the first step with the constraints of water. Many questions should be asked in this step as follow. Is it possible that Thailand will be the leader of textile industry, which needs much groundwater in production, under groundwater ban law? Is it possible to export 10 million tons of milled rice per year under existing irrigation system? If the economic target is not possible, how to use water demand schemes to keep that mark? If the government declares the water demand plans, what is the impact to economic and social structure?

Most researches did not focus on how water using structure changes from changing economic activities, and what is the effect from water policy to the users, how to invest water infrastructure under uncertainties of water demand and supply in the future.

The purposes of this research were: (1) to forecast water demand with effect of changing economic activities by using input-output table; (2) to calculate effects from pricing policy with water demand schemes such as recycle system in each evaluation standard; (3) to increase the value of water infrastructure project by using real option analysis with uncertainties in the future.

2. Methodology

Water demand management model was developed by integrating the engineering, economic, and financial fields in industrial, agricultural, and domestic sectors. The study area is Lower Chao Phraya River Basin that consists of 7 provinces as follow: (1) Bangkok (capital of Thailand); (2) Samut Prakan; (3) Samut Sakon; (4) Nontaburi; (5) Patumtani; (6) Ayutthaya; and (7) Nakon Pathom. The model was developed by using data from year 1985 to 2005 to forecast water situations in year 2006, 2015, and 2025. The outputs of each model were shown in provincial and regional scale.

The model consisted of 4 sub-models as follow: (1) water demand model (to forecast changing water demand in the future from changed economic activities by using input-output table with national and regional development plans); (2) water supply model (to analyze all possible water supplies with constraints and scenarios of demand schemes such as recycle system); (3) integrated water



demand management model (to calculate equilibrium point in each governmental scenario by using pricing policy and water demand-supply curve developed from model 1 and 2, and to evaluate the suitable choice with each evaluation standard); and (4) strategic decision making model (to value flexibility of infrastructure investments supported water demand in the future).

3. Results and Discussion

Total water demands including industrial, household, and agricultural sectors were shown in Table 1. Total water demand in year 2025 was varied from the possible maximum and minimum case between 5,038 and 6,734 million cubic meter, MCM depended on situations in each sector. Possible maximum water demand is summation of industrial water in case of all declared strategies, household water in case of varied water use unit and agricultural water in case of low rainfall. If 100 % of possible recycled water in Japan case was applied, it can be saved 573 MCM in year 2025 or approximately 60 % of capacity of Pasak dam. To validate the results, actual water demand should be surveyed and monitored to analyze effects of declared policies and water measures, however, it is difficult to implement because of limited budget.

4. Conclusions and Recommendations for Thailand

Developing new water sources is more difficult because of limited water supply, conflict with environmental viewpoint, and higher cost of water per cubic meter. Policy maker should use water demand side management especially; (1) water saving such as reuse, reduce, and recycle, (2) pricing policy, (3) water right and sharing, and (4) educate water users with conservation options. Water demand management invokes ways to operate within limits of current supplies. However, combination of both measures is normally best. In viewpoint of economic, it is almost certain that development of industrial activities need more water. From this reason, policy makers should carefully consider the target of economic with constraints of each water source in specific area. In case of study area, main industrial types such as food and textile need groundwater in groundwater critical zone. It is the conflict between the target of economic and constraint of water in this area. Policy makers should make decision of economic planning with the maximum

possible capacity of water. The water rights and sharing in the dry season are always the critical period for water shortage problem. Water management system in Thailand is generally planned from the top-bottom or from central government to users. The problem of this method is that right of water in each user was designed and controlled by policy makers that don't use water in that area. One interesting measure used in Japan is bottomtop method or planning from local committee of each area. The committees consist of only water users in each sector such as factory, farmer, and the head of citizen located in that officers from local-central government and specialists from academic fields play a role as only consultants. By this method, the right and sharing of water and benefit was designed by water users.

 Table 1 Results of forecasted water demand model

Case		Water demand, MCM			
		2006	2015	2025	
T.1	Maximum case	4,064	5,047	6,734	
T.2	Minimum case	3,638	4,235	5,038	
T.3	T.1 with recycle	4,026	4,918	6,161	

Note: T1 or maximum case is summation of industrial sector (case of industrial clusters with FTAs), household sector (case of varied water use unit from changing daily style), and agricultural in drought year. T2 or minimum case is summation of industrial sector (case of normal growth), household sector (case of fixed water use unit), and agricultural in much water year. Recycle means recycled water in industrial sector

Analysis of Biomass Pyrolysis Mechanism for Development in Reactor Design

Weerawut Chaiwat, Takaaki Tani, Kenshi Sunagawa, Isao Hasegawa, Kazuhiro Mae

Department of Chemical Engineering, Kyoto University, Kyoto, Japan Tel.: +81-7-5383-2678, E-mail address: chaiwat@cheme.kyoto-u.ac.jp

Pyrolysis of cellulose using thermogravimetric method was performed under inert atmosphere at different heating rates in order to investigate the pyrolysis behavior of biomass. The decomposition of biomass pyrolysis was shifted to lower temperature when decreasing its heating rate due to longer reaction period. For structural analysis of the residues, FTIR spectra showed a decrease in OH group when increasing pyrolysis temperature. This indicates that the dehydration reaction to produce water proceeded during pyrolysis at low temperature regions. Moreover, XRD patterns also showed a decrease in crystallinity when increasing pyrolysis temperature due to the random glycosidic reaction to produce tar products. Through these analyses, the temperature profile of biomass pyrolysis is very important to effectively design reaction zones for required products distribution and reactor development.

1. Introduction

Biomass has recently been considered as a renewable resource, due to its environmentally benign characteristics. Biomass has a very complex structure, consisting of cellulose (30-50 wt%), hemicellulose (10-30 wt%), and lignin (15-40 wt%); however, cellulose has a simple structure and is often selected for investigations of pyrolysis behavior. Most investigators have studied the mechanism for cellulose pyrolysis, and generally recognize at least two competitive pathways; dehydration, cross-linking i.e. reactions. depolymerization, i.e. the splitting glycosidic bonds. The effects of pyrolysis conditions on product yields and distribution can be explained by these two competitive pathways. In this work, pyrolysis behavior of biomass was preliminarily investigated using thermogravimetric method. The structural properties of biomass pyrolyzed at low temperature region were further studied. Finally, pyrolysis mechanism temperature region was simply proposed.

2. Experimental

Using thermogravimetric (TG) method, cellulose and biomass samples weighed about 1.5-3.0 mg were heated under inert atmosphere at various heating rates, 5, 10, 20, and 50 K·min⁻¹ to 900 °C before they were completely combusted with air to determine carbon conversion and char yields. The samples were also pyrolyzed with a heating rate of 3000 K·s⁻ ¹ using a Curie-point pyrolyszer (CPP) at temperatures for comparison. Moreover, the samples 50-100 mg were also treated under nitrogen atmosphere in quartz tube reactor with the flow rate of 100 cc·min⁻¹ to various low temperatures of 300-500 °C.

Then, the pyrolyzed samples were dried before analysis using Fourier transform infrared spectroscopy (FTIR) and X-ray diffraction (XRD) for structural analysis of the residues.

3. Results and Discussion

3.1 Analysis of Biomass Pyrolysis Rate

Thermogravimetric analysis was used to preliminarily investigate the effect of heating rate on the kinetic behavior of cellulose pyrolysis as shown in Fig. 1. With decreasing the heating rate from 50 to 5 K·min⁻¹, the temperature beginning of cellulose decomposition were gradually shifted from approximately 350 to 300 °C. For pyrolysis with 5 K·min⁻¹, the decomposition of cellulose was completely proceeded before reaching 400 °C, while it almost reached 450 °C for that of 50 K·min⁻¹. This indicates that the pyrolysis with lower heating rate making longer reaction period required lower temperature to complete cellulose decomposition.

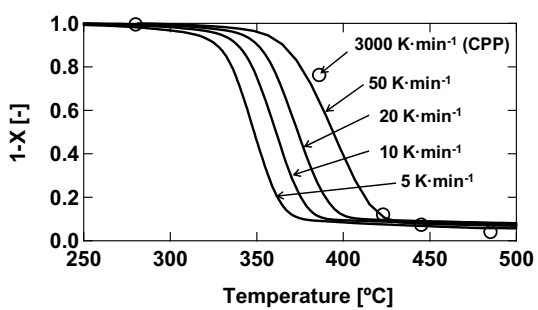


Fig. 1 TG curves of cellulose samples pyrolyzed at various heating rates.



Pyrolysis at Low Temperature Since TG results showed the change of pyrolysis behavior due to its decomposition reaction during low temperature region, the analyses of FTIR and XRD were conducted, which their results are given in Fig. 2 and 3, respectively in order to compare the structure of cellulose residues pyrolyzed at different low temperatures with 5 \dot{K} ·min⁻¹ and 3,000 \dot{K} ·s⁻¹. For FTIR spectra in Fig. 2, absorptions between 3000 and 3600 cm⁻¹ are typically ascribed to hydroxyl groups (OH) or adsorbed water. The spectra of OH peak intensity gradually decreased when the samples were treated to higher temperature. The OH peak was extremely dropped from 320 to 340 °C and from 445 to 485°C for the samples pyrolyzed at 5 K·min⁻¹ and in a flash mode, respectively. However, the spectra of the residues at higher temperature then showed almost the same low intensities of the OH absorptions. This indicates that the dehydration to produce water such as cross-linking reaction was promoted during pyrolysis at low temperature region which has agreement with the results of thermongravimetric analysis.

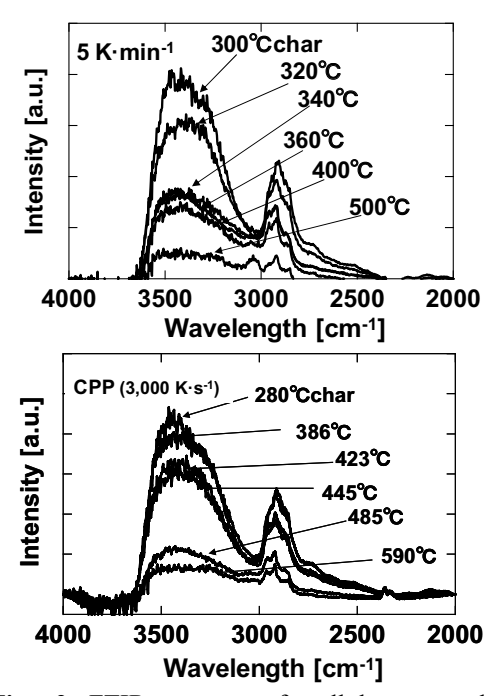


Fig. 2 FTIR spectra of cellulose samples pyrolyzed at 5 $K \cdot min^{\text{-}1}$ and 3,000 $K \cdot s^{\text{-}1}$

Through the analysis of solid crystallinity, XRD patterns of the samples treated with inert gas and air showed the peak intensities at 20 =15-25° as shown in Fig. 3. The peak intensities were continuously decreased with increasing temperature. This indicates that the crystallinity of pyrolyzed residues gradually decreased, and then the sample structure became near amorphous at 340 °C and 485°C

for the samples pyrolyzed at low heating rate and in a flash mode, respectively, because the glycosidic bonds may be randomly decomposed to produce tar when heating to higher temperature.

3.3 Conclusions and Investigations of Pyrolysis Mechanism of Biomass

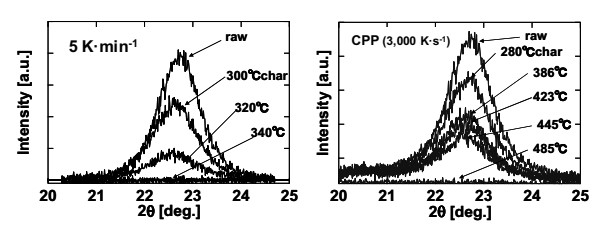


Fig. 3 XRD Patterns of cellulose samples pyrolyzed at 5 K·min⁻¹ and 3,000 K·s⁻¹

Through above analyses, it shows that heating rate has a significant influence on pyrolysis temperature range. Pyrolysis with low heating rate at 5 K·min⁻¹ completely proceeded at 340 °C, while the sample was hardly decomposed for flash pyrolysis at the same temperature. Moreover, lower heating rate at low temperature causes relatively more cross-linking reaction with a OH group. decrease in Consequently, pretreatments of biomass at low temperature may be necessary to change its structure and obtain valuable products. Finally, a simple structural model was also proposed to properly explain the mechanism of biomass pyrolysis.

4. Recommendations for Thailand

Since Thailand has abundant biomass resources, researches on mechanism and reactor technology of biomass conversion such as pyrolysis and gasification should be more focused to control obtained products as renewable energy and valuable chemicals. In conclusion, through the results in this work, the temperature profile of biomass pyrolysis is very important to effectively design reaction zones for required products distribution and reactor development.

Gasification of Cotton and Jatropha Residue Using Supercritical Water

Thachanan Samanmulya¹, Tawatchai Charinpanitkul¹, Yukihiko Matsumura²

¹Center of Excellence in Particle Technology, Faculty of Engineering, Chulalongkorn University, Payathai Patumwan, Bangkok, Thailand ²Department of Mechanical System Engineering, Hiroshima University, Hiroshima, Japan Tel./Fax: +66-2-218-6480, E-mail address: ctawat@chula.ac.th

Among various biomass materials available in Thailand, cotton and jatropha are abundant biomass which has potential as renewable energy resources. Powdery cotton and jatropha residue has been gasified by supercritical water in a tubular flow reactor to produce fuel gas. Effects of gasification temperature in a range of $400 - 700^{\circ}$ C and biomass loading of 0.1-0.5 wt % have been experimentally examined. The gaseous product is composed of hydrogen, carbon dioxide, carbon monoxide, methane and a small amount of ethane and ethylene. The hydrogen yield was dependent on the increasing biomass loading. Elevated temperature and catalyst addition would be required in the gasification of high concentration of feedstock.

1. Introduction

Biomass is one of the most abundant renewable energy resources. A variety of biomass resources can be used to convert to energy. Biomass conversion to energy is undertaken with two main process technologies: thermo-chemical and biological processes. Thermo-chemical gasification of biomass is likely to be a cost-effective process to produce fuel gas [1].

One method for hydrogen production is the steam reforming of biomass. The major problem in gasification by steam reforming is the formation of tars and char as the biomass does not react directly with steam at atmosphere pressure [2].

Supercritical water has an excellent extracting capability which is superior to that of liquid water. Generally, the dielectric constant of supercritical water is much lower than that of water and other solvents. As a result, supercritical water behaves like an effective solvent for many biodegradable materials. It is well known that supercritical water has the ability to dissolve biomaterials which are not normally soluble in water or steam. These properties make supercritical water a very promising reaction medium for the conversion of biomass to value-added products. The objective of this research is to produce a fuel gas from biomass, which are cotton and jatropha seed residues by gasification in supercritical water. Investigation on effects of temperature and biomass loading upon has been gassifi-cation vield conducted experimentally. Analyses of gas compositions obtained from gasification have also been carried

2. Experimental

All gasification has been performed within a tubular flow reactor shown schematically in Fig. 1. The tubular flow reactor had the inside diameter of 2.17 mm and the length of 12 m. Cotton or jatropha residue powder suspension was fed into the reactor by a piston pump (Toyokoatu Co.,

designed for our use). Except otherwise stated, the reactor temperature and pressure were 500°C and 25 MPa, respectively. The reactor was cooled down by the cooler before solid remaining was separated from suspension by the solid-liquid separator. Meanwhile, the exit gas flow was separated by the liquid-gas separator. The gas generation rate was measured by the gas meter (W-NK0.5A, Shinagawa). The gas and liquid samples were analyzed with gas chromatograph (GC-14B, Shimadzu) and TOC (TOC-V_{CPH}, Shimadzu), respectively. In this work, the reaction temperature was varied from 400 to 700 °C and residence time in the range of 80 – 222 s.

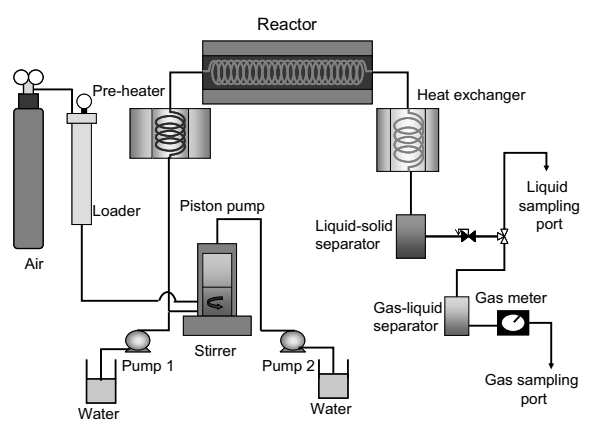


Fig. 1 Schematic experimental set-up

3. Results and Discussion

Effect of biomass loading (0.1-0.3 wt %) in the reactor on gasification product by supercritical water was studied at 500°C, 25 MPa. Figure 2 shows that with an increase in the biomass loading from 0.1 to 0.2 %wt, relative yield of methane, ethylene, ethane and carbon monoxide concentration was reduced while that of carbon dioxide and hydrogen was increased. As the biomass loading was further increased from 0.2 to 0.3 %wt, the hydrogen fraction was reduced while carbon monoxide

and was increased slightly. Based on these results, it would be implied that the gasification of high solid loading of biomass feedstock would be preferable to gaseous product with small molecular size.

Meanwhile, effect of temperature (500-600°C) on gasification of cotton and jatropha residue is shown in Figure 3. When temperature was increased from 500 to 600°C, the yield of hydrogen and methane were increased while the fraction of carbon monoxide and carbon dioxide were reduced. These would be attributable that the selective formation of hydrogen and methane would be more enhanced under higher supercritical conditions.

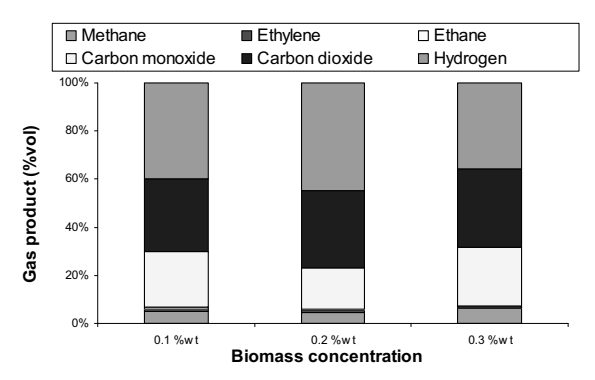
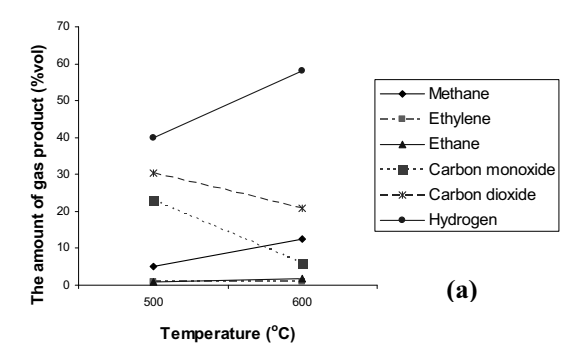


Fig. 2 Effect of loading on gaseous product synthesized from cotton gasification in supercritical water (500°C and 25 MPa.)

4. Conclusion and Recommendations for Thailand

Cotton and jatropha residue could be gasified by supercritical water to produce fuel gas which contained hydrogen, methane, carbon monoxide, carbon dioxide and small amount of ethylene and ethane. Hydrogen production was influenced by operating parameters which were biomass loading, temperature and residence time. With a high solid loading, hydrogen fraction was decreased. Systematic investigation on gasification of both biomass materials would be beneficial to Thailand and Southeastern Asian countries because of their abundance in this region.



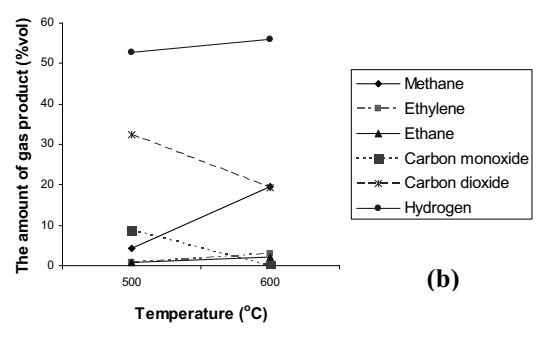


Fig. 3 Gaseous products synthesized from gasification of biomass in supercritical water (P= 25 MPa.); (a)Cotton (b)Jatropha residue

5. Reference

- [1] Y.J. Lu et al., Hydrogen Energy 31 (2006) 822–831.
- [2] M. J. Antal et al. Ind. Eng. Chem. Res. 39 (2000) 4044–4053.

Acknowledgement

This research is partially supported by the Centennial Fund of Chulalongkorn University. TS also gratefully acknowledges the support of HUMAP of Hiroshima University.

129

NS-P03

Liquid Phase Deposition of Anatase Titanium dioxide Nanotubes Arrays and their Performances of Hybrid Solar Cells

Thitima Rattanavoravipa, Takashi Sagawa, Susumu Yoshikawa*

Institute of Advanced Energy, Kyoto University, Kyoto, Japan E-mail address: s-yoshi@jae.kyoto-u.ac.jp

Titanium dioxide (TiO₂) nanotube arrays were deposited on the fluorine-doped SnO2 (FTO) transparent conducting glass oxide by a liquid phase deposition method using ZnO template. Characterizations of the TiO₂ nanotube arrays were performed.TiO₂ arrays on the substrate are suitable for fabricating hybrid solar cells based on the nanotube arrays FTO/TiO₂/N719/P3HT:PCBM/Au structure. Before cell fabrication, the surface modification of the metal oxide surface enhanced the electron injection of the solar cells performance. The power conversion efficiency of the device is determined to be 0.656% under AM 1.5 solar illuminations.

1. Introduction

Over the past decade organic based solar cell are attracting enormous as a low cost, lightweight, and scalable source of renewable energy. The high power conversion efficiency has been reported 4-5% which focused of conjugated bulk heterojunction polymer [1-3]. Hybrid solar cell is an alternative type of the promising devices which combined the donor organic semiconductor together with acceptor inorganic semiconductor. TiO2 is an attractive oxide because of its electron accepting and conducting ability. It has been reported the application of TiO₂ for photovoltaic dye sensitized solar cell and hybrid solar cells as an electron acceptor and transport. In the structure of nanorod/nanotube vertical arrays of the metal oxide, the large interface between the metal oxide materials and straight carrier paths to the electrode can be achieved due to the very short length of diffusion excitons[4].

2. Methodology

ZnO nanorod array on the ITO substrate was prepared by hydrolysis with solution method.. ZnO nanorod arrays were grown by immersing the zinc nanocrystal seeded sample into the solution of zinc nitrate hydrate and sodium hydroxide at 80 °C. After the deposition, substrate were rinsed by distilled water and dried in the air. TiO2 nanotube arrays were synthesis by using ZnO template for deposition (LPD). The template of ZnO nanorod arrays on was immersed into aqueous solution including, ammonium hexafluorotitanate and boric acid. After immersion, the surface modified FTO was washed by deionized water and calcined at 450 °C. Prior to use, FTO coated with TiO₂ nanotube arrays was immersed overnight in N719 dye. After the rising with acetonitrile out the extra amount of dye, mixture of P3HTand PCBM in chlorobenzene was spin-coated on the top of the N719/TiO₂-coated FTO substrate. Subsequently, the sample was immediately annealed at 140 °C. All the device preparations were prepared in the glove box under Ar atmosphere. Finally, gold electrodes were then evaporated under high vacuum in the ULVAC evaporation system.

3. Results and Discussion



Fig. 1 SEM images cross-sectional views of ZnO nanorods arrays (a) and TiO₂ nanotube arrays (b) grown on FTO substrate (inset shows the top view of the tube structure, scale bar 500 nm.).

Fig. 1(a) show the images in cross-sectional view ZnO template on FTO substrate. These nanorods have uniform lengths of ~750 nm and diameters of ~ 80 nm were observed. After the heat treatment XRD patterns shows the predominant anatase phase. The current densityvoltage of TiO2 hybrid solar cells with and without surface modification under simulation of the light at AM 1.5. Modifying the TiO₂ nanotube arrays with N719 ruthenium dye attained V_{oc} of 0.48V, J_{sc} of 5.7 mW/cm², FF of 24 %, and η of 0.656%. On the contrary, unmodified cell demonstrated the V_{oc} of 0.08V, J_{sc} of 1.1 mW/cm², FF of 25 %, and η of 0.02%. Such improvement of the interfacial contact between the organic layer and the electron transporting layer may improve the efficiency of electron transfer because the wettability of the

surface after surface modification of TiO_2 nanotubes with dye molecule by the polymer resulting in enlargement of the contact area where the charge separations occur

4. Conclusions and Recommendations for Thailand

We have successfully synthesized the TiO2 nanotube arrays through one step liquid phase deposition technique ZnO on template perpendicularly on the substrate. TiO2 nanotube arrays on the substrate are suitable for fabricating hybrid solar cells based on the nanotube arrays TiO2/N719/P3HT:PCBM/Au structure. The solar cell performance was improved in terms of the enhancement of the electron injection through the modification of the metal oxide surface by using N719 dye. Finally, this method for fabricating the 1-D aligned TiO2 nanorod/nanotube arrays can provide us for the other application in electronic devices.

- [1] W. Ma, C. Yang, X. Gong, K. Lee, A. J. Heeger, Adv. Funct. Mater. 15 (2005) 1617-1622.
- [2] M. Reyes-Reyes, K. Kim, D. L. Carroll, Appl. Phys. Lett. 87 (2005) 083506.
- [3] Y. Kim, S. Cook, S. M. Tuladhar, S. A. Choulis, J. Nelson, J. R. Durrant, D. D. C. Bradley, M. Giles, I. McCulloch, C.-S. Ha, M. Ree, Nature Mater. 5 (2006) 197-203
- [4] S.-I. Na, S.-S. Kim, W.-K. Hong, J.-W. Park, J. Jo, Y.-C. Nah, T. Lee, D.-Y. Kim, Electrochimica Acta 53 (2008) 2560-2566..
- [5] J.H. Lee, I.C. Leu, M.C. Hsu, Y.W. Chung, M. H.Hon, J. Phys. Chem. B 109 (2005) 13056-13059.

NS-P04

Electrospun Conductive Polymer Nanofibers for Organic Photovoltaic Cells

Surawut Chuangchote, Takashi Sagawa, Susumu Yoshikawa

Institute of Advanced Energy, Kyoto University, Kyoto, Japan Tel: +81-80-3814-9493, Fax: 81-7-7438-3508, E-mail address: surawut@iae.kyoto-u.ac.jp

Organic photovoltaic device is one of the promising alternatives to conventional silicon-based solar cells. A new method for preparation of active layers of conductive polymer-based organic solar cells by electrospinning without any thermal post-treatment to obtain optimal performance is presented. A conductive polymer, poly[2-methoxy-5-(2'-ethyl hexyloxy)-1,4-phenylenevinylene] (MEH-PPV), and its blends with an easily spinnable polyvinylpyrrolidone (PVP) were dissolved and electrospun. Electrospinning was carried out under an applied electrical potential of 15 kV over a collection distance of 15 cm. Electrospun MEH-PPV nanofibers were obtained as a ribbon-like structure aligned with wrinkled surface in fiber direction after the Soxhlet extraction. Crystallinity and electrical conductivity of the obtained fibers is higher than that of the spin cast film. By combination of these electrospun MEH-PPV nanofibers with the fullerene (C_{60}) or its derivative {[6,6]-phenyl- C_{61} -butyric acid methyl ester (PCBM)}, it is possible to fabricate bulk-heterojunction organic photovoltaic cells with relatively high efficiency as compared with that of conventional organic photovoltaic devices. The preliminary power conversion efficiency of ca. 0.2% with detail will be reported.

1. Introduction

Organic photovoltaic device is one of the promising alternatives to conventional siliconbased solar cells. In this sense, bulk heterojunction devices, which are based on the spontaneous phase separation between donor and acceptor materials, have become popular. However, high conversion efficiencies require a thermal annealing during the fabrication of cells.

One of promising materials for organic photovoltaic devices is conductive polymer because of a combination of specific properties from optical and electronic points of views with easy processing. From various forms of the conductive polymers; nanowires and nanofibers are growing broad interest in recent year. In particular, diameters of the polymeric materials can be shrunk to sub-micro or nanometers, bringing several specific characteristics such as improved mechanical performance, relatively large surface area to volume ratio, and flexibility in some surface functionality [1]. Among various kinds of processing techniques, electrospinning, which has become one of the versatile tools for fabrication of ultrafine fibers. In this context, a new method for preparation of active layers of conductive polymer-based solar cells in wide area, by electrospinning, without any thermal posttreatment to obtain optimal performance is presented.

2. Experimental

A conductive polymer, poly[2-methoxy-5-(2'-ethyl hexyloxy)-1,4-phenylenevinylene]

(MEH-PPV), and its blends with an easily spinnable polyvinylpyrrolidone (PVP) were dissolved. As-prepared solutions were electrospun under an applied electrical potential of 15 kV over a fixed collection distance of 15 cm at room temperature. The flow rate and the collection time were fixed for all experiments at 1 ml·h⁻¹ and 1 min, respectively. In order to remove PVP out from as-spun MEH-PPV/PVP fibers, the Soxhlet extraction was carried out. Methanol was used as a solvent at the extraction temperature of 75°C. The extraction time was fixed for 12 h. The samples were then dried overnight at 60°C in vacua. Morphological appearance of the asspun fiber mats was observed by a scanning electron microscope (SEM), operating at an acceleration voltage of 10 kV. Crystallinity of the as-spun fibers was measured by an X-ray diffractometer (XRD). Ultraviolet-visible (UV-Vis) absorption and photoluminescence (PL) of the as-spun fibers were also investigated. The excited wavelength was 385 nm. The photovoltaic properties of obtained devices [Fig. 1(a)] were investigated.

3. Results and Discussion

As-spun fibers from solutions of MEH-PPV/PVP in mixed chlorobenzene/methanol with various concentrations showed beaded or uniform characteristic with relatively small diameter (625 nm - 1.7 μm). In order to study the effects of solution properties and spinning conditions, electrospinning of solutions of MEH-PPV/PVP in chlorobenzene/methanol was carried out at various conditions. The average diameter of fibers was found to



decrease with the increase in the applied electrical potential in the range of 5 to 15 kV and a minimum size was ca. 625 nm when the applied electrical potential was ca. 15-20 kV (MEH-PPV:PVP = 1:3). Further increase of the applied electrical potential led to the increase of the size of as-spun fibers. Moreover, this periodic trend was also observed in the study in effects of content of MEH-PPV in the blended solution, which the minimum size of as-spun fibers was observed at the ratio of MEH-PPV/PVP of 1.5:6. While the average diameter was found to decrease monotonously with increasing the collection distance up to a far enough distance (ca. 20 cm) [1]. Moreover, the average diameter of the as-spun fibers was found to decrease into nanometer scale (smallest diameter was ca. 43 nm in the form of beaded fibers) with decreasing the concentration of PVP and/or addition of a volatile organic salt [2].

Electrospun MEH-PPV nanofibers were obtained as a ribbon-like structure aligned with wrinkled surface in fiber direction after the Soxhlet extraction as shown in Fig. 1(b). Crystallinity of the obtained fibers is higher than that of the spin cast film [3]. By combination of these electrospun MEH-PPV nanofibers with the fullerene (C_{60}) or its derivative $\{[6,6]$ -phenyl- C_{61} -butyric methyl ester (PCBM)}, it is possible to fabricate bulk-heterojunction organic photovoltaic cells [structure: ITO / PEDOT: PSS / MEH-PPV nanofibers:fullerene / Al] with relatively high efficiency as compared with that of conventional organic photovoltaic devices. The preliminary power conversion efficiency of ca. 0.2% with detail will be reported.

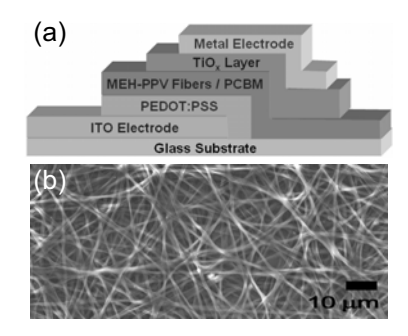


Fig. 1 Cell structure (a) and SEM image (b) of fibers-based photovoltaic cell

4. Conclusions and Recommendations for **Thailand**

Thailand is a tropical country which has sunshine in several months a year, which makes it as an ideal location for the development of renewable energies, especially solar cells. Therefore, this work is quite new and interesting to study in Thailand. The fabrication of nanofibers by electrospinning with above reported conditions seems to be able to carry out in Thailand. However, the preliminary power conversion efficiency reported here is only 0.2%. Therefore, it still needs to undergo further research and development to enhance the efficiency of organic solar cells and the potential to use organic solar cells in a commercial level.

- [1] S. Chuangchote, T. Sagawa, S. Yoshikawa, Macromol. Symp. 264 (2008) 80-89.
- [2] S. Chuangchote, T. Sagawa, S. Yoshikawa, Jpn. J. Appl. Phys. 47 (2008) 787-793.
- [3] S. Chuangchote, T. Sagawa, S. Yoshikawa, Mater. Res. Soc. Symp. Proc. 1091E (2008) 1091-AA07-85.

133

NS-P05

Experimental Study on the Performance of a Single-cell SOFC Prepared by Screen Printing and Co-firing Process

Pramote Puengjinda, Toshiaki Matsui, Koishi Eguchi

Department of Energy and Hydrocarbon Chemistry, Graduate School of Engineering, Kyoto University, Kyoto, Japan Tel.: +81-7-5383-2523, E-mail address: mote moto@yahoo.com

A single-cell SOFC (solid oxide fuel cell) was successfully prepared by screen printing with co-firing technique and its electrochemical performance both impedance spectra and I-V test was investigated. In this experiment, nickel oxide and yttria stabilized zirconia (NiO/YSZ) have been prepared as the anode and La_{0.6}Sr_{0.4}MnO₃ (abbreviated as LSM) as the cathode in contacted with YSZ electrolyte on either side. The preliminary experimental results showed that the fabricated SOFC unit cell provided acceptable performance, which both cathode and anode side were prepared by screen printing technique. However, this experimental study just provides preliminary information of the fabricated SOFC which conducted in the initial step of the prospective future study that will be deliberately conducted by emphasizing on both materials development (i.e., materials with high activity) and also the fabrication methodologies; especially for the anode electrode side, in order to obtain high performance SOFC. The objective of this prospective future work includes obtaining high performance SOFC with effective availability for applying in the industrial applications. As this consequence, the further information and development are strongly required.

1. Introduction

Nowadays it is commonly well known that the energy crisis is seemed to be the major problem which dramatically affected the widening attention of many researchers. Many alternative energy sources are still in their different stages of development. Among the alternative energy sources, ceramic fuel cells, commonly known as solid oxide fuel cells (SOFCs), have been extensively developed for electric power generation applications. The most attractive feature of SOFCs is its clean and efficient production of electricity from a wide variety of fuels. Moreover, the SOFCs has potential to be manufactured and operated cost effectively and, thus, promises to be an important alternative source for generating complementary electric power in the future. However, many various parameters such as operating temperature, cathode, anode and electrolytic characteristics can strongly effect on the efficiency of SOFCs. Among these constituents in the SOFCs, its electrical and physical characteristics greatly affect power generation characteristics of the cell [1]. The performance of an anode is critically dependent on its microstructure [2], which in tune closely dependent on the initial powder preparation and anode forming process [1, 2]. It is usually agreed that the slurry-coating method resulted in single-cell with good reproducibility and reasonable performance, suggesting that this method can be considered for SOFCs fabrication [3].

2. Experimental

With the simple approach of screen printing, both anode and cathode pasting materials need to be previously prepared. For anode substrate preparation, NiO and YSZ were mixed with 4:1 molar ratio and ballmilled for 24 h, respectively. Then the welldispersed powders were sintered at 1400 °C for 12 h. After cooling down to the room temperature, the as-prepared anode powders were mixed with organic binder in an alumina mortar and applying mechanical grinding to enhance the separation of the particles in order to form the well-dispersed anode pasting materials. In this experiment, a 0.5 mm thick YSZ electrolyte support cell was painted by the as-prepared anode pasting materials through screen printing procedure. After pasting the anode material on the center of YSZ electrolyte, then it was sintered instantly again at 1400 °C for 5 h in order to obtain perfect attachment with the support electrolyte. The similar procedure is applied to fabricate cathode electrode; however, for cathode material, La_{0.6}Sr_{0.4}MnO₃ (abbreviated as LSM), La(CH₃COO)₃·1.5H₂O Sr(CH₃COO)₂·0.5H₂O and Mn(CH₃COO)₂·4H₂O were mixed with 300 ml distilled water. The mixture was suddenly heated by hot plate assisted with mind magnetic stirring to vaporize redundant water and other light organic compounds. After complete vaporizing, the cathode powders suddenly generated, and then sintering process was applied at 900 °C for 5 h. After cooling down to the room temperature, then glycol was



used as solvent for the as-prepared cathode powder to form the well-dispersed cathode pasting materials. Screen printing procedure was also applied to cathode side and after sintering the cell at 900 °C; thus, the unit cell was completely prepared.

In order to test this fabricated unit cell, hydrogen saturated with water at room temperature was used as a fuel at the anode side and ambient air was used as oxidant at the cathode side and the cell performance was investigated.

3. Results and Discussion

The anode and cathode pasting material which obtained from previously mentioned methodology are illustrated in Fig. 1a and b, respectively. These materials provide welldispersed powders of both initial components with the appropriate viscosity for pasting on the electrolyte layer (YSZ). However, some agglomerated particles could be observed which can be controlled during the powder preparation procedure. After performance's test was applied to this fabricated cell, the result was illustrated in the Fig 2.



Fig 1 (a) Anode pasting material; (b) Cathode pasting material; (c) Planar unit cell after applying performance test.

This I-V result shows acceptable performance of obtained cell compared to other literatures reviews [2, 3].It can be preliminary accepted that screen-printing can be applied to produce unit cell with good performance. Although, the maximum power density was only 0.008 W·cm⁻²; however the prospective study on fuel

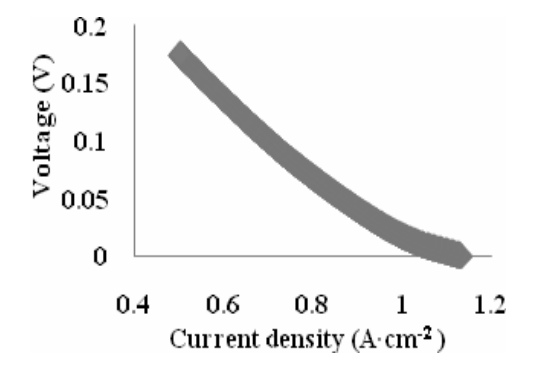


Fig 2 I-V of curve of cell measured at 1000 °C using H₂/O₂ as the operating gas

4. Conclusions and Recommendations for **Thailand**

Screen printing methodology can be applied technically to fabricate the SOFC with reproductively easy for transferring to an industrial scale. The cell shows the acceptable performance. Due this conducted to experiment was in the initiate research procedure; however, the development of the anode materials to obtain the higher activity and performance is still continuously required.

As previously mentioned, SOFCs are promising alternative energy sources which can be applied directly to various industrial applications. For Thailand, my mother land is still a developing country; hence, many useful technologies and research on both commercial and industrial developments are strongly required.

- [1] W.Z.Zhu, S.C. Deevi, Mater. Sci. Eng. A 362 (2003) 228-239.
- [2] S.P. Jiang, S.H. Chan, J. Mater. Sci. 39 (2004) 4405-4439.
- [3] S.D. Souza, S.J. Visco, L.C. De Jonghe, Solid State Ionics 98 (1997) 57.

135 NS-P06

Synthesis of Carbon Nanoparticles by Arc Discharge under Reduced Pressure Air

Chantamanee Poonjarearnsilp¹, Tawatchai Charinpanitkul¹, Apinan Soottitantawat¹, Noriaki Sano², Hajime Tamon²

¹Center of Excellence in Particle Technology, Department of Chemical Engineering, Chulalongkorn University, Bangkok, Thailand

²Department of Chemical Engineering, Graduate School of Engineering, Kyoto University, Kyoto, Japan

Tel./Fax: +66-2-218-6894, E-mail address: ctawat@chula.ac.th

Carbon nanostructures including multiwalled carbon nanotubes (MWCNTs) and multishelled carbon nanospheres (MSCNSs) were formed by DC arc discharge in reduced pressure air within a spherical chamber. The effects of arc current and pressure on the yield and morphology of carbon nanostructures were experimentally investigated. TEM and XRD analyses were performed to characterize the synthesized products. It was found that MWCNTs with relatively small diameter (less than 20 nm) could be found as deposit on the cathode tip. Based on XRD analysis, it was found that MWCNTs synthesized with the arcing current of 35 A had notably high crystallinity. Meanwhile, at higher arcing current of 55 A MSCNSs were obtained as the solid deposit scattering and sticking on the chamber wall. The percent yield of as-synthesized carbon nanoparticles increased with an increase in arcing current and a slight increase in reduced pressure of air. Based on our experimental results, the reduced pressure for the highest yield of MWCNTs was 190 Torr.

1. Introduction

Among several methods for preparing carbon nanoparticles (CNPs), arc discharge is one of the most practical means to yield highly graphitized nanotubes due to the high process temperature. Gas atmosphere under which the arc discharge is generated is one of the most important key factors affecting the yield and morphology of the CNPs. We expected that CNPs could also be produced in an air atmosphere though Cui et al. prepared MWNTs under a nitrogen atmosphere [1]. Because of the ultimate safety and convenience for tooling, dry air can be the most profitable process gas, but there have been few reports related to the preparation of CNTs in an air atmosphere.

2. Experimental

Direct current arc discharge between two pure graphite rods with vertical alignment had been carried out within a spherical chamber. After the chamber was evacuated to a designated vacuum level ranged from 190 to 760 Torr, the direct electrical current of 35 to 75 A was applied to the two graphite rods which were 1-2 mm apart for generating stable arc plasma, in turn vaporizing the anode to generate carbon nanoparticles. Those generated products could be observed as black soot depositing on the cathode tip and the chamber wall. TEM and XRD analyses were performed to characterize the fabricated products.

3. Results and Discussion

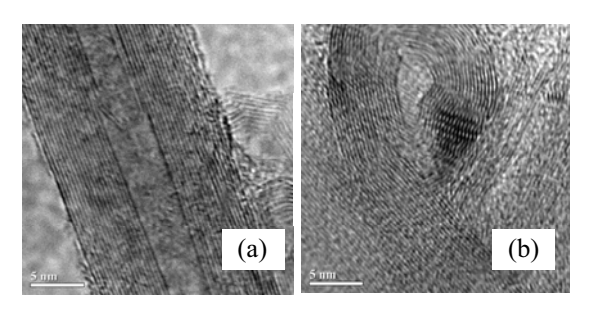


Fig. 1 TEM images of (a) MWCNTs and (b) MSCNSs synthesized at 190 Torr, 75 A and 600 Torr, 55 A, respectively.

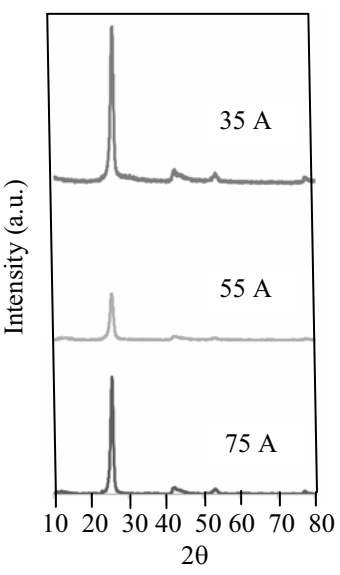
After the arc process without using any catalyst, we found that the quantity of product was remarkably reduced. In the case of using nitrogen as the accommodating gas, the yield of product was acceptably high [1]. But there was lower yield when air was employed. The quantity of as-synthesized product was dependent upon the process conditions such as current and pressure. At high current and air pressure the quantity of product increased but still much lower than that in nitrogen gas. This might be attributed to the efficient oxidation reaction in the air.

Fig. 1(a) shows MWCNTs with small diameter (less than 20 nm) could be fabricated with the arcing current of 75 A in the vacuum of 190 Torr. Meanwhile, fine quasi-spherical multishelled carbon nanoparticles were mainly



collected from the chamber wall deposit when a higher arcing current of 55 A in the vacuum of 600 Torr was employed (Fig 1(b)).

Based on XRD analysis shown in Fig. 2, it could be confirmed that the as-synthesized product, which was obtained when the arcing current of 35 A was employed, exhibit markedly high crystallinity. Moreover, the quality of the CNTs increases with a decrease in the reduced pressure air. In this work, the effects of gas pressure which provide high yield of MWCNT production was examined. Ebbesen et al. reported the optimized pressure to yield the highest amount of MWCNTs was 500 Torr [2]. Furthermore, Waldorff et al. also showed the effective pressure for CNP synthesis was about 200-300 Torr [3]. Based on



experimental results, the air pressure for the highest yield of **MWCNTs** was 190 Torr. It has been believed that accommodating air acts as "quenching media" for carbon vapor, which could attain at supersaturation of carbon clusters, leading nucleation and growth of carbon nanoparticles [4].

Fig. 2 XRD patterns of CNTs synthesized at different arcing current.

It should be noted that with the sufficient low vacuum level and the special configuration of the chamber used in this work, radial flow of carbon clusters emerging from the vaporizing anode would be beneficial for fabrication MWCNTs. This phenomenon accompany with the convective and radiation heat transport mechanism [5]. It should be experimentally observed that with an increase in arcing current the higher irradiation was generated from the arc. A higher gas flow could be visually observed during experiment. The anode consumption rate was drastically increased with the arcing current while the production yield was increased. Arc discharge could vaporize the graphitic anode, resulting in formation of numerous carbon clusters emerging from the arcing zone. Then higher amounts of carbon clusters would flow in all radial direction due to the convective flow mechanism [4]. Therefore, higher amount of MWCNTs could be fabricated.

4. Conclusions and Recommendations for Thailand

With high aspect ratio, MWCNTs would form a percolating network within the nonconductive matrix at much lower loading than traditional fillers. They would be more beneficial to composite applications. Besides composite application, MWCNTs have a broad range of potential applications including nanoelectronics or chemical sensors.

MWCNTs and MSCNSs could be synthesized by a DC arc discharge under reduced pressure of air without using any catalyst. The structure and amount of each type of nanoparticles could be controlled by arc current and the air pressure inside the chamber. Based on XRD analysis, carbon nanoparticles with high crystallinity could be prepared at the low arcing current of 35 A. There are possibilities to make use of such carbon nanoparticles, in particular MWCNTs for developing VOC gas sensors, which would be beneficial to Thailand.

- [1] S. Cui, P. Scharff, C. Siegmund, L. Spiess, et. al., Carbon 42 (2004) 931-939.
- [2] T.W. Ebbesen, H. Hiura, J. Fujita, Y, Ochiai et. al., Chem. Phys. Lett. 95 (1993) 83-90.
- [3] E.I. Waldorff, A.M. Waas, P.P. Friedmann, M. Keidar, J. Appl. Phys. 95 (2004) 2746-
- [4] E.G. Gamaly, T.W. Ebbesen: Phys. Rev. B 52 (1995) 2083-2089.

Improvement of Thermo-mechanical and UV Absorption of

PMMA with ZnO Nanoparticles

Thornchaya Satitpitakun¹, Hisashi Yamamoto², Anongnat Somwangthanaroj¹, Takafumi Seto², Yoshio Otani², Koh-hei Nitta², Tawachai Charinpanikul¹

¹Center of Excellence in Particle Technology, Department of Chemical Engineering, Chulalongkorn University, Bangkok, Thailand ² Department of Chemical Engineering, Graduate School of Natural Science and Technology, Kanazawa University, Japan *Email address: ctawat@chula.ac.th

In this present work, poly (methyl metacrylate)/ZnO nanocomposite has been successfully fabricated by melt mixing method. The concentration of ZnO nanoparticles in PMMA has been varied for examining its effect on the properties of PMMA/ZnO composite by dynamic mechanical analysis (DMA) and ultraviolet-visible (UV-vis) spectrophotometry. The results indicated that the thermal stability of the prepared PMMA/ZnO composite could be significantly improved. The composite glass transition temperature shifted to a higher temperature with the increasing ZnO loading. Furthermore, UV absorption of ZnO PMMA composite was higher when ZnO concentration was increased and the composite with 0.5 wt% of 20-nm ZnO was sufficient for shielding UV irradiation.

1. Introduction

Because of the wide band gap (3.37 eV), high exciton binding energy (60 meV) at room temperature and high mechanical and thermal stabilities, zinc oxide (ZnO) is used as not only semiconductor but also functional filler for polymer composites [1]. Poly (methyl methacrylate) (PMMA) is an optically clear thermoplastic material. It is widely used as an artificial glass because it shows higher impact strength as well as resistant to weak acid. alkaline solutions, non-polar solvents, oils and water. Therefore, PMMA is commonly used for alternative constructing interior instead of glass. It is well recognized that PMMA is excellent host material for nanoparticles of metal and semiconductors. ZnO can absorb a wide range of UV light (λ<400 nm) which could convert photonic energy to excitation energy [2]. Therefore, ZnO could especially be used in shielding UV irradiation, which is beneficial to applications of buildings or automobiles protection. The objective of present work is to improve optical and mechanical properties of PMMA film with ZnO nanoparticles. The effect of concentration of ZnO particles on UV abortion and dynamic mechanical properties was experimentally studied and analyzed.

2. Experimental

In order to prepare composite of PMMA/ZnO, commercial ZnO particles with average size of 20 nm purchased from Wako Pure Chemical Industries and PMMA by Kuraray Co. LTD., were employed.

with nanoparticles designated loading were mixed with PMMA using a tworoll mill at 200°C for 10 min. The mixed materials were subject to compression molding to prepare 0.5 mm thick sheets. The operating condition of the compression molding machine was 200 °C and 100 MPa. Then the specimen was immersed in 0°C water for cooling down.

The optical properties of prepared specimens were studied by UV-vis-NIR spectrometer (Jasco V570). The scanning speed was 400 nm/min in the wavelength range of 200-800 nm. The nanocomposite film samples were cut into rectangular shapes of 20mm×5mm×0.20mm. Dynamic mechanical analysis of the specimens was performed using a DVE-V4 FT with a heating rate of 1 °C/min and frequency 10 Hz.

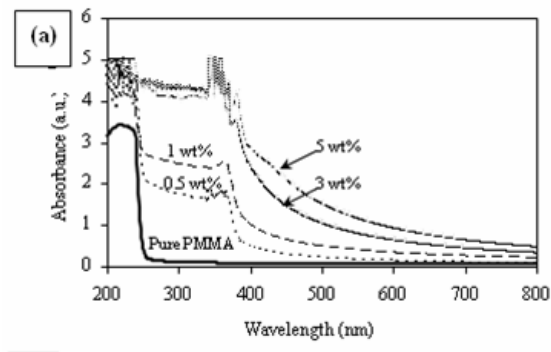
3. Results and Discussion

Figure 1(a) shows the absorption spectra of composite with ZnO concentrations of 0.5, 1, 3 and 5 wt%. The intensity of UV absorbance peak increases with ZnO concentration. Although there were some noises in the absorbance curves at a high ZnO concentration, the peak absorption existed at the wavelength of 367 nm, which is smaller than 378 nm (the theoretical wavelength of bulk ZnO corresponding to band-gap of 3.3 eV). The blue-shift phenomenon for 20-nm ZnO particles is attributed to the quantum effect of nanoparticles. Kanemitsu et al.[3] claim that semiconductive nanoparticles would play a role in the electronic interaction due to the

NS-P07



confinement of excitons and electrons in nanoparticles which would lead to efficient energy transfer.



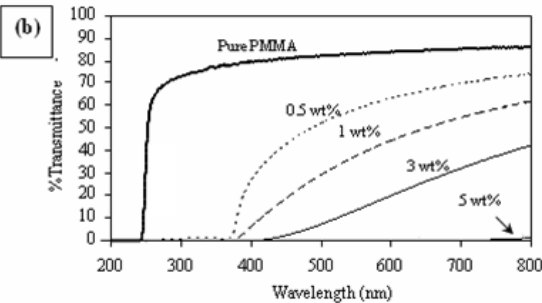


Fig. 1 Optical characteristics of PMMA/ZnO nanocomposite films (a) UV absorbance, (b) UV transmittance

Fig.1 (b) shows specific transmission of UV light. It could be clearly observed that only 0.5 wt% of 20-nm ZnO compounded with PMMA could significantly shield UV irradiation, resulting in a remarked decrease in % transmission. Xiong et al. also reported that 7 wt% of 60-nm ZnO particles added into poly(stryrenebutylacrylate) completely shields UV irradiation [4]. As a result, it is reasonable to imply that the nanocomposite prepared in this study would probably exhibit UV protection. Thereby ZnO nanoparticles could improve the UV durability of the PMMA film.

Meanwhile, the loss modulus (E") of the composites was characterized by a dynamic mechanical analyzer (DMA). The loss modulus relates to the energy loss due to polymer chain movement and the E" peak corresponds to the glass transition temperature (T_g). Figure 2 indicates that the T_g of PMMA/ZnO nanocomposites was shifted with the increment of ZnO content and exceeded that of pure PMMA. This would be attributed to the mobility restriction of PMMA chain due to the entangling ZnO particles within PMMA matrix.

4. Conclusions and Recommendations for Thailand

PMMA/ZnO nanocomposite films have been successfully prepared by a two-roll mill. When concentration of ZnO in the composite was increased, UV absorption of the composite became higher. Based on thermo-mechanical test, the PMMA/ZnO nanocomposite films with higher ZnO content exhibited higher glass transition temperature compared with that of pure PMMA. These results would exhibit possibility to apply PMMA/ZnO composite for UV-cut window, which would be beneficial to many countries including Thailand. However, capability of producing ZnO nanoparticles would be required for Thai manufacturers. Moreover process of manufacturing of UV shielding material should be further studied for finding the most effective route.

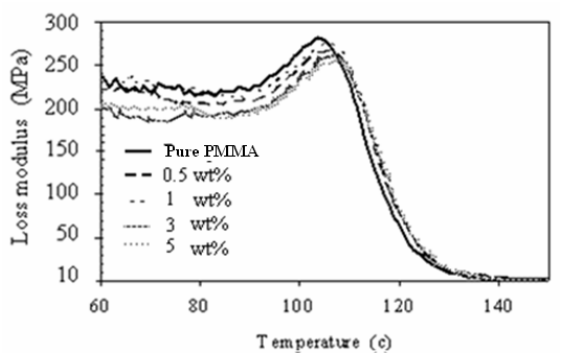


Fig. 2 Effect of ZnO loading on loss modulus of PMMA/ZnO nanocomposite

5. References

- [1] P. Yang, H. Yan, S. Mao, R. Russo, J. Johnson, R. Saykally, N. Morris, J. Pham, R. He, H.-J. Choi, Adv. Funct. Mater. 12 (2002) 323–331.
- [2] B. Mahltig, H. B. ttcher, K. Rauch, U. Dieckmann, R. Nitsche, T. Fritz, Thin Solid Films 485 (2005) 108–114
- [3] Y. Kanemitsu, A. Ishizumi, J. Luminescence 119–120 (2006) 161–166
- [4] M. Xiong, G. Gu, B.You, L. Wu, J. Appl. Polym. Sci. 90 (2003) 1923-1931.

Acknowledgement

This work is partially supported by the Centennial Fund of Chulalongkorn University and KUSEP of Kanazawa University.

NS-P08

Synthesis and Characterization of SiC/SiO₂ Core-Shell Nanowires

Wasana Khongwong, Masamitsu Imai, Katsumi Yoshida, Toyohiko Yano

Research Laboratory for Nuclear Reactors, Tokyo Institute of Technology, Tokyo, Japan E-mail address: khongwong.w.aa@m.titech.ac.jp

 $\rm SiC/SiO_2$ core-shell nanowires were synthesized through a simple thermal evaporation of silicon powders during decomposition of methane (CH₄) gas. The influence of two parameters, reaction temperature (1300, 1350 and 1400 $^{\circ}\rm C$), and soaking time (1, 3 and 6 h), were investigated. X-ray diffractometry, field-emission scanning electron microscopy, transmission electron microscopy, scanning TEM, and high-resolution TEM were used to characterize the as-grown products. The typical synthesized nanowires at different conditions possess the diameter of was not more than 100 nm with several tens micrometers in length. It can be reported that using higher temperature and longer soaking time lead to more complete reaction to attain high yield nanowires. Base on the results, it was also found that the typical nanowires should be grown via the oxide-assisted growth (OAG) mechanism.

1. Introduction

In recent years, one-dimensional (1D) nanoscale structures such as wires, rods, tubes, springs, belts, and etc. have attracted much attention due to their remarkable properties and potential applications as interconnects or functional components in nanoscale electronics, nanocomposites and nanodevices including field-effect transistors [1]. Among these materials, silicon carbide nanowires (SiCNWs) are the leading material, because of its excellent thermal and mechanical properties and large band gap [2].

Various methods have been addressed for preparation SiC nanostructures, including chemical vapor deposition (CVD) [3], laser ablation [4], arc discharge [5], and so on. However, synthesis of SiC/SiO₂ core-shell nanowires by means of simple evaporation of Si have not reported yet.

In this work, we present a simple way to fabricate the β -SiC/SiO₂ core-shell nanowires without adding metal catalysts from outside through thermal evaporation of Si powders among flowing CH₄ gas. The effect of reaction temperature and soaking time on growth of nanowires were studies.

2. Experimental Procedure

Silicon powder, SN (average particle size ≈ 50 nm, 99% nominal purity) was used as raw powder. The experiment was conducted in a horizontal mullite tube furnace. First, silicon raw powder was put in the mullite boat which was then covered by a thin sheet of alumina fiber net. After placing the whole set into the center of the furnace, the chamber was initially evacuated to a pressure below 1.33 Pa. Ar gas was then applied at a flow rate of 0.6 l/min into the tube. The furnace was first ramped to 1200 °C at 10°C/min and then continued to heat but

5°C/min to preset target temperatures of 1300, 1350 and 1400 °C. At maximum temperature, H₂ at a flow rate 20 sccm was introduced for 2 min before flowing of CH₄ gas at a flow rate 10 sccm for 30, 90 and 180 min in batch for soaking time of 1, 3 and 6 h, respectively. The furnace was allowed to cool down to room temperature in Ar atmosphere and then the mullite boat containing as-grown SiC nanowires was moved out from the chamber.

After reaction at different conditions, the products were obtained in the boat. X-ray diffractometry (XRD, CuKα, PW 1700, Philips, Holland), field-emission scanning electron microscopy (FE-SEM, S-4800, Hitachi, Japan), transmission electron microscopy (TEM, H-9000, Hitachi, Japan), and scanning TEM (STEM) were used to characterize the synthesized products.

3. Results and Discussion

3.1 Effect of reaction temperature

The yield of white-blue wool-like products in the boat increased with temperature. The XRD analysis indicated that the as-synthesized products consisted of β-SiC. FE-SEM observation confirmed that the wool-like product from every specimen was wire-like nanostructures. Lengths of the nanowires were up to several tens micrometers and diameter ranging from 5-60 nm. Fig. 1 shows typical FE-SEM image of product synthesized at 1400 °C. The upper right inset of Fig. 1 is a high magnification TEM of a typical nanowire, clearly revealing that the nanowire consists of a dark-contrasted inner core and a light-contrasted outer shell. The result of STEM-EDX selected-area and electron diffraction (SAD) patterns altogether of core and shell indicated that the core part could be indexed with the β-SiC crystal with twins and

the fiber axis direction was found to be {111} of β -SiC, while only diffused spots (d = 0.36) nm) sited along the fiber direction was detected from the un-completed crystallinity shell layer.

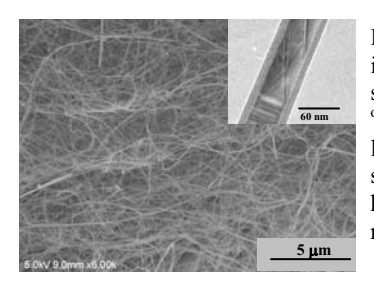


Fig. 1 typical FE-SEM image of product synthesized at 1400 °C, it composed of amount large straight, curved. haphazard distributed nanowires.

The typical thick SiC/SiO₂ core-shell nanowires were observed by TEM. The result shows that higher reaction temperature is, thicker cores are, and clearly to observe thickness of wires increased when using reaction temperature at 1400 °C K. The thickness of core/shell of nanowires synthesized at 1300, 1350 and 1400 °C are 15/5, 20/5 and 40/10 nm, respectively.

3.2 Effect of soaking time

As-synthesized products of SiC nanowires were fabricated at 1350 °C with soaking times of 1, 3 and 6 h. It seems increasing the soaking time increased amount of product.

FE-SEM observation indicated that the all as-grown products consisted of large quantities of randomly distributed wire-like shape products. Lengths of the nanowires are up to several tens of micrometers and diameter less than 100 nm. TEM images of typical thick coaxial structure nanowires under soaking time at 1, 3 and 6 h indicated that only thickness of shell layer increased after change in soaking time from 1 h to 3 h. After synthesized for 6 h, both thickness of core and shell became larger than those synthesized for 3 and 1 h. The thickness of core/shell of typical nanowires synthesized at 1, 3 and 6 h are 20/5, 20/10 and 30/12.5 nm, respectively.

Although the detailed growth mechanism of β-SiC/SiO₂ coaxial nanowires is not still completely understood yet, we infer that the overall reactions of nanowires formation can be written as following reactions (1)-(4).

According to above, the SiC/SiO₂ core-shell nanowires were formed through the reaction of SiO and methane. It seems the SiO is important factor on nanowires growth. Thereby, this mechanism can be classified into the oxide-assisted growth (OAG) mechanism.

4. Conclusion and Recommendations for **Thailand**

Based on the experimental results of the current work, the conclusions can be written as follows. The high yield of very long SiC/SiO₂ core-shell nanowires with diameter not more than 100 nm are fabricated by the simple method through evaporation the mechanism. The yield of as-synthesized products increased with synthesis under using higher reaction temperature, and longer soaking time. The synthesized nanowires at higher reaction temperature and longer soaking time possessed larger core and thicker shell than those nanowires prepared at lower reaction temperature and shorter soaking time.

This research can be applied for many such as fields in Thailand electronic components, nanocomposites, including solar cell because SiC nanowires have very high surface area and the elasticity and strength of an individual SiC nanowire is much higher than that of bulk SiC.

- [1] A.M. Morales, C.M. Lieber, Science 279 (1998) 208.
- [2] H.K. Seong, H.J. Choi, S. K. Lee, J.I. Kee, D.J. Choi, Appl. Phys. Lett. 85 (2004) 1256.
- [3] H.E. Dai, E.W. Wong, Z.H. Lu, H.S.C. Fan, C.M. Liber, Nature, 375 (1995) 769.
- [4] Y. Zhang, K. Suenaga, C. Colliex and S. Iijima, Science 281 (1998) 973.
- [5] T. Seeger, P. Kohler-Redlich, M. Ruhle, Adv. Mater. 12 (2000) 279.

Apiluck Eiad-ua, Takashi Shirai, Hideo Watanabe, Tomohiro Yamakawa, Koji Orito, Masayoshi Fuji*, Minoru Takahashi

Production of Non-firing Ceramic from Paper Sludge Ash

Ceramic Research Laboratory, Nagoya Institute of Technology, Tajimi, Gifu, Japan Tel.: +81-5-7227-6811, Fax: +81-5-7227-6812, *E-mail address: fuji@ nitech.ac.jp

Non-firing ceramic of paper sludge ash have been successfully fabricated by combination of surface activation of the powder and chemical solidification. Surfaces of paper sludge ash powder were mechanochemically activated using a planetary ball-milling, and the mixture of activated powders with 15 wt.% KOH aqueous solution was cast into a mould and keep at 25°C for 7 days under relative humidity of 90%. All the compositions can be solidified at ambient temperature. This proposed process is an attractive route for shaping waste materials into ceramics without using the conventional sintering step.

1. Introduction

Nowadays, paper sludge has become one of the most serious environmental problems. Because the paper sludge dumped on land has increased, environmental burden. The paper sludge is usually landfilled or burned to produce paper sludge ash, which is composed of more mineral such as SiO₂ and Al₂O₃ [1] as starting material of ceramic. Mechanochemical (MC) treatment is considered as potential candidate for initial material pretreatment because of it involves the formation of product phase at the interface of the reactants. The mechanochemical treatment initiated by intensive of milling in highenergy ball mills could be good choice for the ceramic powder preparation [2]. On the other hand, it is well known that alkaline solution as a binder between ceramic particles, which is responsible for solidification to form a strong green body at room temperature [3]. It is possible to convert waste materials into valuable ceramics by using solidification assisted by surface activation of the powder by planetary ball milling under ambient temperature condition. The objective of this work is to fabricate ceramic without firing using the activated particles from paper sludge ash as raw material to reduce industrial waste.

2. Experimental Procedure

The paper sludge ash powder was used as a raw material. Planetary ball-milling was used for mechanochemical treatment of powder. The mill was rotated between 100 to 300 rpm at 60 min of milling time. The products were prepared by mechanical mixing an amount of paper sludge ash and alkaline solution (KOH) to form homogeneous slurry throughout the series of compositions. After being mixed at 2,000 rpm for 5 min with an electric mixer, the

slurry was poured to Teflon mold and kept at room temperature until solidification. After demolding, the specimens were dried at 25°C (RH 90%) for 7 days in the steam oven.

X-ray diffraction was used for the qualitative determination of the crystal phases present in paper sludge ash and microstructural examination of surfaces were carried out using a SEM [4-5]

3. Results and Discussion

Fig. 1 shows the XRD pattern of raw material treated for 0 to 300 rpm at 60 minutes. From this figure, the raw material is mainly composed ofwollastonite (CaSiO₃), gehlenite $(Ca_2Al_2SiO_7)$ and calcium aluminate (Ca₅Al₆O₁₄). Peak intensity of crystalline decreases with increasing rotation speeds. This is because that the particles were involving in miniaturization and amorphilization with influence of high energy action of ball milling. Fig. 2 shows the microstructure of raw material without and

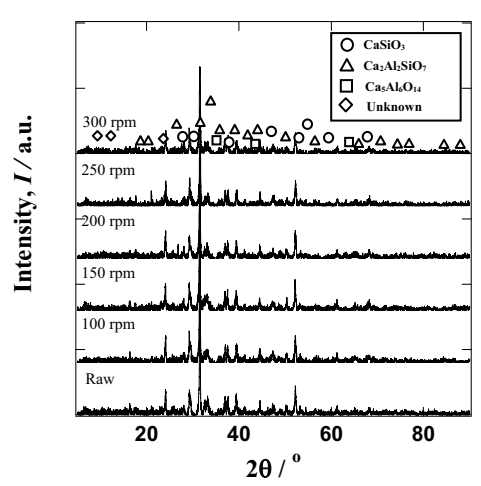
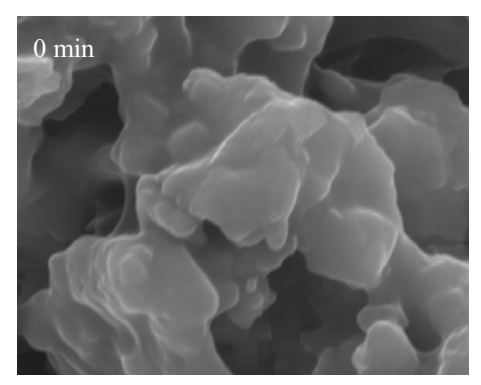


Fig.1 XRD patterns of the initial material treated by planetary ball-milling at 0-300rpm

. **D**00

NS-P09





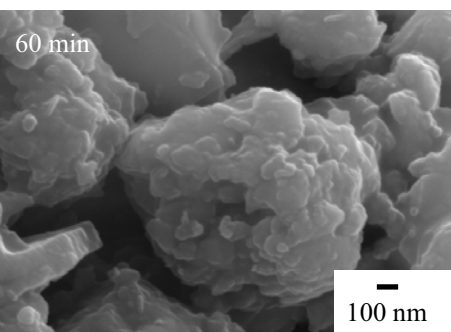


Fig.2 SEM images of initial material treated by planetary ball-milling at different time

with treatment for 300 rpm, 60 minute by planetary ball-milling. This study examined microstructures of samples understand developments on how MC treatment influences the raw material structure. The treated sample consists of the fine particles having decreasing size with an increasing of milling time.

4. Conclusions and Recommendations for Thailand

Non-firing ceramic was successfully fabricated from paper sludge ash. This method was done by combination of the both mechanochemical and chemical reaction of ceramic particles converting waste material into valuable ceramics without using the conventional sintering step. The benefit of this research which contributes to Thailand is to reduce industrial waste such as paper sludge and change it into valuable ceramics. Because Thailand have many industrial wastes such as, paper sludge ash, rice husk ash and palm oil fuel ash, which become the most seriously environmental problem. On the other hand, all the waste material on mentioned above, are composed of mineral of Al₂O₃ and SiO₂ as starting material of ceramic. Therefore, it is possible to reduce waste material from industry by fabricating to valuable ceramics.

- [1] K. Okada, Y. Onoa, Y. Kameshima, A. Nakajima and K. J.D. MacKenzie, J. Hazard. Mater. 141 (2007), 622-629.
- [2] B.D. Stojanovic, A.Z. Simoes, C.O. Paiva-Santos, C. Jovalekic, V.V. Mitic, J.A. Varela, J. Eur. Ceram. Soc. 25 (2005) 1985-1989.
- [3] T. Yamakawa, M. Fuji and M. Takahashi, Proc. Int Symp. on Eco Topia Sci. 2007.
- [4] C. Shi and A. Fernandez-Jimenez, J. Hazard. Mater., B137 (2006) 1656-1663.
- [5] J-A. Kim, J. Eur. Ceram. Soc, 26 (2006) 1023-1034.

143 NS-P10

Characterization of Short Glass Fiber-Reinforced PC/ABS Blends

Nattapon Samakrut¹, Satida Krailas², Sarawut Rimdusit^{1,*}

¹Polymer Engineering Laboratory, Department of Chemical Engineering, Faculty of Engineering, Chulalongkorn University, Bangkok, Thailand ²PTT Phenol Company Limited, Chatuchak, Bangkok, Thailand Tel.: 66-2-218-6862, Fax: 66-2-218-6877, *E-mail address: sarawut.r@chula.ac.th

Polycarbonate (PC) and acrylonitrile-butadiene-styrene (ABS) blends of a high melt flow index formulation are reinforced with short glass fibers at 0 to 30 wt% using a fixed fiber length of 3 mm. From rheological studies, the viscosity of the filled systems increases with an increasing content of the short glass fiber. The viscosity of the compound at 30 wt% fiber content exhibits a value about one order of magnitude higher than that of the neat PC/ABS. Shear thinning behavior was also observed in those filled and unfilled polymers. From thermogravimetric analysis, the degradation temperature of the composite specimen was found to be negligibly affected by the presence of the glass fiber. The technique was also used to confirm good fiber dispersion in this PC/ABS composites. Scanning electron micrographs reveal that the glass fiber adhered relatively well to the PC/ABS matrix which is crucial to the effective reinforcement of the fiber.

1. Introduction

Polycarbonate (PC) is used in specialty applications from its high toughness, higher continuous working temperature, high modulus and good transparency. The drawbacks of PC, however, are high melt viscosity (poor processability) and notch sensitivity. The disadvantages of PC can be effectively overcome by blending with thermoplastics or thermoplastic elastomers of which ABS is the most popular candidate. The addition of ABS not only minimizes the drawbacks of PC but also retains the other superior mechanical properties and also generates other useful properties such as glossiness and low-temperature toughness [1, 2].

For some specific applications that require substantially high mechanical properties (such as a case of notebook etc.), one effective method to improve the properties and to maintain its processability using traditional extrusion or injection is by reinforcing with short glass fiber. Therefore, the major purpose of this study is to investigate the effect of short glass fiber on properties of the resulting PC/ABS composites. The composites are useful for applications in the electronic and electrical appliance industries in Thailand.

2. Experimental

2.1 Materials

PC and ABS pellets used were a commercial product. The short glass fiber was purchased from Chongqing Polycomp. International Corp., China.

2.2 Preparation of PC/ABS Composites

Both PC and ABS pellets were dried to constant weight at 105°C for at least 4 hr in an

air-circulated oven to remove some moisture, which could cause PC degradation and defects [3].

Compounding of PC, ABS and glass fiber was carried out by a twin screw extruder (Thermo Haake Rheomex, Haake PolyLab Co., Ltd., Germany). The fiber contents were varied from 0 to 30 wt%. The extruded strands were cut into pellets (lengths of > 3 mm.) and dried before use.

2.3 Experimental Procedures

2.3.1 Rheological Property Measurement

The melt viscosities of PC/ABS blends having glass fiber loadings of 0 to 30 wt% at a constant shear rate (1 sec⁻¹) were determined using a parallel plate rheometer, Haake Rheo Stress 600, from Thermoelectron Cooperation. The diameter of each plate is 20 mm and the gap between the plates was fixed at 1 mm.

2.3.2 Thermogravimetrix Analysis

The degradation temperature (T_d) and residual weight of the PC/ABS blends at various glass fiber contents were studied using a Perkin Elmer Instrument Technology (SII Diamond TGA/DTA) thermo gravimetric analyzer at a heating rate of 20°C/min . The temperature was scanned from 50 to 700°C under air atmosphere. The purge air flow rate was 50 ml/min.

3. Results and Discussion

3.1 Rheological Properties

From Figure 1, the viscosity of PC/ABS blend reinforced with short glass fibers was increased with increasing the content of the glass fiber. The plots also indicate the decrease in viscosity with increasing shear-rate, the characteristic of shear thinning fluid. The



viscosity value of 30wt% glass fiber filled compound was about one order of magnitude higher than that of the neat PC/ABS used.

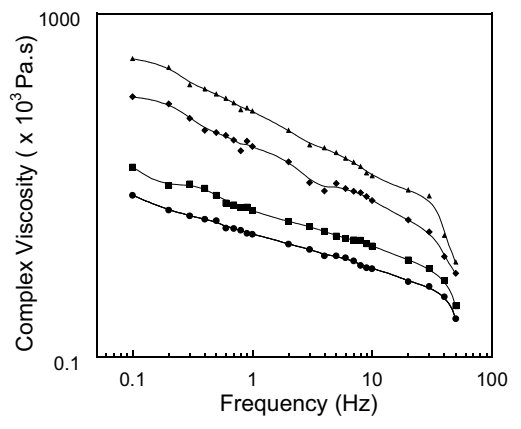
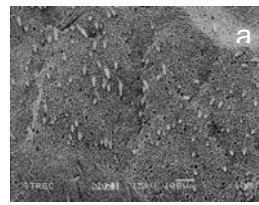


Fig. 1 Viscosity of PC/ABS blend at various glass fiber contents (\bullet) 0%, (\blacksquare) 10%, (\bullet) 20% and (\triangle) 30%

3.2 Fiber Dispersion and Composite Interface from Microscopy

The SEM micrographs of the fracture surface of PC/ABS blend filled with 10 wt% of short glass fiber are shown in Figure 2a and 2b. Figure 2a reveals the relatively good dispersion of the short glass fiber in the PC/ABS matrix. The uniform dispersion is one key feature to yield a good composite property. Figure 2b illustrates also the glass fibers to substantially adhere to the PC/ABS matrix which is essential for its mechanical property enhancement by the reinforcing fiber.



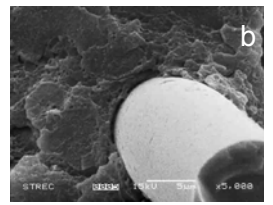


Fig.2 SEM micrographs of fracture surface of PC/ABS/GF (a) (×1000), (b) (×5000)

3.3 Thermogravimetric Analysis

The thermal degradation of glass fiber-reinforced PC/ABS blend is presented in Figure 3. The TGA thermograms of all composites were found to decrease in two steps. The first step was between 360 and 460°C and the second step was approximately 520°C. From the figure, it can be seen that the degradation temperature at 5% weight loss was ranging from 371 to 380°C. Moreover, the residual solid of all composites were found to be consistent with the composition in the molding compounds suggesting good dispersion of the fiber in the PC/ABS matrix.

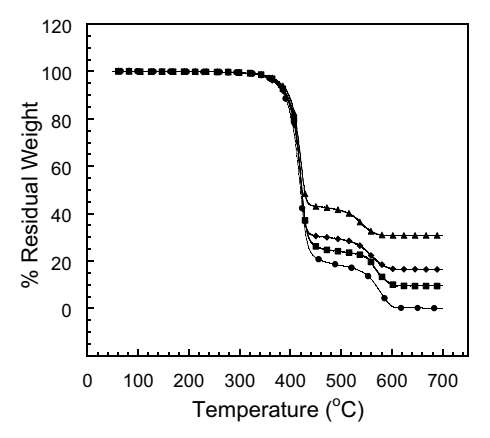


Fig. 3 TGA thermograms of PC/ABS blend at various glass fiber contents (\bullet) 0%, (\blacksquare) 10%, (\bullet) 20% and (\triangle) 30%

4. Conclusions

Short glass fiber-reinforced PC/ABS blends has been widely exploited by the industry in Thailand especially in automotive and electronic applications due to its good processability and thermal properties.

The viscosity of PC/ABS reinforced with short glass fiber increased with increasing the glass fiber content whereas substantial bonding between the glass fiber and the PC/ABS was observed. The processing condition used can provide a specimen with relatively uniform fiber dispersion.

- [1] S. Balakrishnan, N.R. Neelakantan, D. Nabi Saheb, J. P. Jog, Polymer 39[23] (1998) 5765–5771.
- [2] G. Wildes, H. Keskkula, D.R. Paul, Polymer 40 (1999) 7089-7107.
- [3] R. Greco, M. F. Astarita, L. Dong, A. Sorrentino, Adv. Polym. Tech. 13 (1994) 259.

NS-P11

Thermomechanical Properties of TPP-Filled Polycarbonate/Acrylonitrile-Butadiene-Styrene Blends

Teerapat Matchimapiro¹, Potejanee Sornthummalee², Thanyawat Pothisiri¹, Sarawut Rimdusit^{1,*}

¹Polymer Engineering Laboratory, Department of Chemical Engineering, Faculty of Engineering, Chulalongkorn University, Bangkok, Thailand ²PTT Phenol Co., Ltd., 36th Floor, Sun Tower, Chatuchak, Bangkok, Thailand ³Department of Civil Engineering, Faculty of Engineering, Chulalongkorn University, Bangkok, Thailand

Tel. +66-2-218-6862, *E-mail address: sarawut.r@chula.ac.th

Effect of triphenly phosphate (TPP) on thermophysical properties of polycarbonate/acrylonitrile-butadiene-styrene (PC/ABS) blends for flame resistant application was investigated. From dynamic mechanical analysis, two glass transition temperatures (T_g 's) for PC and ABS phases at 158 and 125 $^{\rm O}$ C, respectively, of the blend clearly suggested the immiscible nature of the two polymers though with some degree of mixing. The amount of the TPP additive was systematically varied. The results revealed that the value of the glass transition temperature (T_g) from Tan of the PC/ABS blend decreased with increasing the content of TPP. In contrast, with increasing the contents of TPP, the strange moduli of the blend specimens at room temperature systematically increased. The V-0 category of UL-94 standard of flammability test can also be achieved using the TPP system.

1. Introduction

In recent years, PC/ABS blends have become one of the most frequently used engineering plastics. Their commercial success is due to an appropriate properties combination of the two components: high thermal stability and good impact behavior of PC and easy processability and economy of Furthermore, the PC notch sensitivity is improved by the more reliable notch impact ABS resistance. The flammability of PC/ABS blends strongly depends on the mass ratio of PC and ABS. PC by itself exhibits a V-2 rating in the UL-94 test, whereas ABS has a rather flammable rubber component so it is more combustible and tends to produce heavy black smoke. Furthermore, due to a recent environmental concern, there has been a demand for non-halogenated flame retardant plastics. Phosphorus-base flame retardants are believed to be effective both in gas phase and in condensed phase although a specific flame retardant works dominantly in either of two phases. TPP is the most widely used flame retardants and is reported to exhibit relatively good fire-retarding performances [1]. The additive has been reported to be compatible with both PC phase and ABS phase [1-2].

2. Experimental

2.1 Materials

The polymeric materials used in this investigation were commercialized PC and ABS. The commercial TPP flame retardant was purchased from Fluka Co., Ltd., with 99.98% purity, melting point of 48°C and boiling point of 245°C..

2.2 Preparation of PC/ABS blends

Melt mixing of PC, ABS, and TPP was carried out by a single screw extruder. PC and ABS pellets were dried for several hours to a constant weight in an air-circulated oven, in order to remove any moisture. PC was mixed with ABS as the high impact formula [1], and the blend was compounded with TPP at various weight percentages. The PC/ABS blend was cooled in air and then cut by a pelletizer.

2.3 Dynamic mechanical analysis (DMA) of the blends

DMA was used to characterize the viscoelastic properties of the studied PC/ABS blends. The tests were carried out at a frequency of 1 Hz in the three-point bending mode using NETZSCH DMA242 equipment under N_2 atmosphere. The thermograms were obtained in a temperature range of 30 to 180 °C at 2 °C /min.



3. Results and discussion

Storage modulus curves of the pure PC/ABS in Figure 1 exhibit two step changes corresponding to the positions of T_os of the PC and ABS phases at about 155°C and 122°C, respectively. The presence of two step changes clearly suggested the immiscible nature of the two polymers. This behavior is in good agreement with that reported elsewhere [3-4]. In the case of PC/ABS modified with TPP, the flame retardant was found to systematically enhance the room temperature strange modulus of the PC/ABS blend. The positions of the step changes shifted to lower temperature with the TPP addition. The storage modulus of the system with TPP was found to be higher than that without TPP.

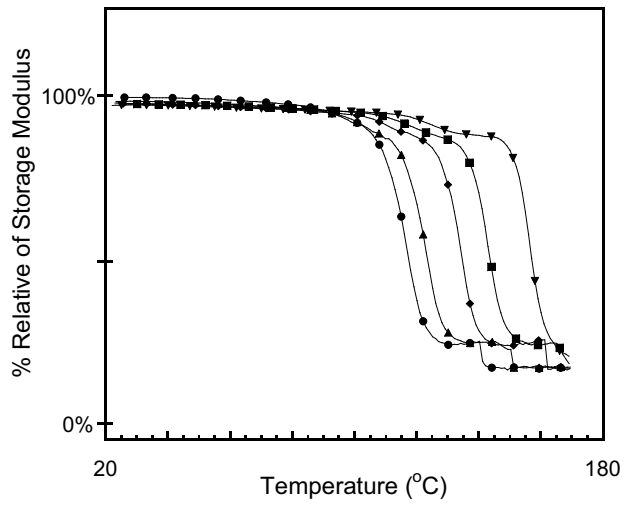


Fig. 1 % Relative of Storage modulus of PC/ABS blends at various TPP compositions.

(**▼**) TPP1, (**■**)TPP2, (**♦**)TPP3, (**△**)TPP4, (**●**)TPP5

Glass transition temperatures PC/ABS/TPP blends were also observed in the DMA thermograms based on the α -relaxation peak of tan δ . Figure 2 shows tan δ of PC/ABS PC/ABS/TPP systems compositions. It can be seen that all of PC/ABS/TPP blend samples exhibited two relaxation peaks of the tan δ which were designated as the T_gs of the PC-rich and ABSrich phases of the blends. The one at higher temperature is of the PC phase, whereas that at lower temperature belongs to the ABS phase. In the case of PC/ABS filled TPP, the flame retardant was observed to cause the lowering of the T_g's of both phases. With adding TPP, Tg values of the PC phase were lower at a larger degree compared to those of the ABS phase (see inset of Figure 2). The behavior suggested that TPP flame retardant might preferably compatible with the PC phase to the ABS phase thus causing the greater reduction in their T_g values with an addition of TPP.

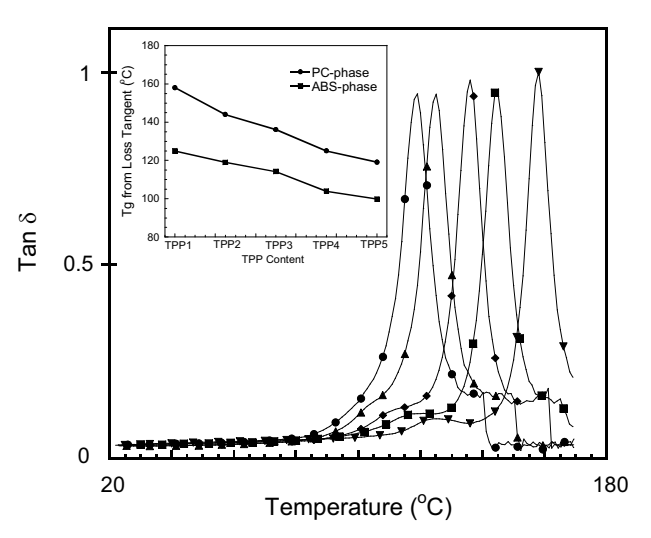


Fig. 2 Tan δ of PC/ABS blends at various TPP compositions.

(**▼**) TPP1, (**□**)TPP2, (**♦**)TPP3, (**△**)TPP4, (**●**)TPP5

4. Conclusions and Recommendations for **Thailand**

The improvement in PC/ABS blends with flame retardant has been widely exploited by the industry in Thailand especially in automotive and electronic applications. Therefore, this research has been conducted. PC/ABS blend exhibited two Tg's of the PCrich and ABS-rich phases as indicated by the existence of two step changes in their storage moduli and the appearance corresponding two tan peaks. TPP flame retardant was found to enhance the storage modulus at room temperature systematically reduce the two glass transitions of the PC/ABS blend.

- [1] S.V. Levchik, E.D. Weil, Polym. Int. 54 (2005) 981–98.
- [2] K.H. Pawlowski, B. Schartel. Polym. Int. 56 (2007) 1404–1414.
- [3] C.J.G. Plummer, C.L. Soles, C. Xiao, C.J. Wu, H.H. Kausch, A.F. Yee, Macromolecules 28 (1995) 7157
- [4] J.E. Mark, Physical Properties of Polymers Handbook, Woodbury, New York, 1996.

NS-P12

Acid Sulfate Soil-landform Relationships in

the Lower Central Plain, Thailand

Naruekamon Janjirawuttikul, Masatomo Umitsu

Graduate School of Environmental Studies, Nagoya University, Nagoya, Japan Tel: +81-5- 2789-2289, Fax: +81-5-2789-2236, E-mail address: naruekamon@gmail.com

The morphology of acid sulfate soils (ASSs) and their relation to landforms of the Lower Central Plain of Thailand were studied. Characteristics of ASSs are categorized into three groups. Group I is ASSs with very strongly to extremely acid conditions throughout profiles. It extends in the area of upper boundary of deltaic plain. Group II is ASSs with reducing C horizons which contain high sulfidic material, after airdried their reactions are decreased to ultra to extremely acid. It occupies in the lower boundary of deltaic plain. Group III represents non ASSs with reducing C horizons which contain low sulfidic material. Most of them extend across in the area of deltaic tidal to tidal plain. ASS is located in the area of recent deltaic plain which considered as developed in condition closely related to the Holocene paleo-environment, especially to the intertidal to deltaic condition at the middle Holocene transgression as mangrove forest and shallow marine environments. In contrast to non ASS, it is distributed in area of embayment during the time of middle Holocene transgression. This indicated sediment of the environment has low sulfidic material content, therefore, ASSs do not develop in the area. However, ASSs are developing in the suitable environment of sulfidic material forming as the eastern active tidal flat of the Gulf of Thailand.

1. Introduction

ASS is one of the serious problem soils. Since the soil contains iron sulfides which produce sulfuric acid when exposed to air [1]. It is especially formed in the estuaries, mangrove swamps, and tidal plains. ASS distributes widely in the Southeast Asia such as Indonesia, Vietnam, and Thailand [2]. The ASS occupies in Thailand around 881,000 ha, and the largest region of distribution is the Lower Central Plain [3], one of the best areas for economic crop of Thailand. However, the occurrence of ASS probably causes of low productivity in the area. Sustainable development requires integrated soil, water and cropping system management over whole landscapes. In the absence of specific information, land use evolves by trail and error, due to insufficient knowledge to conserve and develop land in accurate aspect. For agricultural activities, the wrong is not only causing of decreased yield but also deteriorate capability of soil and impact environment seriously. This paper is aimed to determine the morphology of ASS in the Lower Central Plain of Thailand in relation with the pattern of the paleo-environment of the plain. The recognition of those is importance for soil survey, land use planning, soil database, and environment assessment.

2. Methodology

There are 15 soil profiles were examined in the Lower Central Plain, both the area of ASS and non ASS in southernmost of the plain as deltaic, deltaic tidal and tidal plains landform units. Mainly, the pits were excavated as deep as 2 m. Some profiles can be observed deeper in the case of the bottom of profiles could be opened continuously and they were not collapsed. On the contrary, some were investigated shallower than 2 m due to high level of groundwater of the sites. The study included soil morphology, field pH [4], [5], and 1:1 in H₂O pH [6] were also measured. At each site, sedimentary succession and electric conductivity [7] were determined for better understanding of the depositional environment.

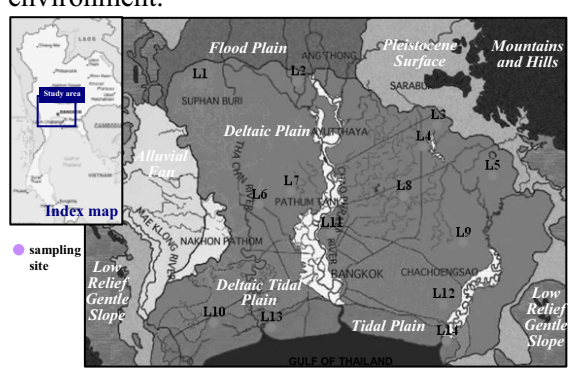


Fig. 1 Landforms classification map of the Lower Central Plain of Thailand [8] and sampling sites.

3. Results and Discussion

Characteristics of ASS are categorized into 3 groups. Group I is ripe ASSs with very strongly to extremely acid condition, including L1-L5. The soils are characterized by various shades of red, brown and yellow mottles which occur as separate zones in profiles, red and brown mottles usually occur at the top whereas yellow mottles of jarosite occur at lower of B horizons. The C horizons commonly contain iron pipes, dead roots, and plant fragments.



Their morphology show oxidation already occurred entire the profiles. Group II is ASSs with reducing C horizons which contain high sulfidic material, including L6-L9 and L14. Reaction of these horizons is neutral to moderately alkaline but becomes extremely acid on oxidation due to the high sulfidic material content. The soils also have red, brown and yellow mottles but occur in the same zone of upper B horizon. A few plant fragments were observed in the C horizons. Group III is non ASSs with reducing C horizons which contain low sulfidic material, including L10-13. Reaction of soils is slightly acid to strongly alkaline and does not become extremely acid on oxidation. Concretions of marl, shell fragments, iron pipes and dead roots could be observed in B and C horizons.

Group I distribute in the upper boundary of deltaic plain, Group II distributes in the lower boundary of deltaic plain and eastern active tidal flat of the Gulf of Thailand. L14 locates in recent environment of ASS development. Group III distributes in the deltaic tidal to tidal plain area.

4. Conclusions and Recommendations for Thailand

ASSs is considered to be developed in condition closely related the Holocene paleoenvironment, especially to the intertidal to deltaic condition during the middle Holocene transgression as mangrove forest and shallow marine environments. Sulfidic material strongly accumulated in intertidal mangrove forest environment to which it was suitable for ASS formation. In contrast to non ASS, it is distributed in the embayment during the time of sea level trangression, then developed to be tidal flat in the period of rapid regression and the southernmost is being tidal flat until the present. At the time of sedimentation, any plant may not grow well in the area and condition was unsuitable for sulfidic material accumulation. Therefore, ASSs did develop in the area of group III.

Land use planning in area of ASS in the Lower Central Plain should considering types of plant to cultivate, select plant which has root system shallower than sufuric horizon (sulfuric horizons of ASS samplings are begin 0-90 cm from surfaces) due to extremely acid condition is inappropriate for general plant growing. Also improvement of plant nutrients of the soil should be finished before cropping. Moreover, excavation in the area of ASS with reduced subsoil should be done and managed carefully,

do not opened the land as deep as horizon containing sulfidic material (upper boundaries of the horizons are 128-170 cm). Due to the material possibly generate serious acid condition on oxidation. Consequently, the land will difficult to apply in any objective.

- [1] A.E. McElnea, C.R.Ahern, J.A.Manders, C.D.Smith, paper presented to 13th Int. Soil Conserv. Org. Conf., Brisbane, 2004.
- [2] Department of Natural Resources and Water, Acid sulfate soils. Queensland Government, viewed 5 December 2007, www.nrm.gld.gov.au/land/ass/index.html.
- [3] Land Development Department, Acid sulfate soil distribution map of Thailand, 1:2 500 000. Bangkok, 2006.
- [4] Soil Survey Staff, Soil Survey Manual. United States department of Agriculture, United States Government Printing Office, Washington, D.C., 1993.
- [5] Soil Survey Staff, Keys to Soil Taxonomy, 10th ed. United States Department of Agriculture, Washington D.C., 2006.
- Survey Center, [6] National Soil Investigations Report No. 42, V. 3.0., United States Department of Agriculture, Washington D.C. 1996, pp. 213.
- [7] T. Yokoyama, in Japan Association for Quaternary Research (Ed.), A Handbook of Quaternary Research V.2, University of Tokyo Press, 1993., pp. 109-118.
- [8] M. Umitsu, S. Tiyapairach, N. Chaimanee, K. Kawase, Proc. of the Symp. on Geol. of Thailand, 2002, pp. 201-206.

NS-P13

Wanwarang Ratananikom¹, Fumihiko Fukuda²

Effect of Intermediate Principal Stress on Bangkok Clay Behavior under Ouasi Simple Shear Condition

¹Department of Civil Engineering, Chulalongkorn University, Bangkok, Thailand ²Graduate school of Engineering, Hokkaido University, Hokkaido, Japan E-mail address: khakhanang_r@hotmail.com¹, fukuda@eng.hokudai.ac.jp²

This paper presents an experimental investigation of the effect of the intermediate principal stress (σ_2). A series of tests was performed on the undisturbed samples of Bangkok Clay by means of a torsional shear hollow cylinder apparatus. The magnitudes of b values were fixed at 0, 0.5 and 1 in each test. The direction of the major principal stress (σ_1) is also fixed at 45° against the vertical axis of the specimens in the entire tests. The results show that when α values were fixed at 45°, significant difference in undrained shear strength is observed at different values of b.

1. Introduction

A lot of experiments proposed that the undrained shear strength measured in the compression mode $(\alpha = 0^{\circ}, b = 0)$ can be significantly higher than that in the extension mode $(\alpha = 90^{\circ}, b = 1)$. This difference can be suggested that the stress conditions, such as the direction of the principal stress and the condition of the intermediate principal stress, have some effects on the soil behavior [1, 2].

Although, several researchers have widely investigated the effects of the principal stress direction and the condition of the intermediate principal stress on many soils, the condition of the intermediate principal stress on the behavior of Bangkok Clay is not available. The objective of this study is to investigate the undisturbed Bangkok Clay behavior with particular attention to the intermediate principal stress effect.

2. Experiments

To clarify these effects, the torsional shear hollow cylinder apparatus was used. Four stress components on the $(\sigma_z, \sigma_r, \sigma_\theta, \tau_{\theta z})$ can be adjusted by controlling the torque (M_T) , the axial force (W), the outer cell pressure (p_o) and the inner cell pressure (p_i) . The average stress components in hollow cylindrical specimen were calculated with reference to the work by Hight et al. (1983) [3]. Undisturbed samples were taken by piston sampler from Ladprao area, Bangkok between the depths of 10.0-12.5 m. The index properties are liquid limit = 85.2-85.8 %, plastic limits = 27.4-33.0 %, plastic index = 52.2-58.4 %, natural water content = 49.3-54.3 % and total unit weight = 17 kN/m^3 . The hollow cylindrical specimens (inner diameter,

 $D_i = 30$ mm, outer diamiter, $D_o = 70$ mm, height, H = 120 mm) used in this study were prepared by using successive drill and enlarged by a wire saw. Three torsional shear tests on hollow cylindrical Bangkok Clay samples were carried out each with a different b values at 0, 0.5 and 1 in undrained condition. The α values were fixed at 45°. The back pressure of 200 kPa was applied to ensure the specimen saturation. After the saturation, Skempton's B value greater than 0.95, all specimens were isotropically consolidated to the pressure which is same as the in-situ vertical stress and than undrained sheared. The undrained shear stage is terminated when the rotation angle of the top part of the specimen reaches 30°. The termination of the isotropic consolidation stage is judged by the dissipation of the excess pore water pressure ($\Delta u < 1$ kPa).

3. Results and discussion

Normalised undrained effective stress paths with α values were fixed at 45° (Fig. 1), whereas b values were varied from 0 to 1. Obviously, the normalised undrained effective stress paths are almost same, irrespective of the values of b when the effective stress path is plot on the q/p_o' versus p'/p_o' . The deviatoric stress is $q = \sigma_1 - \sigma_3$. It can imply that the excess pore water pressure is a function of the principal stress difference. However, it is independent of the intermediate principal stress parameter.

The angle of shearing resistance
$$\phi' = \arcsin\left(\frac{\sigma_1' - \sigma_3'}{\sigma_1' + \sigma_3'}\right) \text{ at the peak shear stress}$$

(the $\tau_{\theta z}$ becomes maximum) with respect to b is shown in Fig. 2. The main observation is that the measured variation in ϕ' increases



when b increase up to 0.5 and remains increase slightly thereafter. This contradictious result may be caused by the effects of stress and strain non-uniformity and/or the different properties of the specimens in the hollow cylinder test.

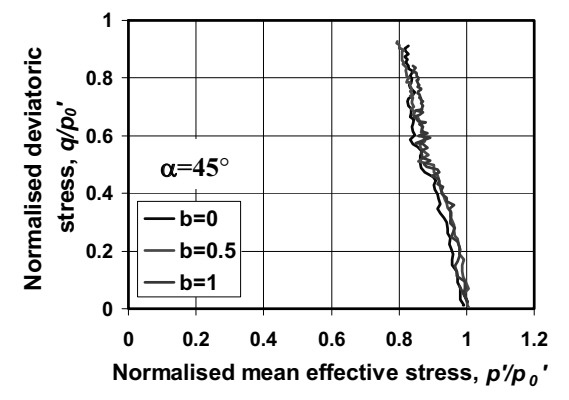


Fig. 1 Normalised undrained effective stress paths with α =45°

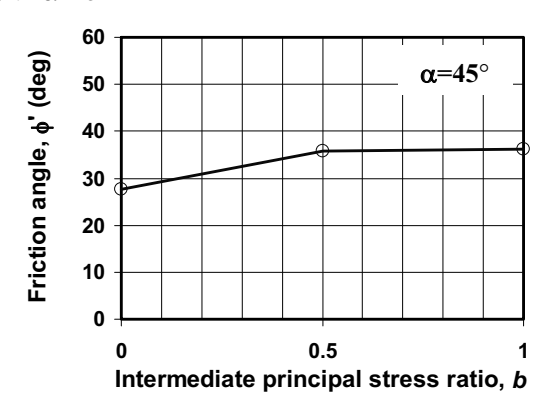


Fig. 2 Friction angle of Bangkok Clay from undrained test with α =45°

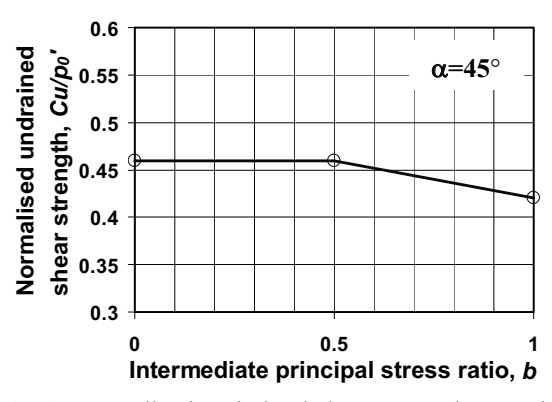


Fig. 3 Normalised undrained shear strength at peak with α =45°

Fig. 3 represents the normalized values of undrained shear strength at the peak shear stress with α =45°. A lower undrained strength is obtained when the shearing is performed with the larger value of b (b=1). The value of Cu/p_0 ′ tends to exhibit constant when b value changes from 0 to 0.5 but difference in Cu/p_0 ′ close to 10% arises at higher values of b. The same trend in behavior has been reported by other researchers [4, 5].

4. Conclusions and Recommendations for Thailand

The influence of intermediate principal stress on the behavior of Bangkok Clay is presented in this paper. When α values were fixed at 45°, the significant difference in the undrained shear strength is observed in shear behavior of Bangkok Clay at different values of b. There is negligible undrained shear strength affected by σ_2 when b<0.5. However, the opposed result of ϕ ' is noticed. This information is achieved accurately; they should be useful for improving the soil model to better represent the real Bangkok clay behavior.

- [1] F. Tatsuoka and K. Ishihara, Proc. of 8th Int. Conf. on SMFE 1[2] (1973) 419-424.
- [2] Y.P. Vaid, A. Sayao, E. Hou, D. Negussey, Can. Geotechnical J. 27[5] (1990) 601-616.
- [3] D.W. Hight, A. Gens, M.J. Symes, Geotecnique 33[4] (1983) 355-383.
- [4] S. Shibuya, Undrained behaviour of granular materials under principal stress rotation, PhD. Thesis, Imperial College of Science, Technology and Medicine, University of London, 1985.
- [5] M. Yoshimine, K. Ishihara, W. Vargas, Soils and Foundations 38[3] (1998a) 179-188.

NS-P14

Stress Analysis of Granular Media Confined in Long Vertical Column

Sokbil Heng, Thirapong Pipatpongsa, Hideki Ohta

Tokyo Institute of Technology, Tokyo, Japan Tel.: +81-3-5734-2121, Fax: +81-3-5734-3276, E-mail address: hengsokbil@ide.titech.ac.jp

Stress analyses of granular media stored in a long vertical axis symmetric column has attracted many interests from granular physics and mechanics. The analyses of stress distributions proposed by Janssen (1895) for corn, and by Jâky (1948) for wheat storage in silos, confirmed good agreement with experimental results, though certain assumptions are needed to improve. This study attempts to indicate the certain theoretical simplification in their assumptions and discusses on the validation aiming to generalize all related formulas. The basic assumption for deriving a well-known coefficient of earth pressure at-rest in soil mechanics proposed by Jâky is examined and clarified in this study. It is clear that Jâky assumed linear shear stress reduction in his analyses of stress distribution not only to sand heaps but also to grains in silos.

1. Introduction

In agricultural and chemical industries, crops and powders are frequently stored in tall silos. In order to design the optimum size of the containing structure with safety and economy, knowledge of storage conditions and stress distributions throughout the granular media is necessary. The study of silo problem has been initiated as early as 1985 by Janssen [1] based on the mechanics of continuous media. The approximation of vertical stress obtained by Janssen's model as well as the phenomenon of saturation pressure has been widely recognized in both physics and mechanics of granular media. However, Janssen's assumption that the vertical and horizontal stresses are principal stresses is not correct. Jâky [2] corrected this inconsistency by considering the distribution of shear stress and imposing that at-rest condition is achieved at the center line of silos. Jâky's analysis firstly introduced the coefficient of earth pressure at-rest K_o , to describe the static of granular media. agricultural products to cohesionless soils, his simplified K_o equation later became the advantage to compute lateral pressures for geotechnical engineers in particular. The analytical method proposed in this study shortcuts the original Jâky's analysis in an attempt to emphasize that Jâky assumed linear shear stress reduction in his (Pipatpongsa et al. [3]). Comparisons of the analytical formulation are made with the published experiments of corn and wheat stored in silos and the results are discussed.

2. Analytical method

The equilibrium equations of stresses in axi-symmetric cylindrical co-ordinates (r,z,θ) are given in radial and vertical directions.

$$\frac{\partial \sigma_r}{\partial r} + \frac{\sigma_r - \sigma_\theta}{r} + \frac{\partial \tau_{zr}}{\partial z} = 0 \tag{1}$$

$$\frac{\partial \sigma_z}{\partial z} + \frac{\partial \tau_{rz}}{\partial r} + \frac{\tau_{rz}}{r} = \gamma \tag{2}$$

where
$$\sigma_{\theta} = \sigma_r$$
, $\tau_{zr} = \tau_{rz}$ (3), (4)

Shear stress at wall
$$\tau_w = \mu_w \sigma_w$$
 (5)

where μ_w is a static coefficient of friction between granular material and silo's wall $(\mu_{w,max}=tan\phi)$, and σ_w is a radial stress exerting to the wall at a given depth.

State of stresses in granular media is assumed to be not mobilized, therefore shear stress τ_{rz} is to reduce linearly with radius r to zero at the center line of silo in Eqs.(6)-(7). Shear and radial stresses along the wall τ_w and σ_w are the boundary conditions to determine τ_{rz} and σ_r from Eqs.(1)-(2). Eq.(8) describes the assumption that vertical stress σ_z is uniform across horizontal section. According to Eq.(2), Eqs.(5)-(7), σ_w can be expressed by Eq.(11).

$$\tau_{rz} = \frac{r}{R} \tau_{w}, \quad \frac{\partial \tau_{rz}}{\partial r} = \frac{\tau_{w}}{R}, \quad \frac{\partial \sigma_{z}}{\partial r} = 0$$
(6), (7), (8)

$$\tau_{w} = \tau_{rz}|_{r=R}, \sigma_{w} = \sigma_{r}|_{r=R}$$
 (9), (10)

$$\sigma_{w} = \frac{R}{2\mu_{w}} \left(\gamma - \frac{\partial \sigma_{z}}{\partial z} \right) \tag{11}$$

According to Eq.(1), using Eqs.(3)-(7), variation of σ_r along the radius can be expressed by Eq.(12).

$$\frac{\partial \sigma_r}{\partial r} = -\mu_w \frac{r}{R} \frac{\partial \sigma_w}{\partial z} = \frac{r}{2} \frac{\partial^2 \sigma_z}{\partial z^2}$$
 (12)

Another boundary condition is given along the center line where state of stress is assumed to be *at-rest condition*. Hence, σ_r and σ_w can be related to σ_z thru Eqs.(12)-(15).

$$\sigma_r|_{r=0} = K_o \sigma_z \tag{13}$$

$$\sigma_r = \int_0^r \frac{\partial \sigma_r}{\partial r} dr + \sigma_r \Big|_{r=0} = \frac{r^2}{4} \frac{\partial^2 \sigma_z}{\partial z^2} + K_o \sigma_z$$
 (14)



$$\sigma_{w} = \frac{R^2}{4} \frac{\partial^2 \sigma_{z}}{\partial z^2} + K_o \sigma_{z}$$
 (15)

Elimination of σ_w from Eqs.(11) and (15), with rearrangement can form a linear homogeneous 2nd order differential equation.

$$\frac{R^2}{4} \frac{\partial^2 \sigma_z}{\partial z^2} + \frac{R}{2\mu_w} \frac{\partial \sigma_z}{\partial z} + K_o \sigma_z - \frac{\gamma R}{2\mu_w} = 0 \qquad (16)$$

The solution of σ_z based on Eq.(16) are carried out by referring to standard formulations given by Eqs.(17)-(21).

$$\xi = K_o \sigma_z - \frac{\gamma R}{2\mu_o} \tag{17}$$

$$\frac{\partial^2 \xi}{\partial z^2} + \frac{2}{\mu_w R} \frac{\partial \xi}{\partial z} + \frac{4K_o}{R^2} \xi = 0$$
 (18)

Let m_1 , m_2 be the real and distinct roots of

$$m^2 + \frac{2}{\mu_o R} m + \frac{4K_o}{R^2} = 0, \qquad (19)$$

where
$${m_1 \brace m_2} = -\frac{1}{\mu_w R} \begin{cases} 1 - \sqrt{1 - 4\mu_w^2 K_o} \\ 1 + \sqrt{1 - 4\mu_w^2 K_o} \end{cases}$$
 (20)

hence
$$\xi = c_1 e^{m_1 z} + c_2 e^{m_2 z}$$
. (21)

 σ_z shown in Eq.(22) is determined from ξ given in Eqs.(17) and (21). Constants c_1, c_2 are solved from Eqs.(23)-(24) as the initial conditions of σ_z at the top of silo where z=0.

$$\sigma_z = \frac{\gamma R}{2\mu_w K_o} \left(1 + \frac{2\mu_w}{\gamma R} \xi \right) \tag{22}$$

$$\sigma_z|_{z=0} = 0, \frac{\partial \sigma_z}{\partial z}|_{z=0} = \gamma$$
 (23), (24)

$$\begin{cases} c_1 \\ c_2 \end{cases} = \frac{\gamma}{2\mu_w (m_1 - m_2)} \begin{cases} 2\mu_w K_o + Rm_2 \\ -2\mu_w K_o - Rm_1 \end{cases}$$
 (25)

3. Results and Comparisons

The asymptotic saturation pressures at the great depth can be ascertained by imposing $z \rightarrow \infty$. Fig. 1 shows the pressures diagram normalized by the saturation pressures versus height of silo normalized by the characteristic depth z_c . It is found that the theoretical equations agreed well with experiments results reported by Janssen and Jâky. At the great depth, stress condition is clearly at-rest state.

$$\lim_{z \to \infty} \xi = 0 , \ z_c = \frac{R}{2\mu_w K_o}$$
 (26), (27)

$$\sigma_z|_{z=0} = \gamma z_c$$
, $\sigma_r|_{z=0} = K_o \gamma z_c$ (28), (29)

$$\tau_w|_{z=\infty} = \frac{R}{2}\gamma, \frac{\sigma_r}{\sigma_z}|_{z=\infty} = K_o$$
 (30), (31)

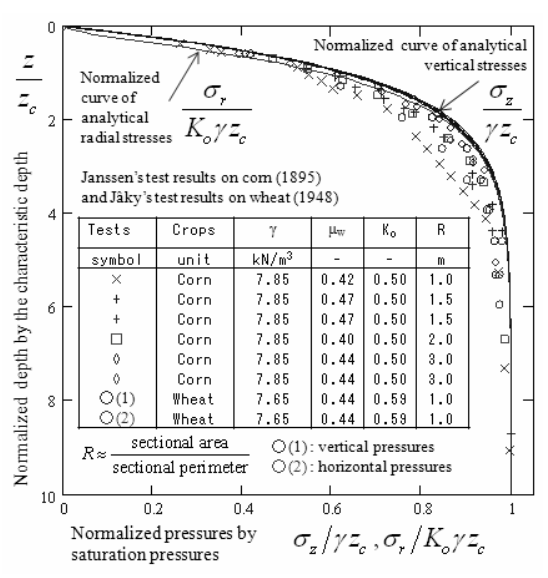


Fig. 1 Stress distributions along the wall of silos

The formula derived in this paper implied by one hand generalized the Janssen's equation of vertical pressure by associating the wall friction with internal friction angle of the material and introduce the coefficient of at-rest pressure, and other hand simplified Jâky's approach of upper and lower section of experimental curve.

4. Recommendations for Thailand

Major exports of Thailand and regional countries are agricultural products which are generally stored in silos. Understanding of storage condition and stress distribution of stored materials can contribute optimized design of containing structures.

- Zeitschr. d. Vereines [1] H.A. Janssen. deutscher Ingenieure 39 (1895) 1045-1049.
- [2] J. Jâky, Proc. 2nd ICSMFE, 1 (1948) 103-107.
- [3] T. Pipatpongsa, S. Ohno, A. Iizuka, H. Ohta, 43rd Proc. JNCGE (2008), 265-266.

Interpretation of K₀-consolidation Processes Illustrated by Randomized Inhomogeneous Strains

Mohammad Hossein Khosravi, Thirapong Pipatpongsa, Hideki Ohta

Tokyo Institute of Technology, Tokyo, Japan Tel.: +81-3-5734-2121, Fax: +81-3-5734-3276, E-mail: mh khosravi@yahoo.com

The Sekiguchi-Ohta model is one of the most fundamental constitutive equations based on critical state theory for anisotropic geomaterials. According to the domain of metastability defined for the inhomogeneous strains at the corner of Sekiguchi-Ohta model, plastic flow is limited by the inequality for generalized strains. The nature of anisotropic virgin-consolidation can be considered as a combined process compression and extension in axi-symmetric condition. This combination is supposed to produce consolidation without overall distortion. Using binary distribution, strain increments can be randomly selected in the domain of metastability. For small number of combinations, inhomogeneous internal strains are obviously seen while the more homogeneous internal strains due to an accumulation random movement can be seen for large number of combinations.

1. Introduction

The Sekiguchi-Ohta model [1] is one of the most fundamental constitutive equations based on critical state theory for anisotropic geomaterials. The yield function $f(\sigma,\sigma_c)$ of this model is expressed by Eq.(1) as a function of a stress tensor σ , and anisotropic hardening stress tensor σ_c .

$$f(\mathbf{\sigma}, \mathbf{\sigma}_c) = M \ln(p/p_c) + \overline{q}/p = 0 \tag{1}$$

where M is critical state frictional parameter, p is mean stress, p_c is isotropic hardening stress parameter and \overline{q} is a relative deviatoric stress. Derivation of these stress variables are shown in Eqs.(2)-(9).

$$p = \frac{1}{3}\mathbf{\sigma}:\mathbf{1}, \ p_c = \frac{1}{3}\mathbf{\sigma}_c:\mathbf{1}$$
 (2),(3)

$$s = \sigma - p1$$
, $s_a = \sigma_a - p_a 1$ (4),(5)

$$\mathbf{\eta}_c = \mathbf{s}_c / p_c$$
, $\overline{\mathbf{s}} = \mathbf{s} - p\mathbf{\eta}_c$ (6),(7)

$$\overline{\mathbf{n}} = \overline{\mathbf{s}} / \| \overline{\mathbf{s}} \|, \ \overline{q} = \sqrt{\frac{3}{2}} \| \overline{\mathbf{s}} \|$$
 (8),(9)

where 1 is second-order identity tensor, s and \mathbf{s}_c are stress deviator of $\mathbf{\sigma}$ and $\mathbf{\sigma}_c$ respectively and η_c is deviatoric second-order tensor associated to anisotropic consolidation. Compressive stresses and strains considered positive, effective stresses are used throughout the paper, single dot (\cdot) , double dot (:) denote single and double contraction of two tensors respectively. Euclidian norm is written shortly by $\| \bullet \| = \sqrt{\bullet : \bullet}$ where \bullet stands for a second-order tensor.

2. Domain of inhomogeneous strains

According to the domain of metastability defined for the inhomogeneous strains at the corner of Sekiguchi-Ohta model [2], plastic flow is limited by the inequality for generalized strains expressed by Eqs.(10)-(11) where \mathbf{z} is an applied strain rate, \mathbf{z} is a volumetric strain rate, \mathbf{z}^p is a second-order tensor of relative plastic strain rate, \mathbf{z} is a constant K_o -consolidated stress ratio, \mathbf{z} is an irreversibility ratio. Provided that the stress point is continuously kept along the corner, the arbitrary strain rate can be varied within the domain of metastability. In other words, uniform possibility of plastic flows can be randomly selected in this domain.

$$\mathbf{\tilde{g}}^{p} = \mathbf{g} - \mathbf{g}_{v} \left\{ \frac{1}{3} \mathbf{1} + (1 - \Lambda) \frac{\mathbf{\eta}_{c}}{\eta_{o}} \right\}$$
 (10)

$$\sqrt{\frac{2}{3}} \left\| \mathbf{\tilde{z}}^{p} \right\| - \frac{\Lambda \mathcal{E}_{v}}{M - \sqrt{3/2} \mathbf{\eta}_{c} : \overline{\mathbf{n}}} \le 0 \tag{11}$$

Under K_0 -consolidation processes, states of stresses and strains are under axi-symmetric condition. Therefore, Eq.(11) can be deduced to Eq.(12) where & is a deviatoric strain rate.

$$\mathscr{E}_{\tilde{s}} \leq \frac{\Lambda \mathscr{E}_{\tilde{v}}}{M \pm \eta_{o}} \tag{12}$$

Descriptions of rate form will be replaced by increment form in the next section by considering that the rate is constant throughout the discretized time increment.



3. Randomized plastic flows

nature of anisotropic virginconsolidation can be considered as a combined process compression and extension. This combination is supposed to produce consolidation without overall distortion [3]. In order to illustrate this condition for a given soil sample, we can assume that for any point of this sample, distortion $\delta \varepsilon_s$ is described by either compression or extension under a constant rate of volume change $\delta \varepsilon_{y}$. We can adopt deviatoric strain increment $\delta \varepsilon_{s}^{(i)}$ as a probability variable where *i* denote step number. To satisfy consistency conditions it is required that,

$$\frac{-\Lambda}{M + \eta_{o}} \delta \varepsilon_{v} \le \delta \varepsilon_{s} \le \frac{\Lambda}{M - \eta_{o}} \delta \varepsilon_{v} \tag{13}$$

The Eq.(13) means that distortion is controlled by compression and extension limits;

$$\delta \varepsilon_{s}^{(i)} = \begin{cases} \frac{\Lambda}{M - \eta_{o}} \delta \varepsilon_{v} & \text{compression} \\ \frac{-\Lambda}{M + \eta_{o}} \delta \varepsilon_{v} & \text{extension} \end{cases}$$
(14)

Using binary distribution we can consider distortion due to volumetric strain increments. Stepwise volume change is obtained by dividing an accumulated volume change with a number of steps n, which represents a number of grain movements. Means of volume and distortion increments $\delta \bar{\varepsilon}_s$ are calculated by,

$$\delta \overline{\varepsilon_{\nu}} = \delta \varepsilon_{\nu}^{(i)} = \frac{\delta \varepsilon_{\nu}}{n} \tag{15}$$

$$\delta \overline{\varepsilon_s} = \frac{1}{2} \left(\frac{\Lambda}{M - \eta_o} \delta \varepsilon_v + \frac{-\Lambda}{M + \eta_o} \delta \varepsilon_v \right)$$
 (16)

Simple computation are made for a rectangular sample composing of 10×10 element points using parameters M = 1, $\Lambda = 0.75$ $\eta_o = 0.5$. Net change in distortion is a summation of all steps emerged from randomized processes.

$$\Delta \varepsilon_s = \sum_{i}^{n} \delta \varepsilon_s^{(i)} \tag{17}$$

Various steps under constant volume change are carried out. Results emanated from binary distribution are illustrated in Fig. Accumulated axial and radial strain increments $\Delta \varepsilon_a, \Delta \varepsilon_r$ can be transformed from accumulated volumetric and deviatoric strain increments by,

$$\begin{bmatrix} \Delta \varepsilon_a \\ \Delta \varepsilon_r \end{bmatrix} = \begin{bmatrix} 1 & 2 \\ 2/3 & -2/3 \end{bmatrix}^{-1} \cdot \begin{bmatrix} \Delta \varepsilon_v \\ \Delta \varepsilon_s \end{bmatrix}$$
(16)

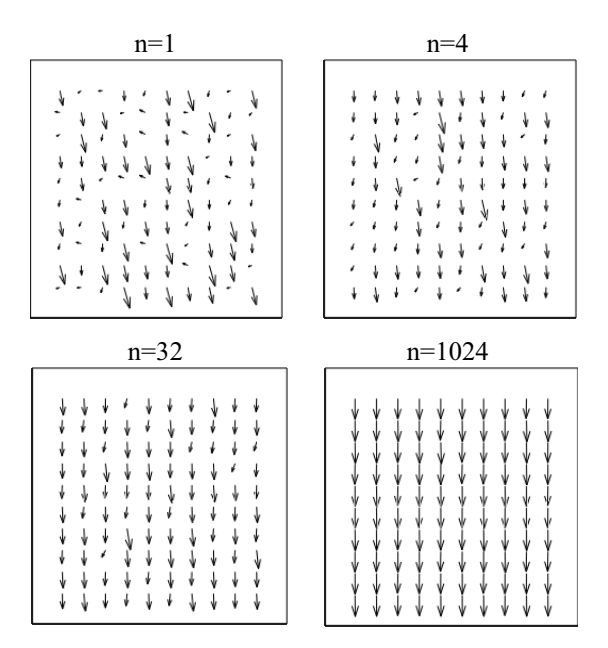


Fig. 1 Vector plots of averaged characterized by binomial distribution

4. Conclusions

For small number of n we can see obviously inhomogeneous internal strain due to the combination of compression and extension while increasing the number of nresults in the more homogeneous internal strain due to an accumulation random movement.

5. Recommendations for Thailand

The Sekiguchi-Ohta model is the most popular soil constitutive model used in Japan. Understanding of the model benefits to academics/researches which contribute to Thailand in the field of Civil Engineering. Soil parameters should be carefully determined when applying to analyses and design.

References

240.

- [1] H. Sekiguchi, H. Ohta, Proc. 9th ICSMFE, (1977) 229-239.
- [2] T. Pipatpongsa, T. Takeyama, H. Ohta and A.Iizuka, Proc. 57th NCTAM (2008) 355-356. [3] K.H. Roscoe, A.N. Schofield, A. Thurairajah, Geotechnique, 13[3] (1963) 211-

NS-P16

Program "PimThai" (Typing Thai by Romanized input)

Pakpoom Sakkamchorn

Tel: +66-86-606-1492, E-mail address: sakgumjorn@yahoo.com www.pimthai.com

This article proposes "PimThai", a program for typing Thai words by Romanized input (Romanization is the representation of word with Roman alphabet). This program will make foreigners who study Thai language and also Thai people who live in foreign countries able to type Thai more effectively. Moreover, this is a good way in promotion Thai language.

1. Introduction

Nowadays, foreigners especially Japanese who are interested in Thai language have become increasing recently. Although they can use Thai, they cannot use Thai keyboard easily because of more than 90 used keys. So if they can type with only 26 keys of English keyboard, it will become more comfortable.

Moreover, if Thai language can be used in Romanization more effectively, we can promote more easily. So this is a good way to heighten Thai language status to be a more universal language. "Promotion Planning for Thai Language as a Foreign Language in Japan" was initiated by Podsatiangool [1]. This idea is an inspiration to make Program "PimThai" (Typing Thai by Romanized input).

2. Methodology

In this project, "タイ文字読み書きの基礎" [2] was use as the reference in Romanization. At present, there are 2 methods, [manual typing method] and [automatic method], in 2 separate versions of program.

The manual typing method, after finishing every syllable and pressing "space bar" button, the program will separate the input word for alphabet and vowel and select Thai alphabet and vowel that match the input and assemble them. Then it show all of the possible words for the input, including all tone marks (wannayuk) that can be chosen whether meaningful or not. For example, when type "KIN" the program will separate K for frontalphabet, I for vowel, and N for back-alphabet. Possible front-alphabet that matches for K is "n". The possible vowel for I is "ຄ". And the possible last-alphabets for N are "u", "a", "a" and "w" (the order of words shown in list is according to frequently of normally used of each alphabet). Therefore the possible words shown in list box for choose are "กิน", "กิญ",

"ña",and "ñw", although some words are meaningless. Moreover, each word can change into different tone marks, for example, "ກື່ມ", "ກື້ມ", etc.

The automatic method (in the other separate version), using a Thai dictionary for the reference of Thai words. Although it does not cover for the entire of Thai words, it is enough for all usually using words. Then convert from Thai to Romanized word and keep it into database. When text is input by user, the program will search from the database for the 20 nearest words. More texts is input, nearer word will be shown. For example, when type K, the first 20 nearest words such as "n", "ถ้", "กก",... will shown in list. When type I (become KI), words in list will change to the new nearest words such as "เกียกกาย", "เกี่ยง", "เกี่ยง งอน". User can select the required word if it is found in the list.

3. How to use

For the manual version, to input Romanized each syllable one by one and then press "Space bar" button, the possible words will be shown in the list box. Select the word from list by pressing "Space bar" continually. If you require tone marks, click "Tab" and Tone marks will be shown. Choose it by click "Space bar". Then press "enter" to select.

For the automatic version, input Thai word by Romanized input. Typing one by one, the nearest word will be shown in list. When the required word is found then press "space bar" button to select the required word. Press the "enter" button to select the required word and Romanized input will be replaced by Thai word. After finish typing, then copy and paste to the require place.



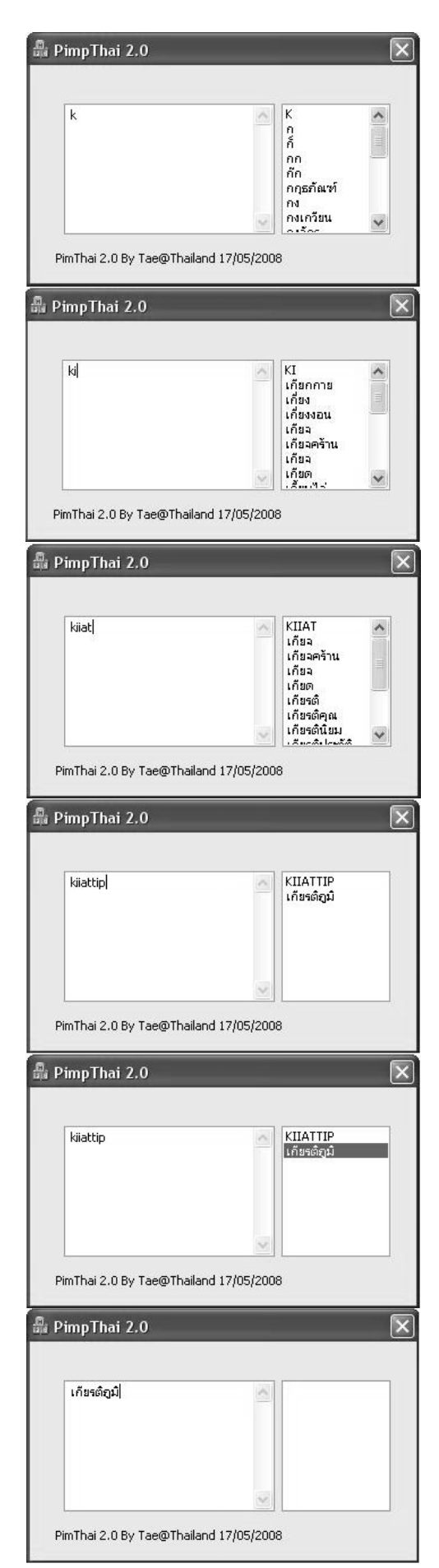


Fig. 1 Using "PimThai" in automatic mode

4. Next Step for This Project

- Combine 2 versions of program together for users can choose both manual and automatic typing.
- Improve the word's database more effectively, such as arranging order of words by frequently of using.
- Patch the program into Microsoft Windows for typing in the require programs such as MS-Office, E-mail, and chatting programs directly

5. Conclusions and Recommendations for Thailand

This application will have an effect on both Thai people and foreigners.

In case of Thai people, they can type in Thai more comfortably because English keyboard has less used keys than Thai. For Thai people in foreign countries, they also Thai easily without remembering positions of each keys.

In case of foreigner, this program will certainly solve the problem of finding keys for each Thai alphabet. And also heighten Thai language status to be a more universal language.

- [1] W. Podsatiangool, Proc. 2nd TJSE conf., 2 (2007)72.
- [2] タイ文字読み書きの基礎, Wilai Tomornkul, TPA, 2003.

Workplace Environment and Personal Exposure of PM and PAHs to Workers in Natural Rubber Sheet Factories Contaminated by Wood Burning Smoke

Thitiworn Choosong ¹, Jiraporn Chumanee², Witchaya Petliap³, Fumie Yoshikawa⁴, Perapong Tekasakul⁵, Surajit Tekasakul², Pitchaya Phakthongsuk³, Yoshio Otani¹, Masami Furuuchi¹

¹Graduated School of Natural Science and Technology, Kanazawa University, Ishikawa, Japan

²Faculty of Science, Prince of Songkla University, Songkhla, Thailand

³Faculty of Medicine, Prince of Songkla University, Songkhla, Thailand

⁴Practical Engineering Education Program, Kanazawa Institute of Technology, Japan

⁵Faculty of Engineering, Prince of Songkla University, Songkhla, Thailand

Workplace environment in factories producing Ribbed Rubber Smoke Sheet (RSS), inside of which are heavily contaminated by wood burning smoke, has been evaluated focusing on concentrations of particulate matter and particle bond PAHs as well as their exposure to workers during January, 2006 – February, 2008 in Thailand. Seasonal changes in the particulates and PAHs concentrations were related to the production amount of RSS and weather conditions. Based on the measurement in four different factories, which have different types of ventilation facilities, influences of ventilation were also discussed. The concentration of total suspended particulates (TSP) in workplace increased linearly with RSS production although it showed a slight dependency on the wind direction to a factory building probably because of the configuration of open sides of the building. TSP concentration in the workplace and at the worker's breathing zone ranged 0.02 to 0.28 and 0.14 to 0.56 mg/m³, respectively. Those are still less than the working environmental standard but rather high PAHs concentrations (94.6 ~ 131 ng/m³ in workplace and 153 ng/m³ at breathing zone) were observed. Ventilation by roof turbines as well as a ridge vent roof may not be efficient enough to remove smoke particles. The workers in the RSS factory were found to have a risk of exposure to rather high concentration of PAHs, which may be both from wood burning and a diesel engine operated inside.

1. Introduction

Ribbed Rubber Smoke Sheet (RSS) is a main product from rubber latex. In the southern provinces of Thailand, there are currently 444 small-scale manufacturers operating, which are commonly called 'RSS cooperatives'. Since a management system is carried out in a cooperative function [1]. The main process of RSS production is drying the latex sheets by smoke and heat in the drying rooms. This requires the burning of solid fuel, which is rubber Therefore, wood. combustion is considered the major emission source of smoke in RSS factories. During incomplete combustion, polycyclic aromatic hydrocarbons (PAHs) are formed, especially a major group of carcinogens [2]. Exposure to particulate matter and chemical components such as PAH is reported the potential harm to health damage [3]. Hence, this study will investigate the worker's exposure level to particle and PAH concentration over 12 months. The influences of particulate matter dilution by the current ventilators will be clarified.

2. Location and general characteristics of Ribbed Rubber Smoked Sheet (RSS) factories

Four RSS factories were selected to represent the general characteristics of RSS factories. Three of them are located in Songkhla and another one is in Phattalung Province. In the study area, the main interest was a new model without (w/o) ventilation. This RSS factory was

built in the 'new' design with 4 drying rooms in a dimension of 4×5 m. The total diameter is 18×25 m, which was the same as the 'old' design. The 'old' design has 7 drying rooms with a dimension 3×7 m. The ventilation systems (vent.) in the study areas are 2 kinds that consist of a turbine and a ridge vent on the roof. Around 4-8 workers were employed to produce RSS.

3. Air sampling and chemical analyses

Air sampling was done at the worker's breathing zone (BZ) and workplace area (PS) using personal sampling pumps (Gilair-5, Sensidyne Inc; SKC Universal PCXR8, SKC Inc, flow rate 2 lpm) with quart fiber filter (ADVANTEC, OR-100). Workplace sampling was done continuously during August 2006 to February 2008 which sampling points comprised three points. All samples were weighted to determine the particulate matter with a 5-digit balance (in mg), and then were wrapped in aluminum foil and stored at -20°C until chemical analysis. Fifteen - sixteen PAH components were analyzed using a high performance liquid chromatograph (HITACHI, L-2130/2200/2300/2485).

4. Results and discussion

4.1 Rubber production

The RSS production in the new model w/o vent is varied depending on the amount of natural latex, weather, season, and the price of RSS on the central RSS market. Therefore, the production figures over 12 months were not constant.



4.2 Particulate matter concentration

The 50th percentile of the particle size distribution in the new model w/o vent was at 1 micron, which is consistent with smoke characteristics [4]. The particulate matter concentrations of PS and HV were 0.09±0.07 0.16 ± 0.08 mg/m³, respectively. different concentrations might be influenced by location and height, as the HV was located near the opening area of the drying room.

The particulate matter concentration at the worker's breathing zone was 0.17±0.1 mg/m³, which was higher than the concentration at the PS and HV sites. This might be the influenced by the job characteristics; for example, a worker has to check the RSS quality in the drying room. In addition, the exposure to particulate matter is related to the increase of the amount of RSS production. Therefore, the worker might be exposed to higher concentrations during higher production season.

4.3 Total PAH concentration

The average total PAH concentration at PS and HV point were 94.6 ± 7.2 and 131 ± 120 ng/m³, respectively, whereas at the worker's breathing zone it was 153±10.6 ng/m³. The higher total PAH value at BZ might be the worker's exposure to PAH from two sources. The main source of PAH were the drying rooms and another source was the diesel engine of the squeezing machine which was the total PAHs concentration at 0.5 m. was 365 ng/m³. In addition, the total PAH gas-phase concentration in workplace was $3.6\pm5.3 \,\mu g/m^3$.

Table 1 Concentration of total dust (mg/m³) and PAH (ng/m³) in 4 RSS factories

PAH (ng/m) in 4 RSS factories					
	RSS cooperation type				
		Hybrid	Old	New	New
		model	model	model	model
		w/t vent	w/t vent	w/o vent	w/t vent
Particle conc. (mg/m³)	PS	0.13±	0.11±	0.09±	0.13±
		0.05	0.03	0.07	0.04
		(n=12)	(n=7)	(n=47)	(n=7)
	BZ	0.29±0.2	0.14±0.1	0.17 ± 0.1	0.24±
		(n=7)	(n=4)	(n=30)	0.1
		(n-/)	(11-4)	(11–30)	(n=6)
	HV	-	-	0.16 ± 0.1	
				(n=47)	
	AN	0.12	0.15	0.22	0.21
		(n=1)	(n=1)	(n=1)	(n=1)
Total PAH (ng/m³)	PS	255±190	113±61	94.6 ± 7.2	517±380
		(n=6)	(n=7)	(n=35)	(n=7)
	BZ	932±101	95.2±74	153±10.6	147±120
		(n=3)	(n=3)	(n=29)	(n=4)
	HV	-	-	131±120	
				(n=31)	
	AN	83.01	224	790	1408
		(n=1)	(n=1)	(n=1)	(n=1)

These total **PAH** particle-phase concentrations, showed at the middle range of the study in the sinter plant and carbon black manufacturing, were found 42±23 to 365±203 ng/m^3 [5] and 4.95 - 612 ng/m^3 [6], respectively. All particle concentrations were less than the recommend airborne concentrations [7], which should be less than 10 mg/m³. However, the total PAH concentrations of the RSS factories were in a serious situation.

4.4 Geometric of plantation and ventilation

According to the plant design, all of the RSS factories were semi-open small scale enterprises. The open site of the new model w/o vent was in the W to SEE direction and the close sites were the other directions. During sampling period, 33.33% of the wind directions were through the open site, whereas through the close site was 66.67%. This had an effect on the particle concentrations, as the concentrations at the open site (0.08±0.02 mg/m³) were lower than at the close sites $(0.12\pm0.08 \text{ mg/m}^3)$.

Table 1 showed that the particle concentration both at PS and BZ were in various ranged. This may be some ventilators, roof turbine ventilators, and ridge vents on the roof were installed. During a high production period, the RSS cooperative w/t ridge vent of roof showed no turbulences air flow in the workplace, while RSS factories w/o vent showed several times of turbulences air flow.

5. Conclusion

The 50th percentile of particle distribution in RSS factories was 1 micron. The total dust concentrations in all RSS factories were lower than occupational exposure limit values. However, the total PAH concentrations were relatively high and close to the range of PAHs in medium and heavy manufacturing. According to RSS cooperative plant's design, rain and wind directions might influence the particle concentrations. The general ventilation is not appropriate to dilute PAHs and smoke from the workplace. The workers in the RSS factories were exposed to PAHs from smoke particles from the drying room and the diesel engine.

- [1] Office of the rubber replanting aid fund, Ministry of agriculture and cooperative, Thailand. (www.rubber.co.th). Access since January 2008.
- [2] Environmental Health Criteria International Programme on Chemical Safety, United Nations Environmental Programme. International Labor Organization, World Health Organization. 1998.
- [3] WHO. World Health Report 2002: Reducing risks, promoting life. (www.who.int/whr/en/).
- [4] C.H. William, aerosol technology: properties, behavior, and measurement of airborne particles, 2nd ed., John Wiley& Sons, INC. USA, 1999.
- [5] Y. Lin, W. Lee, S. Chen, G. Chang-Chien, P. Tsai, J. Hazardous Materials, In Press, Corrected Proof, Available online 12 February
- [6] P. Tsai, H. Shieh, W. Lee, S. Lai, J. Hazardous Mater. 26 (2002) 25-42.
- [7] The American Conference of Governmental Industrial Hygienists, 2005 TLVs and BEIs, ACGIH, Cincinnati, USA, 2005.

An Integer Programming-Based Method of Predicting RNA Secondary Structure with Pseudoknots and Its Relation to Simple Linear Tree Adjoining Grammar

Unyanee Poolsap, Yuki Kato, Tatsuya Akutsu

Bioinformatics Center, Institute for Chemical Research, Kyoto University, Kyoto, Japan Tel.: +81-774-38-3018, Fax: +81-774-38-3022, E-mail address: unyanee@kuicr.kyoto-u.ac.jp

RNA secondary structure prediction is one of the major tasks in bioinformatics because it helps to understand the function of RNA molecules. Various prediction methods have been proposed so far. Pseudoknot is one of the substructures appearing in several RNAs, and plays an important role in some biological processes. Prediction of RNA secondary structure with pseudoknots is still challenging since the problem is NP-hard when arbitrary pseudoknots are taken into consideration. We proposed a new method of predicting RNA secondary structure with pseudoknots based on integer programming. In our formulation, we aimed at minimizing the value of the objective function that reflects free energy of a folding structure of an input RNA sequence. We also conjectured that our integer programming formulation has a one to one relationship with simple linear tree adjoining grammar, which can describe a subclass of RNA pseudoknots. We compared the experimental results of our method for a set of real RNA sequences with an existing method. For a set of sequences of small length, our approach achieved good performance in both sensitivity and specificity. We successfully employed the flexibility of integer programming to model the problem of RNA structure prediction. This research could be helpful to studies related to biomedicine and agriculture, and important for the promotion of science in Thailand.

1. Introduction

An RNA molecule plays many important roles in cells. For example, it serves as carrying messenger (mRNA) genetic information from DNA in order to translate into proteins. However, many RNAs are not translated into proteins, called non-coding RNAs (ncRNAs). Functions of some ncRNAs are known such as RNA splicing, processing and editing; but some are yet unknown. Secondary structure analysis helps understand the function of RNA. laboratory process to determine RNA structure is costly. Therefore, secondary structure prediction of RNA is important.

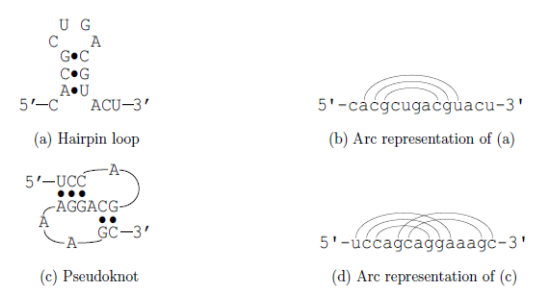


Fig.1 An example of RNA secondary structures.

A molecule of RNA can be viewed as a single strand of the nucleotides (bases) adenine (A), guanine (G), cytosine (C) and uracil (U). A-U, C-G and G-U can form a base pair via hydrogen bonding. Due to this property, an RNA strand can fold back on itself to form a secondary structure (Fig. 1).

We can represent a secondary structure of RNA by drawing a sequence of bases as a horizontal line and arcs over or under the sequence connecting two bases to represent the base pairs. If there are some crossing arcs, the secondary structure is said to contain a *pseudoknot* (Fig. 1 (c) and (d)).

An often-used thermodynamic hypothesis states that RNA always forms a secondary structure with the lowest free energy. Hence, the problem of RNA secondary structure prediction is modeled as an energy minimization problem. Many algorithms have been developed to solve this problem. Existing algorithms can predict a secondary structure with pseudoknots in $O(n^4)$, $O(n^5)$ or $O(n^6)$ time, where n is the length of an input sequence. Moreover, prediction of an arbitrary planar secondary structure including pseudoknots is proven to be NP-hard [1].

We proposed an integer programmingbased method of predicting RNA secondary structure with pseudoknots. Despite the theoretical drawbacks in computational complexity, it is practical and reasonable to model the prediction of pseudoknotted structure by integer programming.

2. Methodology

Integer programming (IP) is an optimization problem, which optimizes a linear function subject to linear equality and/or inequality constraints. An IP problem is